A Study of the Ocean-Atmosphere Interface from Satellite and *In Situ* Measurements

Thesis submitted for the degree of Doctor of Philosophy at the University of Leicester

by

Thomas Sheasby B.Sc. (hons) M.Sc.

Department of Physics and Astronomy
University of Leicester

September 2000

1 Abstract

A Study of the Ocean-Atmosphere Interface from Satellite and *In Situ* Measurements

by

Thomas Sheasby

The Along Track Scanning Radiometers (ATSR-1&2) on ESA's Remote Sensing Satellites (ERS-1&2) are validated using *in situ* radiometric data from Mutsu Bay, Japan. One validation point for ATSR-1 was obtained and it was found to have an offset of –0.03K from the *in situ* radiometric data. Four validation points were obtained for ATSR-2 and it was found to have an offset of 0.07±0.17 K in this region.

The so-called 'skin effect' is investigated to improve the characterisation of the ocean-atmosphere interface. The two contrasting data sets – one from sheltered waters and one from open ocean are compared. The data presented here show that, in open oceans, at wind speeds greater than $6ms^{-1}$, ΔT tends to a constant value of about -0.14 ±0.1K.

The *in situ* radiometric data were taken using the SISTeR radiometer, designed and built by T.J. Nightingale. The absolute accuracy of this radiometer is assessed over a number of years and during the last campaign was found to be better than 0.025 K with an rms error (with a clean scan mirror) of less than 0.03 K.

The data sets required to do this work were collected during 3 field campaigns during the summers of 1996, 1997 and 1998. MUBEX'96 and '97 took place in Mutsu Bay, Japan and CHAOS'98 was a research cruise from Tenerife to Iceland on the RRS Discovery.

2 Acknowledgements

2.1 Personal

I would like to thank my supervisor Prof. David Llewellyn-Jones for his help and advice throughout my project. I would also like to thank the following people for their help in specific parts of my project:

Dr. Isabelle Parkes – for her support and council during her time at Leicester, especially during the MUBEX campaigns.

Dr. Tim Nightingale – for everything SISTeR related and his general advice on everything from blackbodies to Japanese ice cream

Dr. Craig Donlon – for his advice and life saving IDL code on all aspects of radiometry and for helping me get published

Nigel Houghton – for providing the ATSR imagery, sometimes at very short notice

Dr. Chris Merchant – for providing the ATSR coefficients and explaining their use

Dr. Paul Morris – for advice on atmospheric models and modelling

I wish to express my gratitude to my fellow PhD students William Rathman, Helen LeCore and Ian Ridley for the help and support over the years. I also wish to thank my housemates Norm and Jez and all the members of ULBC, both past and present, for a wonderful time at Leicester. And finally, a special thanks to "Mols" for keeping me going.

I would like to acknowledge the Natural Environmental Research Council (NERC) who provided the funding for my work, and RAL and ESA for providing the ATSR data.

2.2 MUBEX'96 & '97

I would like to thank the members of the MUBEX team, especially Dr. Sumio Tanba and Professor Ryuzo Yokoyama, for their help and advice during the campaign. I would also like to thank Mr. Kazue Hosokawa for the use of his vessel and facilities during the campaigns and to pass on my condolences to his family. I would like to acknowledge the Royal Society, the British Council, the Japan Society for the Promotion of Science, NASDA, the Japanese Ministry of Education, NERC and DAIWA for their financial support.

2.3 CHAOS'98

I would like to thank Dr. Denise Smythe-Wright for giving me the berth on the cruise and for her advice on my first research cruise. I would also like to thank Dr. R.W. Pascal and Dr. S.A. Josey for allowing me to use their meteorological data from the cruise and for their wealth of experience of collecting data at sea. I would also like to thank the Captain and crew of the RRS Discovery, and the scientific party for all their help and advice throughout the cruise. The cruise was funded by NERC and the Southampton Oceanography Centre.

3 Introduction

3.1 General

3.1.1 Objectives

The main objective of this thesis is to assess the accuracy of the Along-Track Scanning Radiometers (ATSR-1 and 2), flown on the ERS-1 and ERS-2 satellites. This is done using *in situ* radiometric data rather than a traditional 'bulk' temperature. The skin-bulk temperature difference, or 'skin effect', is important when studying heat fluxes between the ocean and the atmosphere. A second objective of this thesis is therefore to improve the characterisation of the skin effect. In order to achieve these objectives it was necessary to assess the accuracy of the radiometer used to take the *in situ* measurements (SISTeR) and to go on various field campaigns.

3.1.2 Layout of Thesis

This thesis consists of four main chapters. Chapter 3 is an introductory chapter, giving a general overview of this thesis and the background information on sea-surface temperature. Chapter 4 describes the satellite data used and the field campaigns from which the *in situ* data were obtained. Chapter 5 describes the instrument (SISTeR) used to obtain the *in situ* radiometric data. It also assesses the accuracy of that instrument. Chapter 6 presents the results of validating satellite derived sea surface temperatures (SSTs) with *in situ* data from the field campaigns. The results of studying the so-called 'skin effect' are presented in chapter 7. The conclusions and further work are presented in chapter 8.

3.1.3 Scientific Justification and Methodology

Oceans cover 70 per cent of Earth's surface. Their interaction with the atmosphere plays a dominant role in determining the weather, climate and circulation of the oceans. An understanding of the processes driving these systems, and of their interactions with each other, is important for meteorological and climate modelling and so predicting any climate change. This thesis is concerned with the study of the ocean-atmosphere interface and pays particular interest to the accuracy of satellite derived sea surface temperature (SST). Knowing the accuracy of these satellite derived SSTs is of particular importance when they are used for climate change studies or ocean-atmosphere modelling.

This thesis starts by introducing the data sets used, and then assesses the accuracy of the *in situ* radiometer used to obtain the *in situ* validation data. Knowing the accuracy of the *in situ* radiometer, the accuracy of the satellite data is then assessed and then the ocean-atmosphere interface investigated.

3.2 Sea Surface Temperature (SST)

3.2.1 History (Bulk record)

The sea surface temperature (SST) is an important quantity as it is the temperature of the actual ocean-atmosphere interface and therefore plays a direct role in controlling fluxes of heat and gases between the oceans and atmosphere. The SST is also recognised as being one of the indicators of global climate change (Allen 1993). Traditionally the temperature used in models, such as that of the U.K. Meteorological Office, was a sub-surface bulk temperature as this was the only data available. The bulk temperature is typically measured at a depth from 0.5 to 10 metres depending on the method used. The skin SST defines the temperature of the actual interface, and so it is this that should be used in ocean-atmosphere models. Currently, the bulk–skin temperature difference forms part of the parameterisation of the air–sea interface. Using the skin SST directly, eliminates a stage of this parameterisation. Attempts are currently being made to change these models to use SST values, but this requires much effort and is still some way off. Therefore, there is still a user-driven demand for a "pseudo-bulk" temperature from the SST values obtained from Earth observing satellites.

Traditionally the bulk temperature was measured with a mercury-in-glass thermometer from a bucket of water hoisted onboard ships at sea. This was not a very accurate method as it suffered from solar heating, radiative cooling, and human handling and measurement errors. It also depended on the depth from which the water was obtained which was generally very imprecisely determined. More recently, thermistors located on the hulls of ships have been used but care must be taken to ensure they are located at a specific depth and not near any heat source, such as the engine water-cooling exhaust. Regular calibration of such instruments is very difficult and the area covered by instruments on ships and scientific buoys is limited. Ship data tends to be confined mainly to the shipping lanes and buoy data to either specific points (in the case of fixed buoys) or random paths (in the case of drifting buoys). Satellites give global coverage, typically every few days. They use radiometers to measure the SST indirectly. Most earth observing satellites carry these instruments, for example the ERS (European Remote Sensing) series that carry the ATSR (Along Track Scanning Radiometer) and NOAA (National Oceanic and Atmospheric Administration) series which carry the AVHRR (Advanced Very High Resolution Radiometer).

3.2.2 Why we need an accurate SST record

The use of sea surface temperature measurements for detecting and measuring climate change is potentially one of the most useful methods available. This is not only because oceans cover two thirds of the surface of the planet but also that seawater has a large thermal inertia. This helps in filtering out the high frequency noise (from weather patterns etc.) that can swamp measurements made from other methods such as land surface or air temperatures. Satellites enable scientist to obtain the global coverage, high levels of accuracy and consistency needed for such work. The World Climate Research Programme in 1981 stated that a global SST accurate to ±0.2 K is required in order to reliably detect any change. The climatic applications of the international Tropical Oceans Global Atmosphere (TOGA) programme stated the allowed error to be ±0.3 K (e.g. Barton 1992). This is after all systematic, detector and atmospheric errors have been accounted for. The most widely used satellite radiometer is the Advanced Very High Resolution Radiometer (AVHRR) on the NOAA polar orbiting series of satellites. The AVHRR instrument uses bulk buoy data to calibrate the SST. This means that the satellite produces a pseudo bulk temperature from a skin SST. It also has only one blackbody calibrator on-board. It uses deep space (assumed to be at 2.7 K) as a second calibration target. These two calibration points are rather far apart. Various studies (e.g. Robinson *et al.* 1984, May *et al.* 1992) have shown that SSTs obtained from the AVHRR instrument are accurate to 0.6-0.7 K. This lies outside the range set in place by the World Climate Research Panel (WCRP) and TOGA.

The ATSR instruments with their dual-look capability, two blackbodies, and cooled detectors should be more accurate than the AVHRR instruments. Smith *et al.* 1994, suggest that the design accuracy of ATSR lies at ±0.3 K for the 0.5 by 0.5 degree cells, which lies within the limits set by WCRP and TOGA. Parkes *et al.* 2000 show that the image pixel (1 km resolution) error is of order 0.5 K. When these are averaged up to the 0.5 by 0.5 degree average SST (ASST) pixels, the error is reduced to the order of 0.01 K, well within the limits set. The work presented in chapter 6 of this thesis shows that with careful geolocation or in open ocean the pixel error falls to 0.04 ± 0.17 K. This further reduces the error of the ASST pixels and this indicates that ATSR is now meeting the accuracy requirements for climate change studies although further work is required. The current limitation to using the ATSR-1 and ATSR-2 data sets for climate change detection is the limited time series. Allen *et al.* 1994 state that 10-15 years is the minimum timescale that is needed before a trend can be stated with any confidence. Therefore, the stability of the ATSR instruments is important. There has been an ATSR instrument flying since July 1991 so there is currently almost 9 years of continuous data. Allen *et al.* 1994 also stated that if the El Niño signal could be successfully removed then the minimum detection time could be reduced by 1-2 years. Therefore, if the El Niño signal can be removed from the current ATSR data series it can be used to detect climate change. This is currently proving to be difficult due to the short time series available and more data are needed. As time progresses and with the launch of the next generation ATSR (AATSR) in 2001 the length of the data series and so the level of confidence of any trends detected will be improved. Currently ATSR-1 data has been reprocessed with the ATSR-2 processing suite (SADIST-2) to give a consistency in the processing method especially with regard to cloud clearing. There is a known problem with the ATSR-1 data in that the processing does not take account of the warming of the detector over the later part of the instruments life. Work is currently being undertaken to account for this and the data will be reprocessed once this has been done (see chapter 6). The ATSR-2 data is currently processed using an early version of C.J. Merchant's global coefficients. Unfortunately, there was an error found in the dual-look algorithm and so the data need to be reprocessed using the new coefficients released in March 2000. Work is also being done to reduce a possible latitude dependence found when using the global coefficients (Murray 2000) and it is likely that in the future all these effects will be accounted for and the data reprocessed.

3.2.3 The 'Skin Effect' and Diurnal cycle

Two important processes that need to be considered when studying the sea surface temperature are the 'skin effect' and the diurnal cycle. Infrared radiometers measure radiation from the top 10-20μm of the sea. This radiance can be converted into a temperature that is representative of this so-called 'skin' layer of the sea. The 'skin' temperature is important for ocean-atmosphere interaction studies, as this is the temperature of the actual interface. This temperature may differ from the 'bulk' temperature measured conventionally just below the surface. The 'skin effect' is the temperature difference between the 'skin' temperature of the ocean and the 'bulk' temperature. This difference can typically be 0.1 - 0.5 degrees warmer or cooler depending on the weather conditions. The author is referred to Robinson (1985) and Robinson *et al.* (1984) for a detailed description of the skin effect.

Traditionally the depths of the bulk measurements have varied depending on the method used, typically being between 1cm and 5m below the surface. This varying depth of bulk measurements can affect studies of the skin effect, as the temperature of the top 5m of ocean is rarely uniform. This means comparisons between data sets might not be consistent. This is especially true in calm, daytime conditions when strong diurnal thermoclines can build up. In certain conditions, temperature differences of order 3 K have been measured in the top few metres of the sea surface. In these conditions, the depth of the bulk temperature measurement can have a large effect on any skin effect measured. In extreme cases, a warm skin may appear to be present when in fact a strong diurnal thermocline is masking a cool skin. Yokoyama *et al.* (1995), and Yokoyama and Konda (1996) give a good description of these effects in Mutsu Bay and of their effect on AVHRR validation.

3.2.4 Need for Skin Validation

It is important to validate satellite SST data to ensure that all the algorithms used to generate the temperatures are working correctly, especially the atmospheric correction. *In situ* data are often used to derive and validate atmospheric correction schemes for satellite SST measurements. These *in situ* data have traditionally been bulk temperature measurements. With the increase in the accuracy of atmospheric corrections, the skin effect has become a limiting factor in the accuracy of SST validation efforts, especially when using bulk data. Validating satellite SST data with bulk data leads to errors in the derived SST due to the skin effect, so ideally satellite SST data should be validated with *in situ* radiometric data. The AVHRR instruments are validated using bulk data and are calibrated to give a pseudo-bulk temperature not the skin temperature. However, the ATSR processing is designed to give a more accurate skin temperature, so it is important to validate the instruments with *in situ* radiometric skin data. It was for this reason that the SISTeR radiometer, used to collect the data in this thesis, was designed and built (see chapter 5).

3.2.5 Validation Programme

In order to validate satellite SSTs globally, it will be necessary to collect data from a large number of match-ups between *in situ* and satellite SSTs to reduce the effect of errors that are discussed later. These data sets should ideally contain the following measurements:

- The *in situ* radiometric skin data
- The temperature of the sky at the complimentary angle to the sea measurement (ideally with the same radiometer) in order to calculate the down-welling radiation and so a sky correction.
- Further sky temperature measurements for improved sky corrections
- Wind speed (and direction) measurements, preferably at a 10 metre height
- Bulk SST measurements from a range of depths to give an idea of the temperature profile – at least a 'zero' cm depth (from a soap-on-a-rope type instrument) and a deeper bulk measurement (3 or 5 metres).
- Air temperature (10 metre)
- Humidity (10 metre)
- Short-wave solar flux
- Atmospheric pressure
- Measurements any cloud cover present
- Sun angle or bearing to allow for sun glint
- Atmospheric profiles (radiosonde) are useful for updating models etc.

These measurements should be made for a period of time before and after the overpass to obtain an understanding of the local conditions and how they are varying (as a temporal average is used to approximate a spatial average).

These match-ups must come from a variety of locations and latitudes to ensure that there are no regional or latitudinal variations in the algorithms used to generate the satellite SSTs. There should also be a temporal range in the data to ensure that there are no errors due to the annual cycle or by long-term drift of the satellite instruments. The data presented in chapter 6 are hopefully the first of many data sets that will be combined to form a master validation data set that will be used to validate a variety of satellite radiometers. The table in section 6.9 summaries the results of this chapter and is one of the main results of this thesis.

4 Measurement Programme

4.1 Introduction

This chapter describes the data sets acquired and used in this thesis. The first section describes the satellite data that are used, the accuracy of which is investigated in chapter 6. The second section describes the field campaigns that were undertaken during the summers of 1996, 1997 and 1998 in order to collect the *in situ* data.

4.2 The Satellite (ATSR) Data

4.2.1 The Along-Track Scanning Radiometers (ATSR)

The satellite data used in this thesis come from a series of instruments called the Along-Track Scanning Radiometer (ATSR). The ATSR instruments are carried on the ESA Remote Sensing (ERS) satellite series, ATSR-1 on ERS-1 and ATSR-2 on ERS-2. The original ATSR-1 instrument was developed by a consortium of research institutes from the UK, Australia and France. It was an infrared only instrument with channels centred on 12μm, 10.8μm, 3.7μm, and 1.6μm. The ERS-1 satellite was launched on the 17th July 1991. In June 1996 it was put into hibernation mode as a backup for ERS-2, and was eventually lost on Friday 10 March 2000 by a failure in the on board attitude control system. Data from the 3.7μm channel was not available after May 1992 when this channel failed. The ERS-2 satellite was launched in April 1995 and carried the second ATSR instrument (ATSR-2). This is an enhanced instrument, it has the same infrared channels as ATSR-1 but also carries three additional visible/ near infrared channels centred on 0.55μm, 0.67μm and 0.87μm. Table 1 shows the wavelength and width of each channel on the ATSR instruments and their main purpose. The next generation ATSR, AATSR (Advanced ATSR), is due to be launched on ESA's ENVISAT satellite in June 2001 and is part-funded by the UK DETR (Department of the Environment, Transport and the Regions).

Feature	**Wavelength**	**Bandwidth**	**ATSR-1**	**ATSR-2/ AATSR**
Cloud Clearing	1.6μm	0.3μm	Y	Y
SST retrieval (Night)	3.7μm	0.3μm	Y	Y
SST retrieval (Day/Night)	10.8μm	1.0μm	Y	Y
SST retrieval (Day/Night)	12.0μm	1.0μm	Y	Y
Chlorophyll	0.55μm	20nm	N	Y
Vegetation Index	0.67μm	20nm	N	Y
Vegetation Index	0.87μm	20nm	N	Y

Table 1: This table shows the centre wavelength, width and main purpose of each ATSR channel. (From Mutlow *et al.* 1999)

The ATSR instruments constitute an enhancement on earlier space-based radiometers due to improved instrument stability, calibration and detector noise performance. The ATSR-1 instrument had noise equivalent delta temperatures (NEΔT) of better than 50mK at the beginning of the mission when the instrument's detector temperatures were at their coldest (~91 K). This rose to 60mK in the 11μm channel and 130mK in the 12μm channel at the end of the mission. This was due to the degradation of the closed Stirling cycle cooler that allowed the detector temperature to rise to over 110K (Mutlow et. al, 2000). The ATSR-2 11 and 12 μm channels have typical NEΔT values of 36 and 46mK respectively. The better performance is achieved because the cooler has been able to maintain the detectors at 81±1K throughout the mission. The instruments were also extensively calibrated before launch to fully characterise the them, especially with regard to any detector non-linearities. The infrared channels of the ATSR instrument are calibrated once each scan by two on-board blackbody calibration targets spanning the expected range of top of the atmosphere radiances over the sea. One blackbody is cold, at typically -10°C and the other warm at around 30°C. The infrared calibration and corrections for detector non-linearities are automatically applied during the ground processing. The scanning mechanism of the ATSR instruments is such that it enables the instrument to look at the same spot on Earth twice at different angles. The instrument first views a scene in the 'forward' view at an angle of roughly 55°

from vertical then again about 150 seconds later in the 'nadir' view. Figure 1 shows how the conical scanning mechanism of the ATSR instrument enables the instrument to view the surface twice.

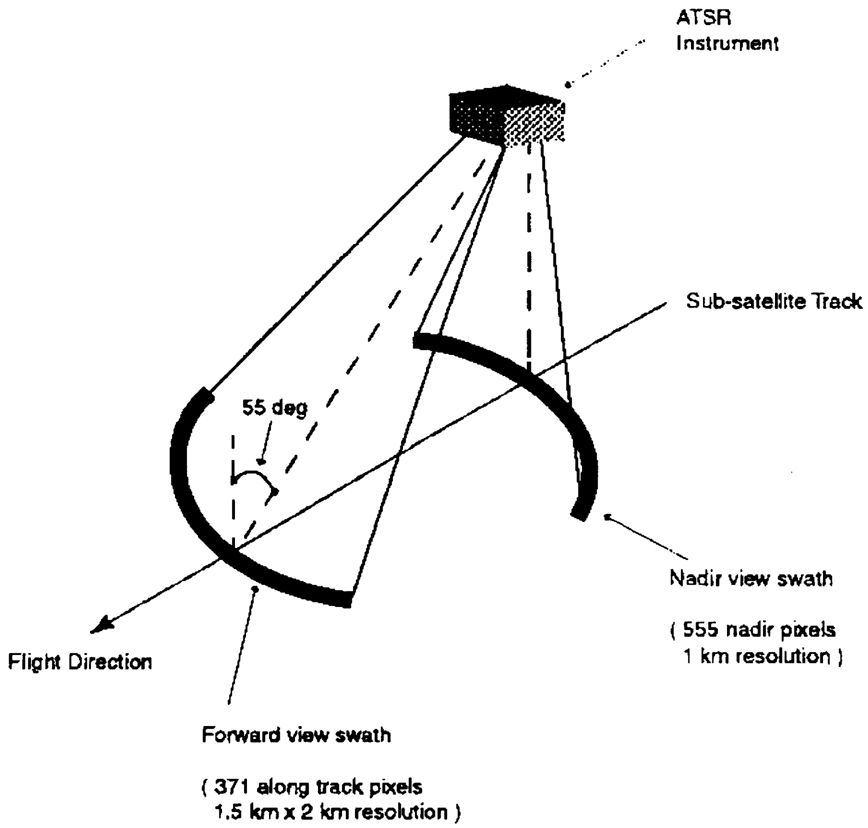

Figure 1: A diagram showing the 'dual-look' viewing geometry of the ATSR instruments that enables them to have both a 'nadir' and 'forward' view. (From Mutlow *et al.* 1999)

This 'dual-look' method helps to provide a better atmospheric correction as the same scene is viewed twice through different atmospheric path lengths. This atmospheric correction is applied during the data processing on the ground. Mutlow *et al.*, 1994 state that the dual view and lower instrument noise enable ATSR to obtain an rms error of 0.36K. One of the main objectives of this thesis was to validate ATSR measurements using *in situ* radiometric data (see chapter 6).

4.2.2 The Data Processing Method

Space-borne radiometers measure the flux of electromagnetic radiation from the top of the atmosphere. This is the flux emitted from Earth's surface modified by the atmosphere. The effect of the atmosphere is corrected for using an atmospheric model. In the case of ATSR, the raw satellite data are processed using a software package called SADIST (Synthesis of ATSR Data Into Sea-surface Temperatures) produced by the Rutherford-Appleton Laboratory (Závody *et al.*, 1994). Initially, ATSR-1 data were produced using SADIST-1 and ATSR-2 data using a newer version called SADIST-2. Recently however, the ATSR-1 data have been reprocessed using the SADIST-2 processing suite to provide consistency between the data sets. The SADIST-2 processing suite is from time to time upgraded and at the time of writing this thesis the most up to date version was version 320. The SADIST processing produces a variety of products that can be obtained by end users. The SADIST-2 manual (Bailey, 1995) and ATSR-1/2 Users Guide (Mutlow *et al.*, 1999) give detailed descriptions of each data product. The two products used in this thesis are the gridded products and the spatially averaged products. The gridded products contain 512 by 512 co-located pixels that have been mapped onto a 1km grid. The spatially averaged products have been spatially averaged to a ten-arcminute or half-degree resolution. Each of these products can be sub-divided into brightness temperature (BT) and sea surface temperature products (SST). The BT's are simply the top of the atmosphere radiances converted into a temperature using the on-board calibration and any detector corrections. The SADIST processing also generates an SST from these BT's using the multi-channel method similar to that used by the Advanced Very High Resolution Radiometers (AVHRRs), flown on the NOAA series of satellites. The dual-look of the ATSR instruments however, enables them to obtain a much better atmospheric correction. There is fundamental difference between the two instruments in that the ATSR instruments use an atmospheric model to generate skin SSTs whereas the AVHRR instruments are validated using a network of buoys so generate a pseudo-bulk SST. The ATSR SST is calculated using the following formula to correct for atmospheric effects. This is a simple linear approximation to a very complex function:

$$SST = a_0 + \sum_{i=1}^{n} a_i T_i$$

where, SST is the Sea Surface Temperature of a given pixel

a_0 is the offset coefficient

a_i is the coefficient for channel i

i is the channel number

n is the number of channels available

T_i is the brightness temperature of channel i

ATSR has three channels that can be used to calculate an SST – the 3.7μm, the 11μm and the 12μm. During the night all three channels can but used but during the day the 3.7μm channel cannot be used because the brightness levels of emitted radiation are comparable to reflected sunlight at this wavelength. Therefore, with the dual-look there are six brightness temperatures that can be used to calculate a night-time SST (three-channel algorithm) and four to calculate a daytime SST (two-channel algorithm). The 3.7μm channel on the ATSR-1 instrument failed in May 1992 so from this date onwards only a two-channel SST can be generated for ATSR-1 data. The coefficients (a_0, a_i) are upgraded from time to time, as is the exact method of applying the coefficients to each pixel. The method of applying the coefficients is complicated by the conical nature of ATSR's scan mechanism. Details of exactly how the coefficients are currently applied are given in chapter 6. Due to the nature of the scan mechanism, the exact size of a pixel varies depending on its position in the scan cycle. The field of view (FOV) of ATSR consists of two, 512 km wide curved swaths (nadir and forward). The nominal pixel size at the centre of the nadir swath is $1km^2$ and 1.5-2 km^2 at the centre of the forward swath. The high-resolution SST product that SADIST-2 generates is mapped onto a 512 by 512 grid of 1 km^2 pixels. The latitude and longitude of the centre of each pixel is then calculated and provided as a similar 512 by 512 grid. The ASST product is obtained by spatially averaging the high-resolution product to a 0.5° grid.

The SADIST-2 processor also generates a cloud mask that has a numerical flag associated with each pixel. Various cloud-clearing algorithms are applied to the data to test for the presence of clouds. A 12-bit number is then assigned to each pixel and the value of each bit gives information on whether the pixel has passed each test. Table 2 gives the value associated with each cloud test. Further details of the SADIST cloud detection scheme are given in Bailey, 1995 and Mutlow *et al.*, 1999.

Bit Number	Decimal Value	Meaning if set
0	1	Pixel is over land
1	2	Pixel is cloudy (result of all tests)
2	4	Sunglint detected in pixel
3	8	1.6μm reflectance histogram test shows pixel cloudy (day-time only)
4	16	1.6μm spatial coherence test shows pixel cloudy (day-time only)
5	32	11μm spatial coherence test shows pixel cloudy
6	64	12 μm gross cloud test shows pixel cloudy
7	128	11/12μm thin cirrus test shows pixel cloudy
8	256	3.7/12μm medium/high level test shows pixel cloudy (night-time only)
9	1024	11/3.7μm fog/low stratus test shows pixel cloudy (night-time only)
10	2048	11/12μm view-difference test shows pixel cloudy
11	4096	3.7/11μm view-difference test shows pixel cloudy (night-time only)
12	8192	11/12μm thermal histogram test shows pixel cloudy

Table 2: A table showing the bit number and equivalent decimal value of the SADIST-2 cloud-clearing/land flags.

For example, if a pixel has a decimal cloud flag of 38 associated with it, from the table it can be seen that bits 1, 2 and 5 have been set (2+4+32=38). This means the pixel is cloudy, suffering from sunglint, and has failed the 11μm spatial coherence test. In the SADIST-2 processing, if both the forward and nadir pixels are flagged as clear (numerical value 0) then a 3-channel SST is generated as described above. If the forward pixel is flagged as cloudy and the nadir is clear then a nadir only SST is generated. If both pixels, or just the nadir pixel, are flagged as cloudy then a dual-view SST is generated and the interpretation of the pixel is left up to the user.

There is more information on the SADIST-2 products in the SADIST-2 manual (Bailey, 1995). The reader is referred to this source and to the ATSR-1/2 Users Guide (Mutlow *et al.*, 1999) for further information.

4.2.3 Satellite Orbits and Data Availability

ERS-1 and ERS-2 were inserted into near-circular low Earth orbits (LEO) at a mean height of 780 km. The orbit is a retrograde, sun-synchronous orbit so the satellite passes the equator at the same local solar time every orbit. The overpasses are at roughly 10.30 am and 10.30 pm local time (local time with respect to longitude not time zone). The orbit gives a sub-satellite velocity of 6.7 km s^{-1} across Earth's surface and an orbital period of about 100 minutes. The ERS spacecraft are usually in 'Yaw Steering Mode', in which the satellite is continually rotated to compensate for Earth's rotation such that the satellite is always aligned with the direction of motion along Earth's surface. The ERS-2 spacecraft was placed into an orbit with a 1-day lag behind ERS-1. Therefore, during the Tandem mission phase, ATSR-2 viewed the same location as ATSR-1, in the same orbit, the following day. Occasional orbital correction manoeuvres are used to maintain the sub-satellite track to within ±1 km from nominal.

Over its lifetime, the ERS-1 platform was placed into various orbits for specific missions. Table 3 shows the dates of and reasons for each type of orbit. When ERS-1 was in its ice phases, the 512 km wide swath of ATSR meant that global coverage could not be obtained (see Figure 2 and Figure 3). This leads to gaps in the SST data during these periods.

Date Range	Repeat Cycle
ERS-1	
31 July 1991 – 10 December 1991	3-day (Commissioning Phase)
10-26 December 1991	ERS-1 orbit manoeuvres
26 December 1991 – 30 March 1992	3-day (Ice Phase)
30 March 1992 – 14 April 1992	ERS-1 orbit manoeuvres
14 April 1992 – 17 December 1993	35-day (Global Phase)
17-21 December 1993	ERS-1 orbit manoeuvres
21 December 1993 – 10 April 1994	3-day (Second Ice Phase)
10 April 1994 – 19 March 1995	168-day (Geodetic Phase)
19-21 March 1995	ERS-1 orbit manoeuvres
21 March 1995 -	35-day (Global Phase/Tandem Phase)
ERS-2	
22nd April 1995 – present	35-day

Table 3: This table shows the dates of the various ERS orbit cycles. (From Murray 1995)

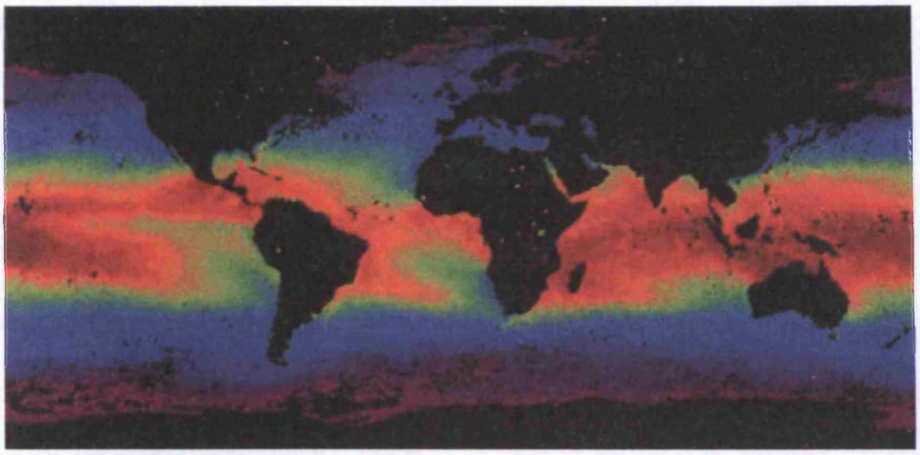

Figure 2: An image showing the typical coverage of the monthly averaged 35-day repeat cycle. Areas where an SST could not be generated (due to cloud, missing data or the instrument being over land) are shown in black. (From Murray, 1995)

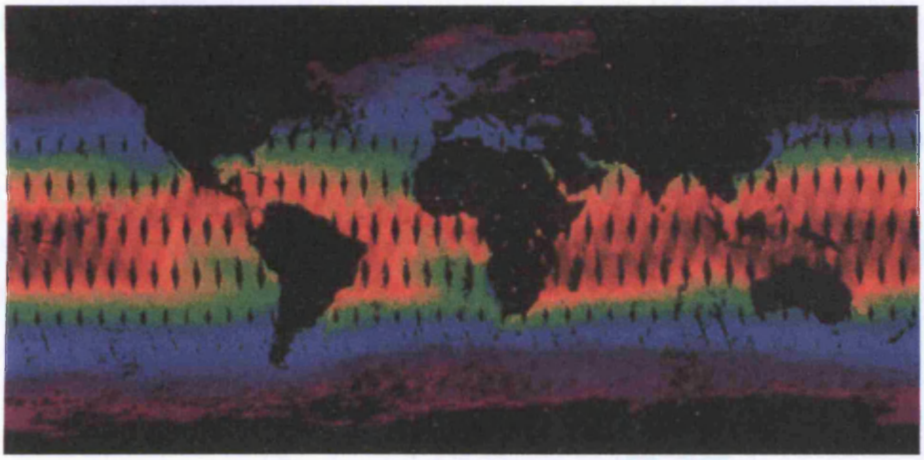

Figure 3: This image shows the typical coverage of the monthly averaged 3-day repeat cycle coverage. Areas where an SST could not be generated (due to cloud, missing data or the instrument being over land) are shown in black. The regular pattern of missing data is due to the nature of the 3 day orbit. (From Murray, 1995)

The orbit of ERS-2 has not been changed from the 35-day repeat cycle so ATSR-2 data do not suffer from missing data.

4.3 Description of Field Campaigns

4.3.1 Introduction

In order to obtain skin SST data sets to use for the validation of satellite SSTs and the study of the skin effect, three field campaigns, two in Mutsu Bay, Japan, and one in the Atlantic Ocean were undertaken. The *in situ* skin SSTs were measured using the SISTeR radiometer (see chapter 5) designed and built by T.J. Nightingale at the Rutherford-Appleton Laboratory (RAL). The data were taken during the summers of 1996, 1997 and 1998. The first two data sets (MUBEX'96 and MUBEX'97) contain the validation data used in chapter 6 and the last two data sets (MUBEX'97 and CHAOS'98) contain the data used for the 'skin effect' studies in chapter 7. The following two sections describe the MUBEX and CHAOS campaigns in more detail.

4.3.2 The Mutsu Bay Experiments, 1996 and 1997

MUBEX (Mutsu Bay Experiment) was an international collaboration between the Universities of Leicester, Iwate, Southampton, and Tokyo along with the Rutherford-Appleton Laboratory (RAL). It was a three-year project studying the ocean-atmosphere interface from satellite and *in situ* measurements. The MUBEX'95 campaign was carried out during the summer of 1995, MUBEX'96 took place in July/August 1996, and MUBEX'97 was held in July/August 1997. The project involved taking a number of detailed *in situ* measurements in Mutsu Bay on the northern side of Honshu Island in Japan. The main experiments were carried out during the summer immediately after the rainy season when cloud free days (essential for satellite observations of SST) are most likely. The author participated in the MUBEX'96 and MUBEX'97 campaigns.

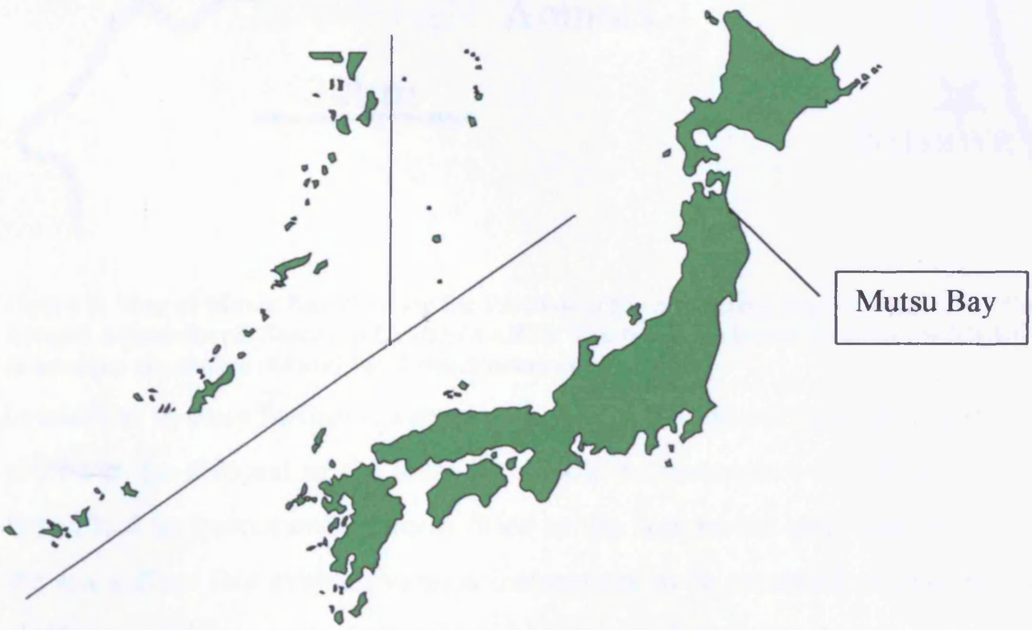

Figure 4: A simple map of Japan showing the location of Mutsu Bay.

Mutsu Bay is located at the Northern end of Honshu Island, Japan (see Figure 4) at roughly 141°E and 41°N. It is a relatively sheltered bay and covers an area of 1600 km^2 to a mean depth of 35m. There is a considerable clam farming and fishing industry in the bay. Over the last 20 years, considerable investment has been made in the area by the Japanese fishing industry producing a network of measuring systems (see Figure 5). This system is run by the Aomori Aquacultural Research Centre (AARC) and these extensive marine and meteorological data were made available to the campaign.

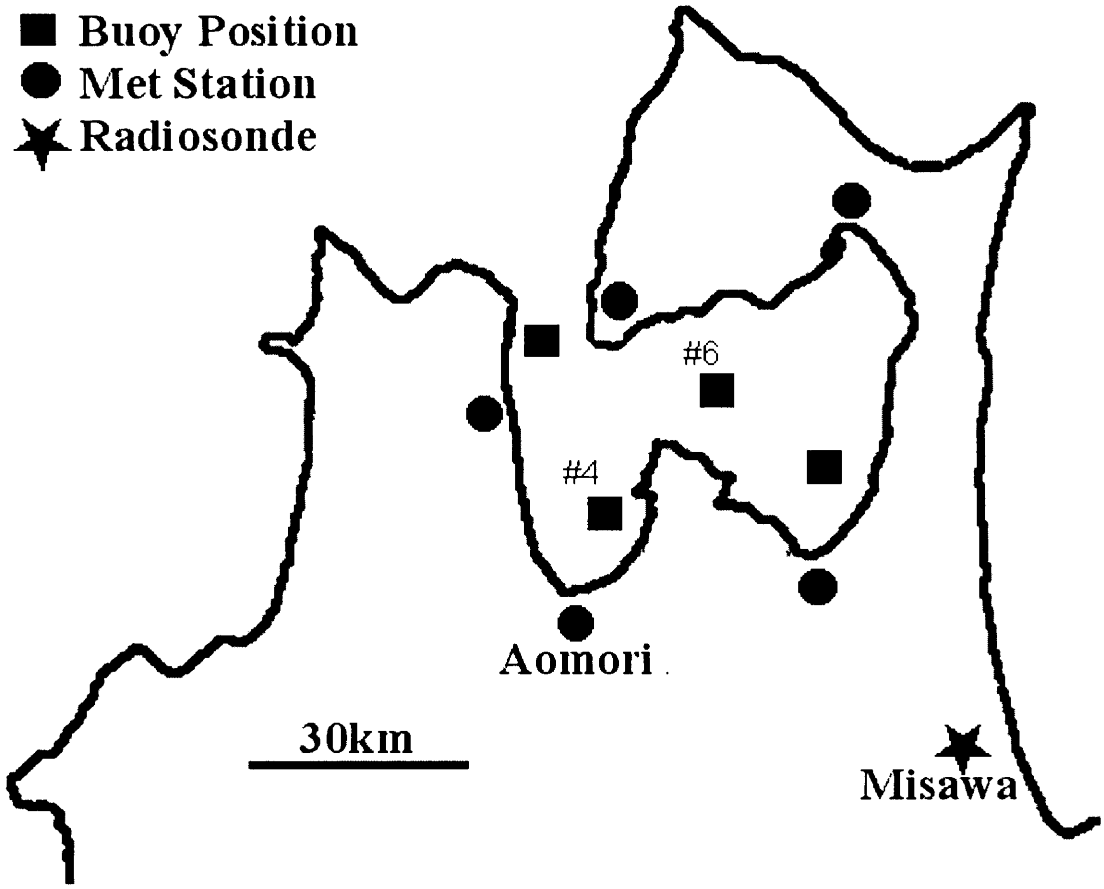

Figure 5: Map of Mutsu Bay showing the location of the measuring system installed by the Aomori Aquacultural Research Centre (AARC). The two main buoys used for the MUBEX campaigns are shown (#4 and #6). From Parkes et al., 2000.

In addition to these facilities, a research boat, the Dai-Ni-Misago (see Figure 6), was placed at the disposal of the team by a local businessman – Mr. Hosokawa. The vessel had an instrument platform fitted to the bow of the ship, five metres above the sea surface that enabled various instruments to be mounted so that they had a clear view of the ocean uncontaminated by the ship's wake or shadow.

Figure 6: A photograph of the research vessel the Dai-Ni-Misago used during the MUBEX campaigns.

Installed on the Dai-Ni-Misago was a variety of instrumentation (see Table 4 and Figure 7). The radiometric SST used in this thesis was measured using the SISTeR radiometer (see section 5) installed on the front of the instrument platform. It was programmed to look at the sea surface at an angle of 18 degrees to nadir and at the complementary angle (162°) in order to obtain a brightness temperature for the sky correction (see Appendix 2). The angle of 18 degrees was chosen to give a viewing angle as close to vertical as possible and still have the FOV outside the ship's wake and shadow. Two types of low-cost radiometers, a thermal imaging camera (TIC) and sea and sky video cameras were also installed on the instrument platform. The bulk temperature was measured using a Conductivity Temperature and Depth probe (CTD) that was hung over the port side of the vessel. The temperature sensor was at a nominal depth of 0.75 metres but this depth varied by ±0.5m as the ship rolled. There was also a temperature-profiling device, deployed by the Japanese side, called the Moving Sea Surface Observer (MSSO). This was a thermistor chain that measured the bulk temperature at a variety of depths down to two metres. Unfortunately, analysis of the data from this instrument raised doubts about the accuracy of its absolute calibration (S. Tamba, personal communication 1999) so the data were not used for this thesis. Also installed on the vessel were a meteorological station, a sun photometer and GPS receivers. Table 4 summarises the main instruments deployed on the Dai-Ni-Misago and Figure 7 shows a schematic of their locations.

Instrument	Parameter being measured	Notes
SISTeR	Radiometric SST	Suffered from noise during MUBEX'96
CTD	Bulk SST	Measured at a depth of roughly 0.75m
Meteorological station	Humidity, air temperature, pressure, wind speed & direction, solar radiation	Failed at the end of July during the MUBEX'97 campaign
GPS receiver	Latitude and longitude	
TIC	Radiometric SST	
Low-cost radiometers	Radiometric SST	A variety of makes were tested during the MUBEX campaigns
Sea Video Camera	Sea State	
Sky Video Camera	Cloud cover	
MSSO	Bulk SST profile	Absolute calibration suspect

Table 4: A table listing the main instruments deployed on the Dai-Ni-Misago during the MUBEX campaigns.

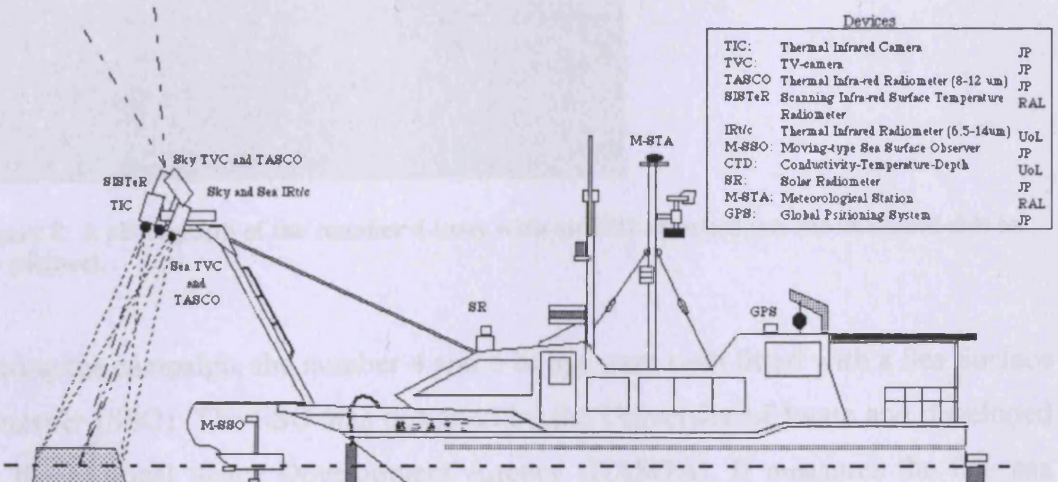

Figure 7: A schematic diagram showing the location of instruments mounted on the research vessel the Dai-Ni-Misago during MUBEX.

In the bay itself, there are a series of moored buoys operated by the AARC (Aomori Aquacultural Research Centre). Each buoy measured different parameters, but most measured the sea temperature at a depth of 1, 15, 30, and 45 metres. The Dai-Ni-Misago usually aimed to be at one of the two more instrumented buoys (number 4 or 6) at the time of a satellite overpass. Figure 8 shows a picture of the number 4 buoy.

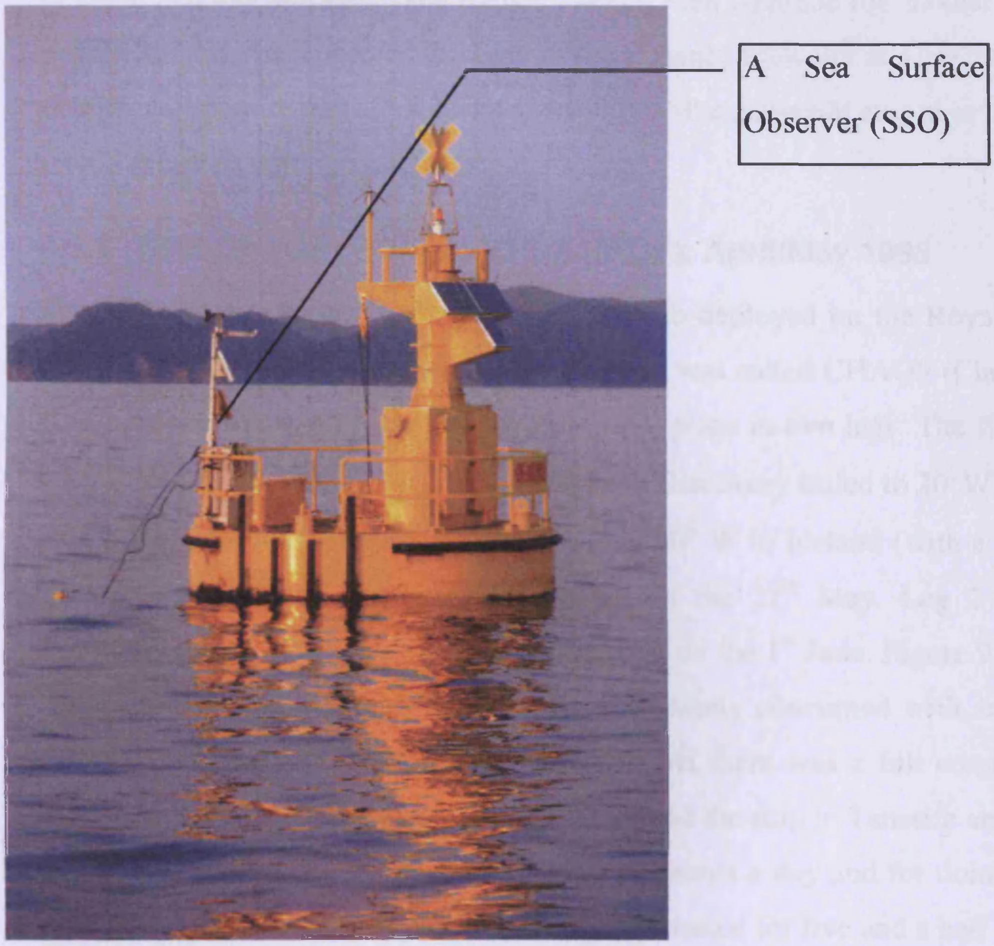

Figure 8: A photograph of the number 4 buoy with an SSO attached (on the left-hand side in the picture).

During the campaign, the number 4 and 6 buoys were each fitted with a Sea Surface Observer (SSO). The SSO was designed by the University of Iwate and developed by the National Space Development Agency (NASDA). It measures the fine sea temperature profile to two metres depth (0, 30cm, 1m & 2m), the air temperature, relative humidity, solar radiation, wind speed, and wind direction.

The team operated from a dock house in Aomori and the Dai-Ni-Misago would typically leave base a few hours before a satellite overpass (ERS or NOAA). The vessel would head to the region of either the number 4 or 6 buoys depending on weather conditions. The number 6 buoy was preferred as it was in more open waters so tended to have less thermal structure and pollution. Typically an hour before each overpass, a validation transect was started where the Dai-Ni-Misago would travel at a speed of roughly one knot towards the respective AARC buoy, aiming to be at the buoy for the overpass. The direction of the transect was chosen to reduce the effects of swell and any sun glint. The transect would then continue for another hour after overpass. Data was collected throughout the transect, typically at 1 Hz. If there was another overpass within a few hours the Dai-Ni-Misago would stay at sea. If not she would return to base.

4.3.3 RRS Discovery Cruise 233 (CHAOS), April/May 1998

The SISTeR radiometer (see chapter 5) was also deployed on the Royal Research Ship (RRS) Discovery on cruise 233. The cruise was called CHAOS (Chemical and Hydrographic Atlantic Ocean Survey) and took place in two legs. The first leg left from Tenerife on the 23rd April 1998. The RRS Discovery sailed to 20°W, 20°N and then followed a long meridional section along 20° W to Iceland (with a dog-leg to the coast of Ireland) arriving at Reykjavik on the 21st May. Leg 2 was from Reykjavik on the 22nd May to the Clyde arriving on the 1st June. Figure 9 shows the cruise track of the campaign. The cruise was mainly concerned with sources and sinks of halocarbons (Smythe-Wright, 1998), and there was a full compliment of meteorological data being taken. The author joined the ship in Tenerife and was part of the team responsible for oxygen chemistry 8 hours a day and for doing work on the SISTeR radiometer 4 hours a day. The cruise lasted for five and a half weeks.

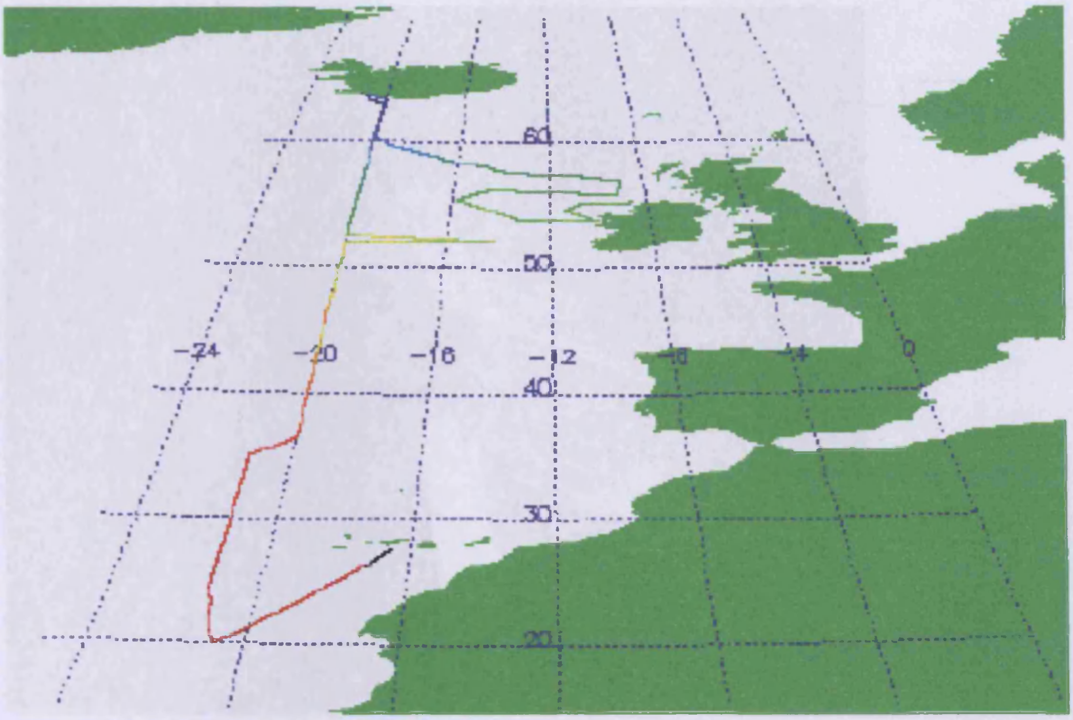

Figure 9: A map showing the cruise track of the RRS Discovery during the CHAOS'98 cruise. The colour of the cruise track gives a rough indication of the SST with red being warm and blue cold.

Two suitable mounting points were chosen for the SISTeR radiometer on the RRS Discovery. Mounting plates were designed for each point and were constructed by the Physics Department workshops at the University of Leicester. The first mounting point was up the foremast of the RRS discovery on the port side (see Figure 10), the second on the bow (see Figure 11). The mounts and cabling for both points were installed and SISTeR tested '*in situ*' before sailing. It was decided in Tenerife, after discussions with the captain, that as access to the foremast in bad weather (when SISTeR would need to be covered) was limited for safety reasons, that the bow was a preferable mounting point. The disadvantage with the bow was that sea spray was more likely to reach SISTeR, resulting in it having to be covered more often. The main advantage was that if the weather turned severe, or it started to rain, then at least on the bow there was access to the instrument and it could be covered, or removed, as necessary.

Figure 10: A photograph of the foremast of the RRS Discovery with the SISTeR instrument mounted on the port side.

Figure 11: A photograph of the bow of the RRS Discovery with the SISTeR instrument mounted on the bow looking 45° to starboard.

SISTeR was mounted so that it was looking at an angle of 45° to starboard. The radiometer was programmed to look at the sea at an angle of 30° from nadir and at three sky angles of 120°, 150° (the complimentary angle) and 170° from nadir. The radiometer was left running continuously during the cruise except during rain, high swell or high winds when the radiometer was covered. During severe weather, the radiometer was removed from the bow and taken inside.

R.W. Pascal and S.A. Josey from the Southampton Oceanographic Centre (SOC) collected the meteorological and bulk SST data. The bulk SST was measured using a so-called 'soap on a rope' or soap for short. This is a thermistor attached to an armoured cable that is weighted so that it skims along just below the sea surface as the ship is moving. The soap was deployed on a long pole from the port side of the bow. Due to the nature of the instrument, it was impossible to deploy it so that it was in completely clean water i.e. out of the bow wave. It was possible, however, to deploy the soap so that it was only affected by the first, small bow wave. This meant it was measuring the temperature of roughly the top 10-20 cm of water. When the ship was on station and so stationary, the soap would sink to a depth of roughly five metres. Therefore, only data from when the ship was moving were used. The meteorological and soap data were measured every 5 seconds, then averaged and logged at one-minute intervals. The wind speed was measured using two sonic anemometers mounted up the fore mast at a height of 13 metres above the sea. The wind speed was corrected for the ship's speed using data from the ship's navigation system. It was then necessary to correct the wind speed to a standard 10-metre height for comparison with other data sets. This was done following Smith 1988. The RRS Discovery also had its own meteorological station but this was less well calibrated than R.W. Pascal's and S.A. Josey's data so was not used. The vessel also had a thermosalinograph (TSG) with a platinum resistance thermometer (PRT) at the water intake at a depth of 5m. Unfortunately, it was noticed that this temperature would jump spuriously and settle back to the correct temperature over a period of hours. The cause of this jump could not be found so these data could not be used.

Although it was not possible to obtain satellite validation points due to poor weather, this was the first deployment of SISTeR on one of NERC's research vessels and provided useful data on skin-bulk temperature differences.

5 The Scanning Infrared Sea-surface Temperature Radiometer (SISTeR)

5.1 Introduction

This chapter describes the Scanning Infrared Sea-surface Temperature Radiometer (SISTeR) that was used to collect the radiometric data presented in this thesis. The SISTeR instrument was designed and built by T.J. Nightingale at Rutherford-Appleton Laboratory (R.A.L.) near Didcot, Oxfordshire. It is a self-calibrating infrared radiometer, designed for the validation of satellite derived sea surface temperatures - specifically the Along Track Scanning Radiometers (ATSR 1&2) flown on the ESA Remote Sensing Satellites (ERS-1&2). There is currently one SISTeR radiometer (Alice) which was used to collect the data in this thesis. A second instrument (Beth) is currently nearing completion. A detailed description of the radiometer is given in Nightingale (2000).

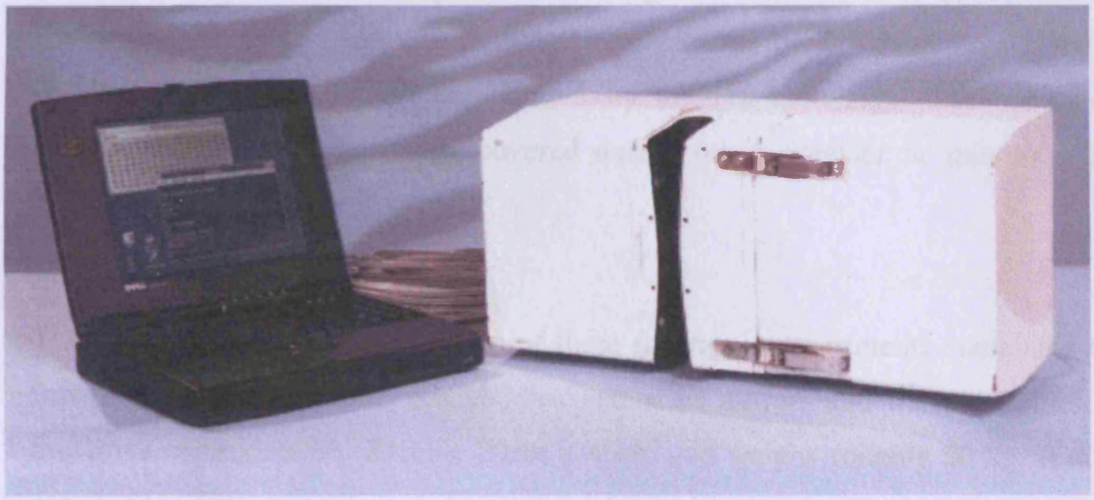

Figure 12: A photograph of SISTeR and its PC-based ground station. (Source T. J. Nightingale)

This chapter gives a brief description of the instrument and presents the results of external calibrations performed on the instrument from its first field deployment in 1996 through to 1998. The data from the MUBEX'96 and '97 campaigns were collected by the members of the MUBEX team (mainly the author, T.J. Nightingale, I.M. Parkes and S. Tamba) and the data from the CHAOS'98 cruise were collected by the author. These were the first deployments and assessments of the radiometer's accuracy and they show how the accuracy of SISTeR improved as the instrument was developed using feedback from the results present here.

5.2 Requirements

In order to validate satellite sea surface temperatures and to study local surface phenomena (such as the 'skin effect') in the field, a radiometer was needed that:

1. had a high radiometric accuracy
2. had low power consumption
3. had good sea worthiness
4. was easy to deploy
5. was easy to operate
6. could be deployed and maintain its calibration for long periods of time (2-3 months)

The first requirement is clearly the most important for satellite validation and the study of local surface phenomena. It can be seen below that the SISTeR instrument did not meet most of these requirements during early deployments. Feedback from the initial campaigns, and the resulting improvements by T.J. Nightingale, meant that the instrument m*et al*l but point 3 by the last campaign. The instrument currently needs to be manually covered during rough weather or rain so is not completely sea worthy.

5.3 Description

The SISTeR instrument is made up of three separate compartments containing the fore-optics, the calibration blackbodies and scan mirror, and the electronics. It measures approximately 20cm x 20cm x 40cm and weighs roughly 20 kg. It does not have a completely sealed optical system, as it would be impossible to compensate for the build-up of contamination on the front-most part of the optical chain in such a system. This means that the radiometer needs to be externally sealed during rain or rough weather and so cannot be used during these times. It also means that the instrument needs to be constantly manned. The SISTeR instrument has been carefully designed to minimise the contamination caused by sudden rain or freak waves. The front-most part of the SISTeR instrument's optical chain is the scan mirror (see Figure 13). In the harsh marine environment, the scan mirror becomes degraded by sea spray and dirt and needs to be cleaned or replaced after long campaigns. However, the effect of this degradation on the absolute accuracy of the derived temperatures was shown to be minimal using data taken during the CHAOS'98 cruise (see section 5.4.3).

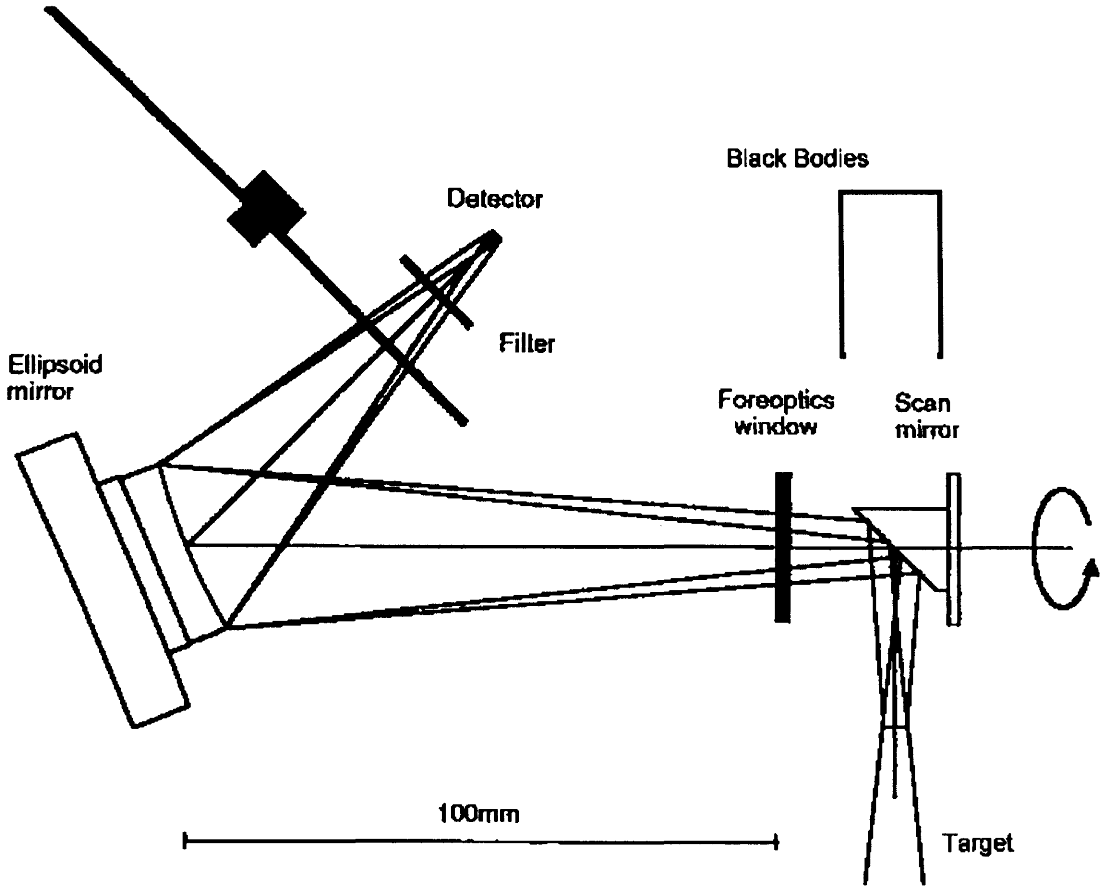

Figure 13: A diagram of the optical chain of SISTeR showing the relative positions of the detector, filters, mirrors and blackbodies. (Source T.J. Nightingale, 2000)

Filters have been built for the radiometer matching the ATSR-2 thermal infrared channels. There was only one channel available, centred on 10.8μm (see Figure 14), during the period of this thesis, so only data from this channel are presented in this document. The instrument's detector is a 2mm diameter DLATGS (Deuterated L-Alanine Tri-Glycine Sulphate) 99 series detector (P5305) that was designed for Fourier transform spectrometers, and built by GEC Marconi. The detector itself has a zinc selenide (ZnSe) window that cuts off below 0.6 μm and above 23 μm. The instrument has a field of view of 12.9°.

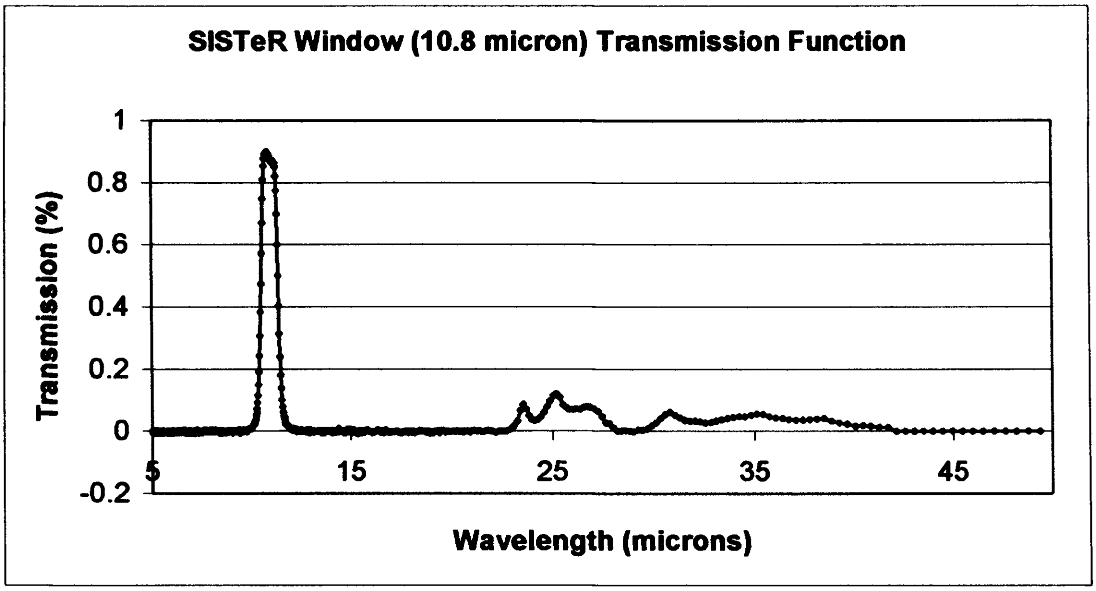

Figure 14: A graph showing the window function of the 10.8 μm channel on the SISTeR radiometer. The detector itself cuts off above 23 μm and below 0.6 μm. (Data provided by T.J. Nightingale)

A further ZnSe window at the entrance to the fore-optics compartment has an anti-reflection coatings on both faces which cut off at 3μm and 15μm. The SISTeR instrument has a movable scan mirror that can be programmed to point in any direction in a vertical plane. It can look at an external target over a forward semicircle from nadir to zenith. This is to enable it to measure both up-welling and down-welling radiation in order to do a sky correction (see Appendix 2). The rear semicircle of the scan mirror's range looks inside the instrument where two internal blackbodies are located. One blackbody is heated to approximately ten degrees above ambient temperature whilst the other floats at the instrument's ambient temperature.

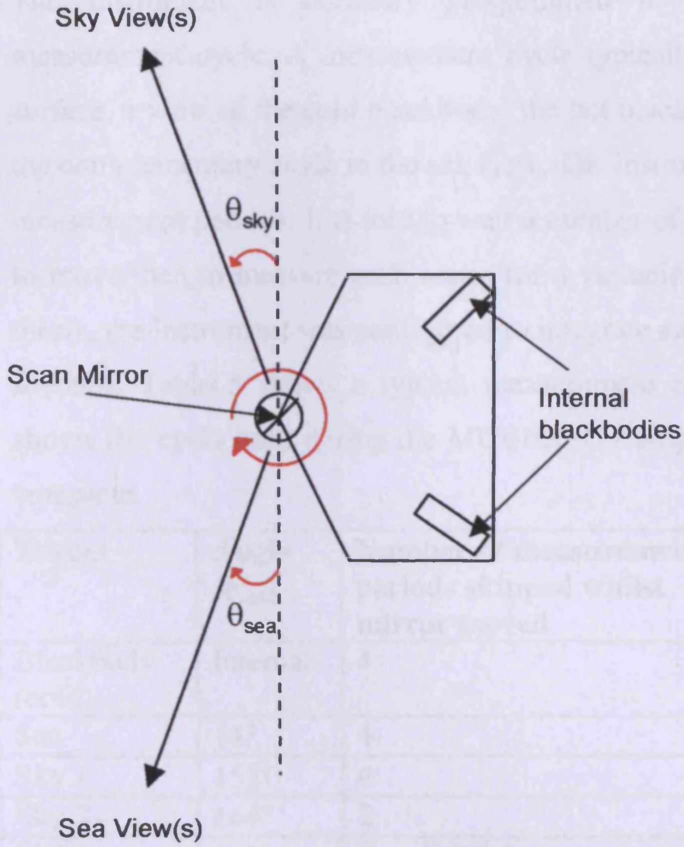

Figure 15: A schematic cross-section of the SISTeR instrument showing how its scan mechanism works. The scan mirror can be programmed so that the instrument views any angle (Θ_{sea}) from nadir to zenith or its internal blackbodies.

Figure 16: A photograph showing SISTeR opened so that the middle compartment containing the two blackbodies is visible. The blackbodies are the two light grey tubes. (Source T.J. Nightingale)

The instrument is normally programmed to view the blackbodies every measurement cycle. A measurement cycle typically consists of a view to the sea surface, a view of the cold blackbody, the hot black body, and finally a sky view at the complementary angle to the sea view. The instrument is programmed in terms of measurement periods. It is told to wait a number of periods to allow the scan mirror to move then to measure each scene for a variable number of periods. During this thesis, the instrument was configured to integrate each measurement period over 0.8 seconds. Table 5 shows a typical measurement cycle used during this thesis. It shows the cycle used during the MUBEX'97 campaign that took 108.8 seconds to complete.

Target	**Angle (θ_{sea})**	**Number of measurement periods skipped whilst mirror moved**	**Number of measurement periods of target**
Blackbody (cold)	Internal	4	8
Sea	14°	4	32
Sky 1	152°	4	4
Sky 2	166°	2	4
Sky 3	180°	2	4
Blackbody (hot)	Internal	4	8
Sea	14°	4	32
Sky 1	152°	4	4
Sky 2	166°	2	4
Sky 3	180°	2	4

Table 5: A table showing a typical measurement cycle of the SISTeR radiometer. This cycle is from the MUBEX'97 campaign and takes a total of 108.8 seconds to complete. Note: Each measurement period takes 0.8 seconds.

The instrument temperature changes minimally between measurement cycles (typically 1 minute) so this approach is valid. This approach is also valid for slow but significant temperature changes between calibration cycles as the interpolated calibration will change (to first order) in the same way as any actual change in instrument calibration. The SISTeR instrument measures radiance, not temperature. In order to generate a target 'brightness temperature' some calculations are needed. The temperature of the two blackbodies is accurately measured with four-wire rhodium-iron thermometers embedded in the base of each blackbody. The radiance of each blackbody can then be calculated from the convolution of the filter response with the Planck function for the given blackbody temperature. A simple linear fit is then applied to these radiances in terms of the signal counts recorded during views to each blackbody. It is then possible to compare the signal counts from external targets to the signal counts from each blackbody and, knowing the radiance from each blackbody, interpolate to get each target's radiance. All emissivity corrections are calculated on radiances before finally converting to temperatures with the inverse of the temperature-to-radiance function. In reality, because the 'cool' blackbody is not actively cooled (active cooling greatly increases the complexity of the engineering and electronics required) it tends to be slightly above the sea surface temperature. This means the instrument actually extrapolates the temperature (see Figure 17) rather than interpolates. The detector was designed to be very linear so errors induced by extrapolating are kept to a minimum.

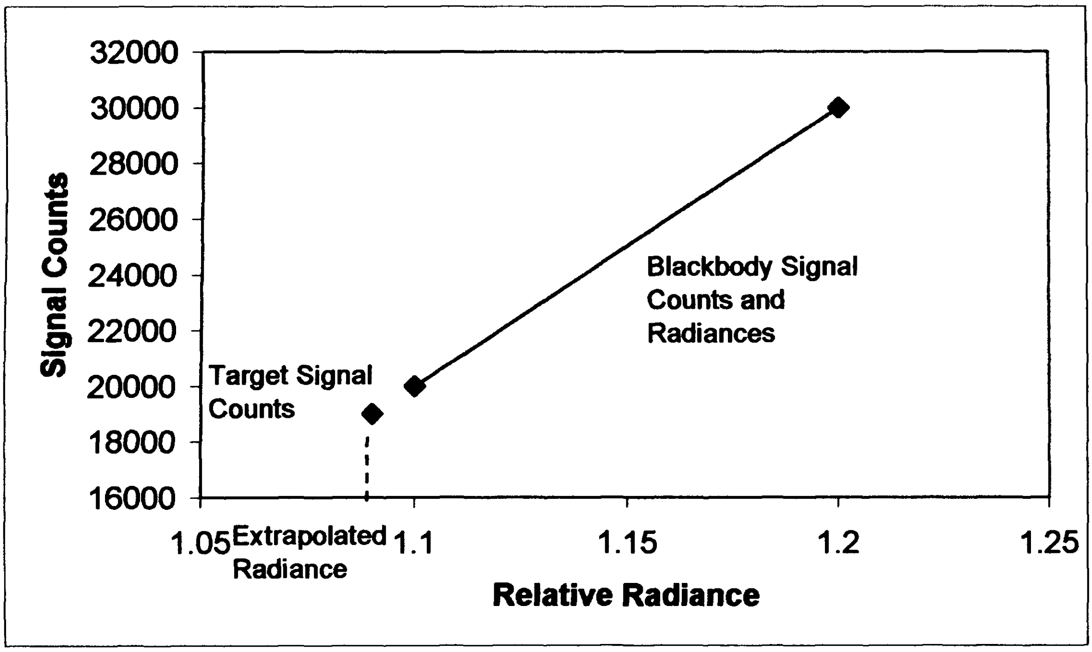

Figure 17: A diagram showing how the SISTeR radiometer extrapolates a target radiance from its internal blackbody radiances.

The instrument contains a small PC that can be interrogated or controlled with a simple C program. Communication with the PC based laptop ground station is via a fibre optic or RS422 link to keep induced noise to a minimum. All data, including all instrument characteristics, are sent to the ground station and recorded. It is then possible, from these data, to calculate a radiometric skin sea surface temperature (see Appendix 2). The instrument was designed to have an accuracy of better than

0.1 K and a noise-equivalent temperature of better than 0.03 K for a one second sample (T.J. Nightingale – personal communication, 1996).

5.4 Accuracy

During the MUBEX'96, 97 and CHAOS'98 campaigns, the SISTeR radiometer was regularly calibrated against an external CASOTS (Combined Action for the Study of the Ocean Thermal Skin) blackbody. The CASOTS project was an EU programme, coordinated by the University of Southampton, with the aim of bringing together the various research groups studying the ocean's thermal skin. The CASOTS blackbody was designed specifically as a portable standard for the calibration of radiometers in the field (Donlon et. al 1999a). The cavity of the blackbody is immersed in a water-bath and the water vigorously stirred with a strong pump. The emissivity of the cavity, for a spot radius less than 30mm, is > 0.999 (Donlon et. al 1999a). Two high accuracy thermometers placed in the water bath measure the temperature of the blackbody. For the MUBEX campaigns, the blackbody temperature was measured with piezoelectric quartz thermometers and during the CHAOS cruise, high accuracy platinum resistance thermometers, calibrated to NAMAS standards, were used. Both sets of thermometers are quoted as being accurate to ±0.02 K. A low power water heater was used to gradually increase the temperature of the water bath giving a continuous range of calibration points.

5.4.1 MUBEX'96

The MUBEX'96 campaign was the first deployment of the SISTeR radiometer and it suffered from a cyclic noise that was traced to power supply noise in the detector pre-amplifier and later corrected. In order to use these data it was necessary to devise a correction scheme. This noise was of the order 1 K and was composed of two parts. The largest part was a cyclic interference with a regular period (see Figure 18). By Fast Fourier Transforming (FFT) the data and removing the corresponding peak in frequency space, it was possible to reduce this noise dramatically (see Figure 19). The increasing magnitude of 'oscillations' at either extreme of the FFT-smoothed fit are edge effects caused by the step in signal level between the end and beginning of the measurements and any discontinuity in the phase of the interference signal.

The second component of the noise was white noise of the order ±0.5 K. A six-minute running mean of the data could therefore reduce this (see Figure 20). The data processing method was tested by using it to process data taken during the external calibrations of SISTeR and comparing the SISTeR and blackbody temperatures.

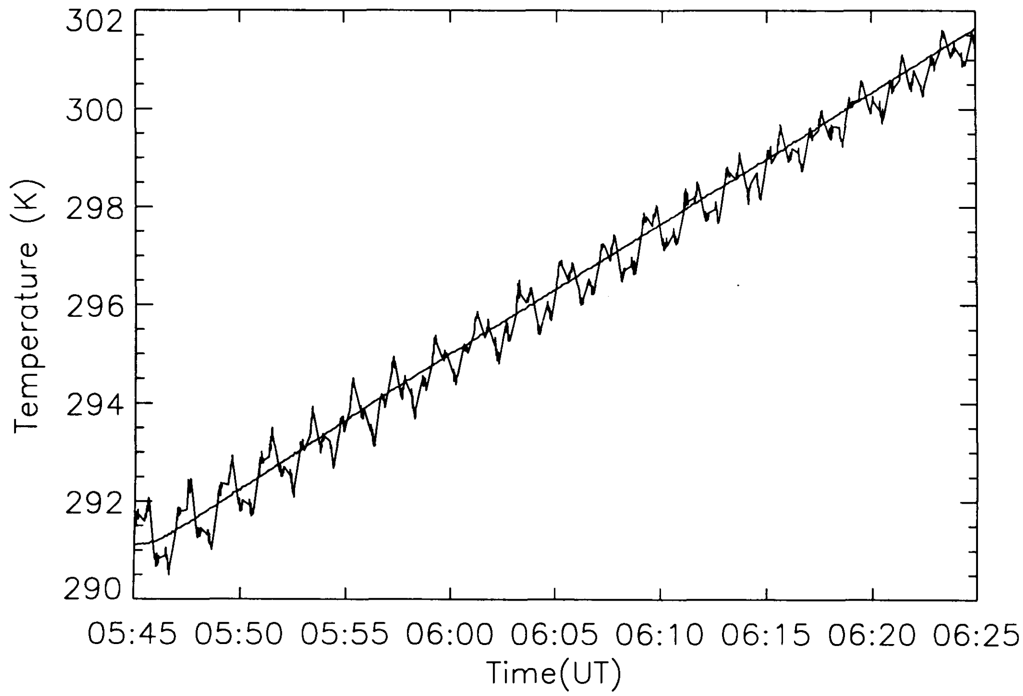

Figure 18: A graph showing the uncorrected radiometric SISTeR temperature and the blackbody temperature (straight line) as a function of time.

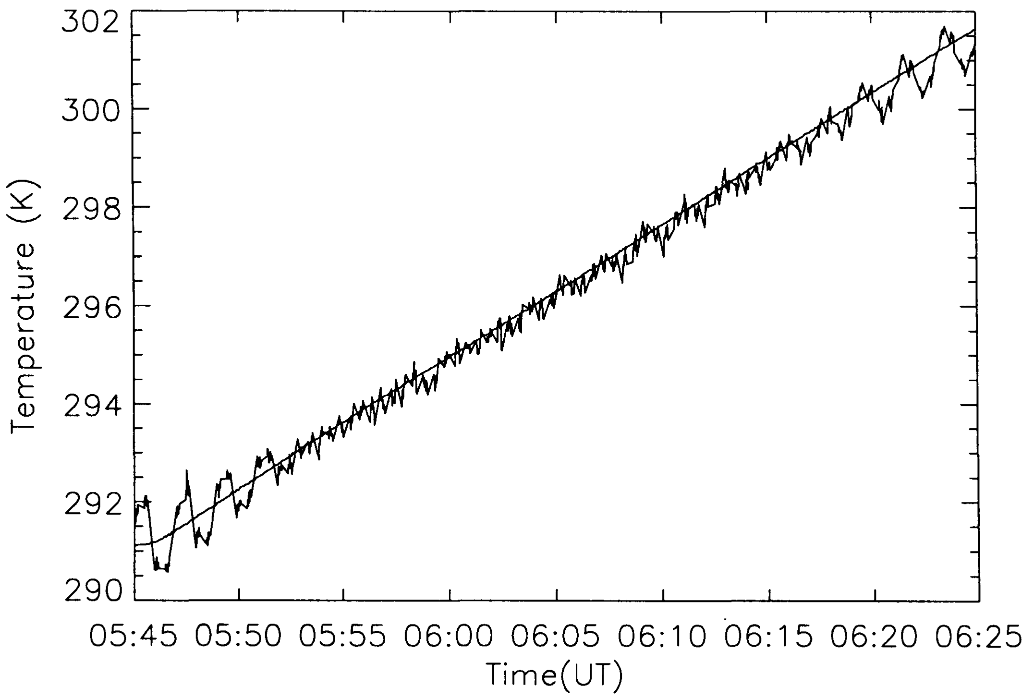

Figure 19: A graph showing the radiometric SISTeR temperature, with the periodic noise removed after the Fast Fourier Transform, and with the random component remaining. The blackbody temperature is the straight line. Note the cyclic signal at the beginning and end of the data are an artefact of the FFT processing used to remove the cyclic noise.

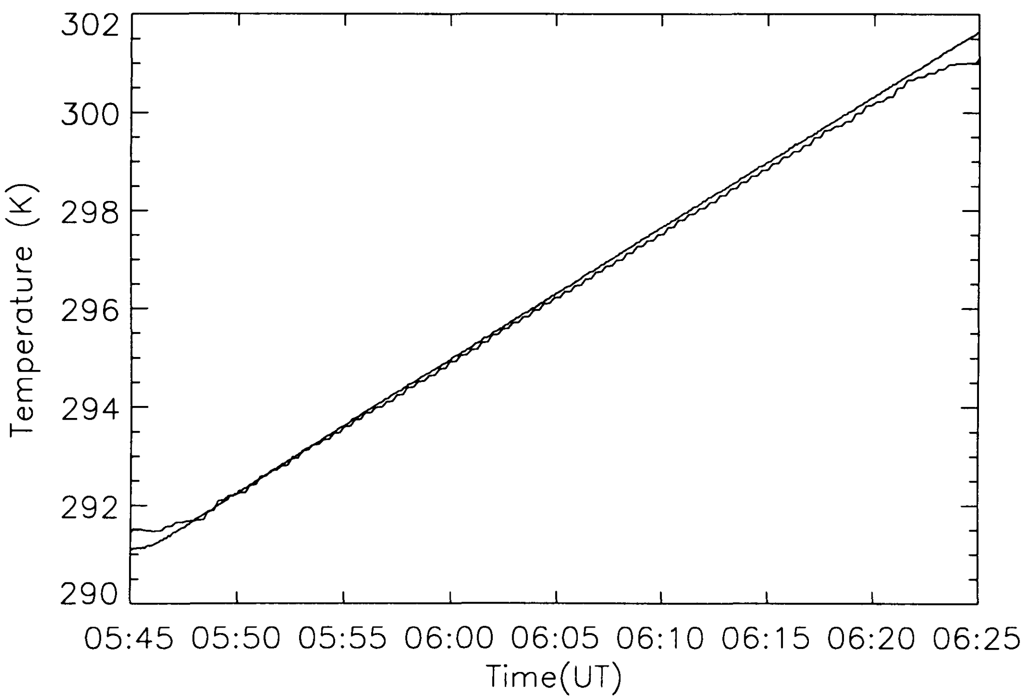

Figure 20: A graph showing the fully corrected radiometric SISTeR temperature (with both the cyclic and periodic noise removed) and the blackbody temperature (straight line) as a function of time.

The corrected data was found to have an absolute accuracy of better than ±0.1 K, which is accurate enough for satellite validation.

5.4.2 MUBEX'97

T.J. Nightingale corrected the problem with the power supply noise in time for the MUBEX'97 campaign. Unfortunately, during an external calibration of SISTeR it was noticed that the calibration of the thermometry on one of the internal blackbodies had changed. Figure 21 shows the effect this incorrect calibration had on the measured temperature. This incorrect calibration led to a bias that ranged from approximately -0.8 to -0.6 K depending on the temperature of the source (See Figure 22).

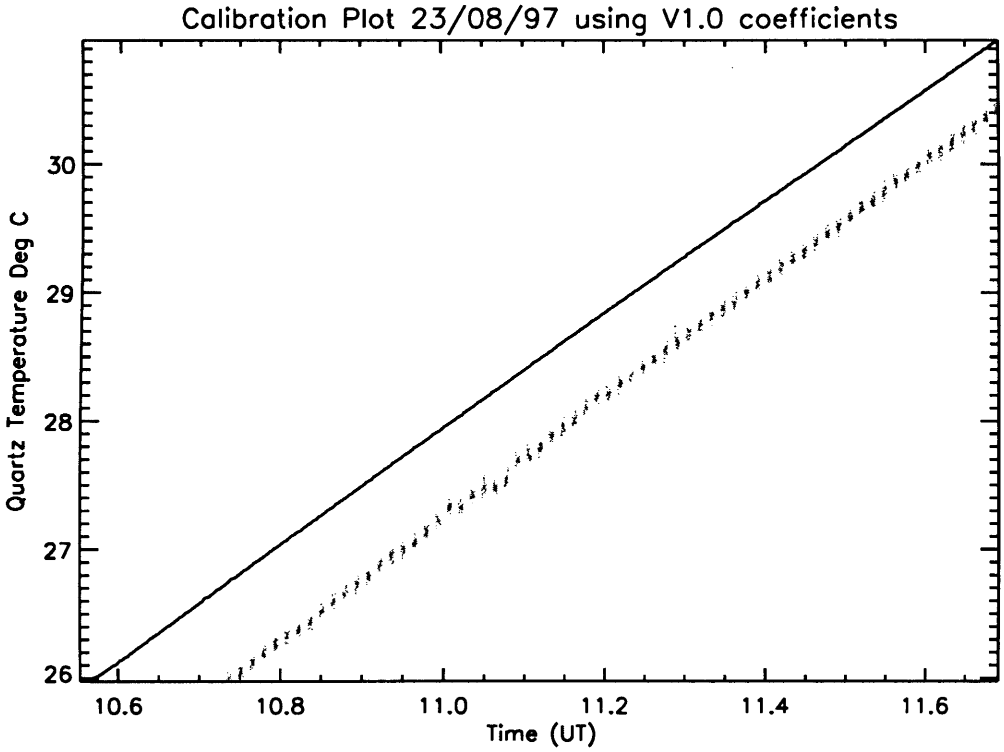

Figure 21: Data from an external calibration run showing the effect of the incorrect internal blackbody calibration. The SISTeR data are the grey dots and the CASOTS blackbody data the black line.

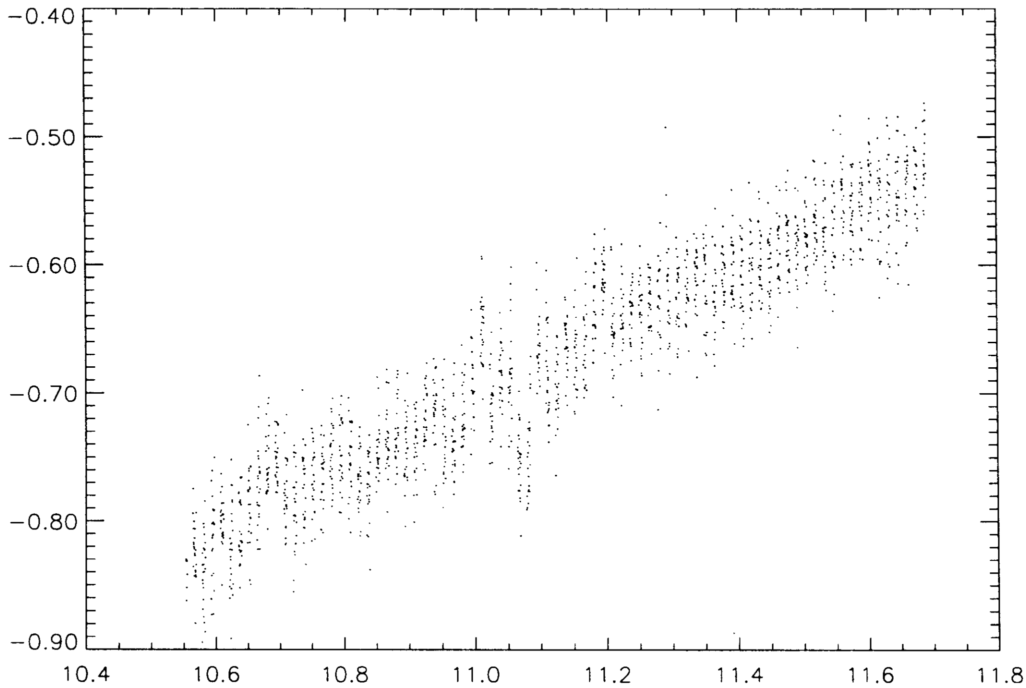

Figure 22: Graph showing the difference between the SISTeR data (using the original internal blackbody calibration) and the CASOTS blackbody temperature as a function of time as the CASOTS blackbody slowly warmed.

This raised the possibility that the calibration had changed during the MUBEX'97 campaign either suddenly or slowly over time and would mean the data were suspect. After the campaign, the blackbodies were recalibrated and the new calibration function tested by applying it to the data taken during calibration runs and checking the difference. It was later found that the instrument had been exposed to an incorrect environment before the MUBEX'97 campaign, and this had probably led to a step function change in the calibration.

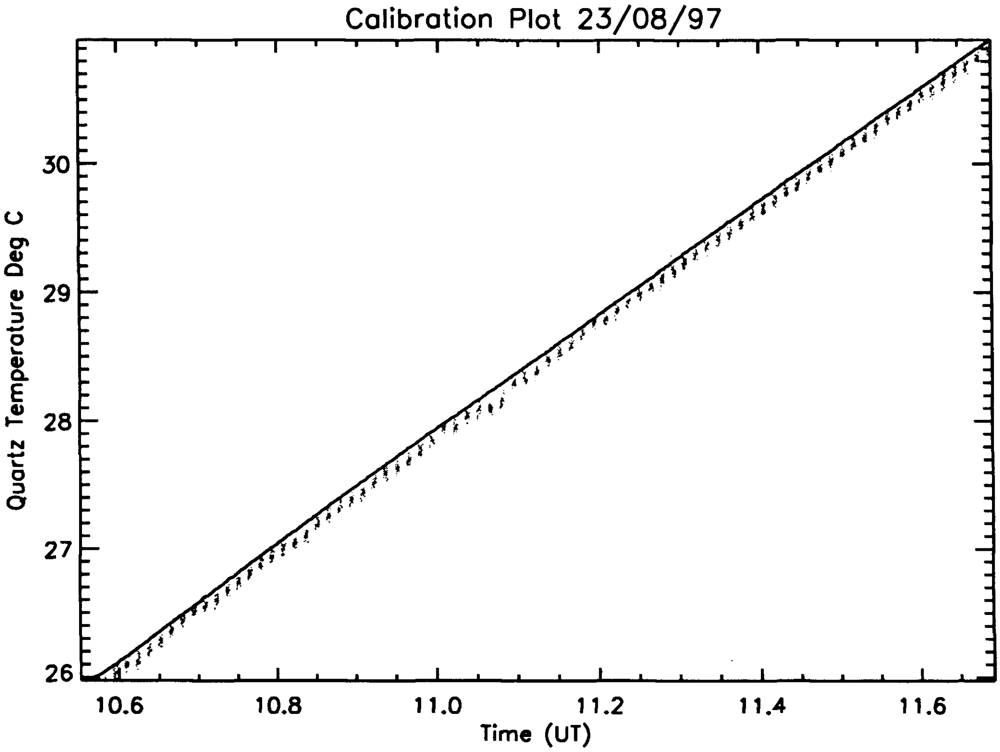

Figure 23: Graph showing the same data as Figure 21 with the new blackbody calibration coefficients. The SISTeR data are the grey dots and the CASOTS blackbody data the black line.

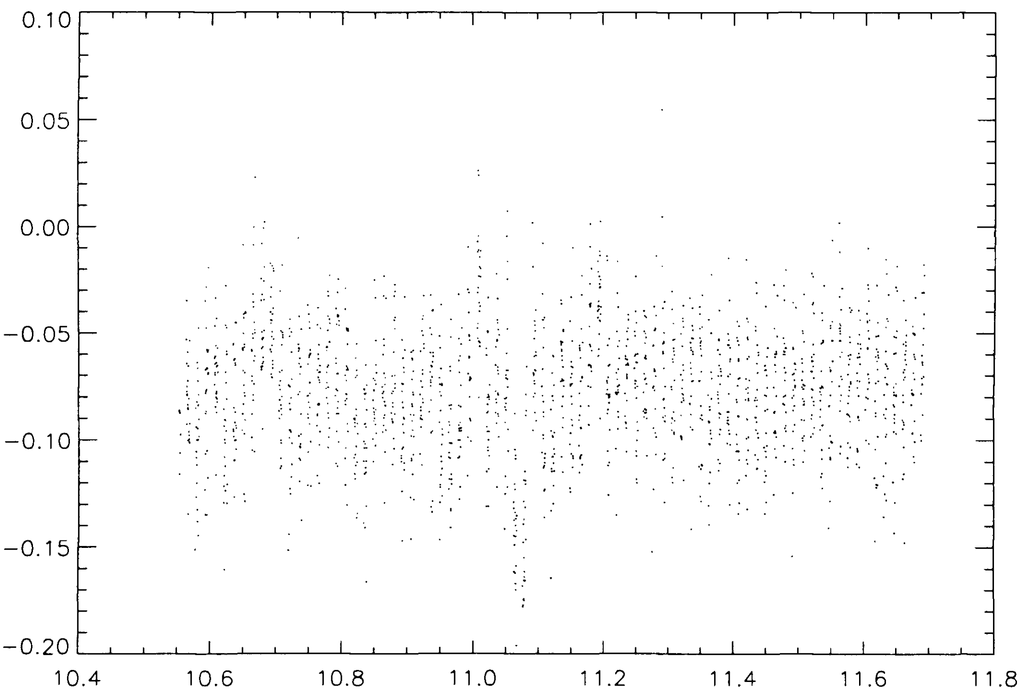

Figure 24: Graph showing the difference between the SISTeR data (using the revised internal blackbody calibration) and the CASOTS blackbody temperature as a function of time as the CASOTS blackbody warmed.

Figure 23 and Figure 24 show the results of applying the revised calibration coefficients to the internal blackbody. It can be seen that the offset between the radiometric temperature and the blackbody temperature has been reduced and the offset is now no longer temperature dependant.

Date of External Calibration	Mean offset (K)	SD of offset (K)
26/07/97	-0.092	0.044
12/08/97	-0.081	0.033
23/08/97	-0.077	0.029

Table 6: Table showing the mean offset and standard deviation of the offset for the three external calibrations of the SISTeR instrument during the MUBEX'97 campaign. The offset is defined as SISTeR-CASOTS blackbody temperature.

Table 6 shows the data from the three calibration runs done during the campaign. It can be seen that the revised calibration was successful in reducing the offset to a mean difference of approximately -0.08 K. The revised calibration was therefore applied to all SISTeR data taken during MUBEX'97. It was decided not to apply an offset to the SISTeR data as the mean offset was close to the uncertainty of the blackbody thermometry.

5.4.3 CHAOS'98

During the CHAOS'98 campaign, the SISTeR radiometer was again calibrated externally using the CASOTS blackbody but this time the new NAMAS (National Accreditation of Measurement and Sampling) certified thermometry was used. The SISTeR instrument was calibrated three times during the campaign, at the beginning, middle and end of the campaign.

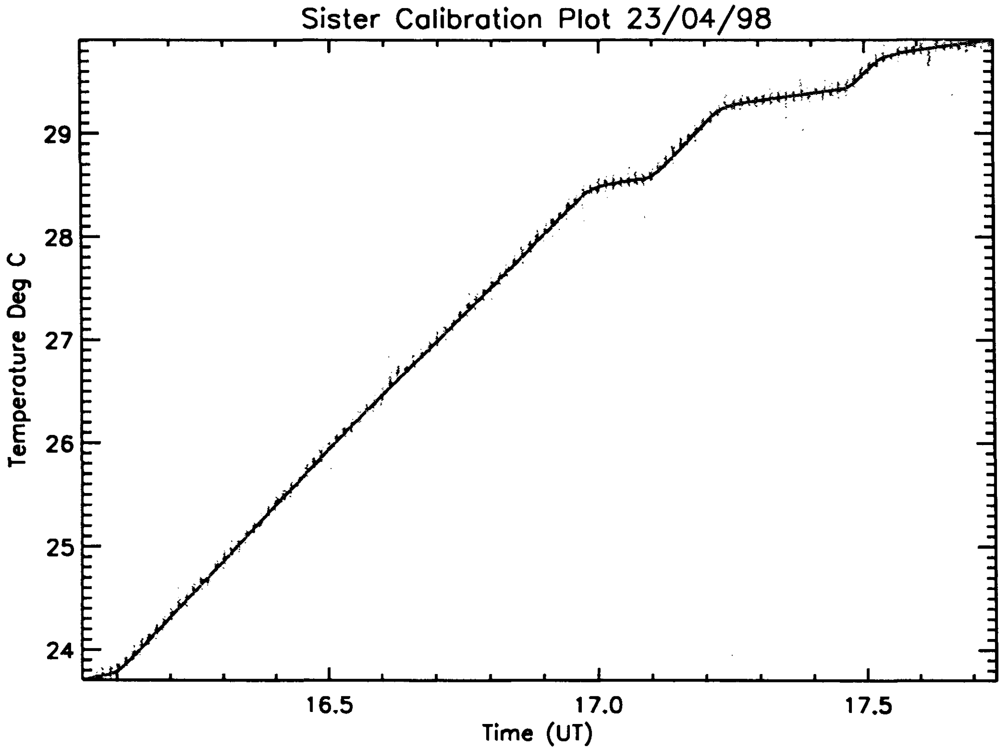

Figure 25: Graph showing data from the external calibration of the SISTeR radiometer at the beginning of the CHAOS'98 cruise. The SISTeR data are the grey dots and the CASOTS blackbody data the black line.

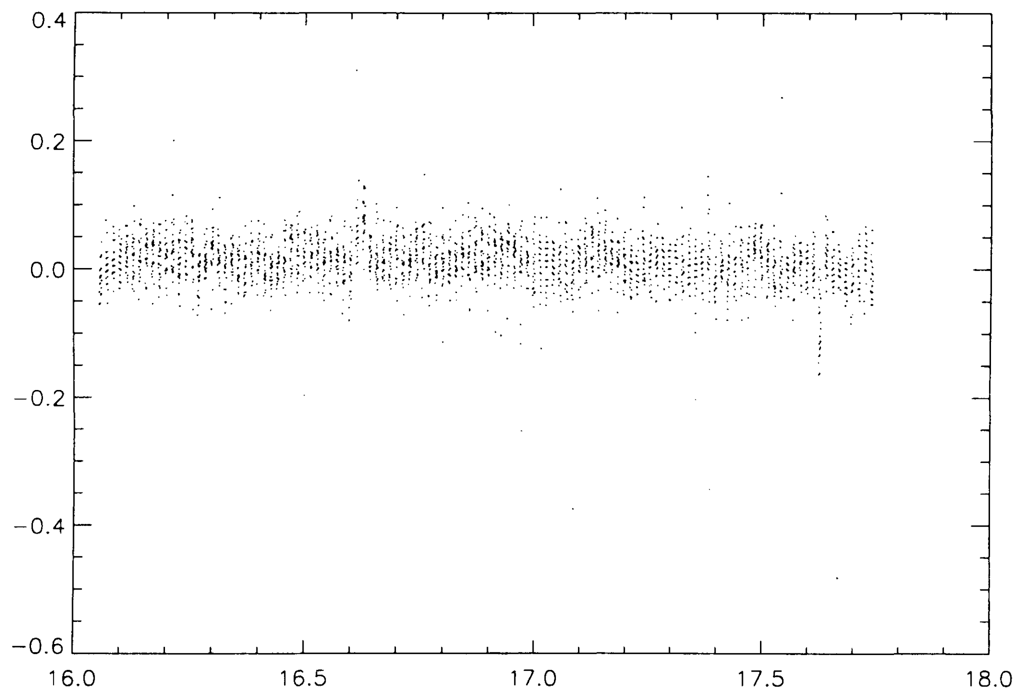

Figure 26: Graph showing the difference between the SISTeR temperature and the CASOTS blackbody temperature measured with the NAMAS certified PRT's.

The SISTeR instrument performed satisfactorily and met its accuracy specification during the CHAOS'98 campaign. Figure 25 shows the results of a typical external calibration run done at the start of the campaign. It shows that the SISTeR instrument followed the warming blackbody temperature very closely. Figure 26 shows the difference between the SISTeR radiometric temperature and the blackbody temperature. It shows a negligible offset and an rms noise of about 0.04 K.

Date of External Calibration	Mean Offset (K)	SD of Offset (K)
23/04/98	0.011	0.037
11/05/98	0.021	0.046
12/06/98	0.004	0.050

Table 7: Table showing the mean offset and standard deviation of the offset for the three external calibrations of the SISTeR instrument during the CHAOS'98 cruise. The offset is defined as SISTeR-CASOTS blackbody temperature.

Table 7 shows the results of all three external calibration runs. It shows that the SISTeR radiometer agreed very closely with the CASOTS blackbody throughout the cruise. It is interesting to note that the mean offset does not change significantly during the cruise but that the standard deviation does increase. This is to be expected, as the level of noise should increase as the scan mirror becomes contaminated with sea spray and dirt during the cruise. This shows the advantage of having a non-sealed radiometer system in that, despite the fact that the front-most part of the optical chain has been obviously contaminated, the system still functions accurately. It should also be pointed out that the mirror used during the CHAOS'98 cruise had been used on a previous campaign and SISTeR with a new mirror would have a lower rms noise of about 0.03 K (as can be seen from the MUBEX'97 data).

5.5 Summary

During the early deployments of SISTeR, it suffered from teething trouble that affected its accuracy and it was unable to meet its design requirements. However, during the three years of data collection for this thesis it developed into a highly accurate radiometer. The data from the CHAOS'98 cruise show that SISTeR now has an absolute accuracy of better that 0.025 K and an rms error (with a clean scan mirror) of less than 0.03 K. These are within the accuracy requirements set by T.J.

Nightingale. In order to obtain sufficient satellite validation points for a comprehensive programme, many *in situ* radiometers are needed (see chapter 6). Unfortunately, the high cost (about £70,000 each) of each SISTeR instrument limits the number that can be built and deployed. In addition, the fact that SISTeR currently needs to be constantly manned, in case of rain or rough weather, also limits its use in the field. Therefore, it cannot be regarded as completely sea worthy in its current design.

C.J. Donlon, with T.J. Nightingale and others, is currently designing and building a cheap, autonomous, self-sealing radiometer that can be deployed on ships of opportunity (oil tankers, freighters etc.) without the need of a scientist to operate them. It is intended that the SISTeR radiometer would be used to make spot-check measurements on the accuracy of such instruments, before and while they are at sea, whilst still being used for high accuracy validation work.

6 Validation Results

6.1 Introduction

This chapter discusses the validation of the ATSR instruments using *in situ* data collected during this thesis. All the validation points come from the later two MUBEX campaigns as no clear overpasses were obtained during the CHAOS'98 cruise. The first part of this chapter discusses early validation results that are published in Parkes, Sheasby *et al.* 2000. The rest of the chapter deals with data that was processed just before writing this chapter using the most up to date version of the SADIST-2 processing suite (V320). Firstly, a direct comparison is made between the standard product obtained from RAL and the *in situ* data without any attempt to correct for errors in geolocation. The SSTs calculated using coefficients provided by C.J. Merchant are also generated for comparison and the method used to generate these SSTs is described in this section. Next, each validation point is looked at in detail and new SSTs generated after correcting for geolocation errors by lining each BT image up with the outline of the bay. The overall accuracy of ATSR is then discussed.

6.2 Previous Work

Previous work on the validation of ATSR-1 is scarce and the only published data on the validation of ATSR-2 (with *in situ* radiometric data) are in Parkes *et al.* 2000. Previous validation work can be broadly split into two categories. The first category, bulk match-ups, attempts to validate ATSR with *in situ* bulk temperatures, usually from buoy networks (e.g. Mutlow *et al.* 1994, Harris *et al.* 1995, Harris and Saunders 1996). These are generally over much larger spatial and temporal scales than the second category, skin match-ups, but do not compare like with like due to the skin effect. Efforts have been made to attempt to account for the skin effect using models of the physical processes occurring (e.g. Merchant and Harris 1999, Murray *et al.* 2000). Skin match-ups, are more appropriate as they compare *in situ* skin temperatures with the satellite skin temperatures (Smith *et al.* 1994, Thomas and Turner 1995, Barton *et al.* 1995, Donlon *et al.* 1998 & 1999b, Parkes *et al.* 2000). Unfortunately, the difficulties and cost of obtaining *in situ* radiometric data mean that currently there are only about 50 such validation points in limited areas of the globe.

ATSR-1 data obtained pre-1998 are processed with various versions of the SADIST-1 processing suite. Authors typically reported a cool bias in ATSR SSTs of varying order (although Barton *et al.* 1995 report a warm bias of 0.2 K in the Southern hemisphere). Authors report (summarised in Merchant *et al.* 1999) that this cool bias was due to two effects. The first was due to the eruption of Mount Pinatubo in the Philippines shortly before the launch of ERS-1. Závody et. al 1995 assumed that the stratosphere could be characterised as aerosol free. Unfortunately the eruption sent large amounts of aerosols into the stratosphere and this leads to a bias of up to ~1.5 K in the first year of operation. The second cause of the bias was due to the inadequate parameterisation of the water vapour absorption continuum in the 10-13μm region. This caused a bias of up to ~0.4 K that would be present in all the data.

After 1998, attempts were made to derive new coefficients that reduced or eliminated these errors (Brown *et al.* 1997, Barton 1992, Merchant *et al.* 1999). The coefficients published in Merchant *et al.* 1999 were used by RAL during 1999 to reprocess the ATSR-1 data using the same data processing suite as ATSR-2 (SADIST-2 V320). Merchant finds a bias of 0.23±0.22 K for the three-channel algorithm and a bias of 0.07±0.27 K for the two-channel algorithm in agreement with the data in this chapter (Merchant and Harris 1999 and Chapter 6.4.1). There is still a recognised problem with the ATSR-1 data due to the gradual increase in the detector temperature with time. Work is underway on an algorithm to account for this warming and new coefficients are expected in the future.

At the time of writing, ATSR-2 data are being processed with an equivalent set of coefficients to that of ATSR-1 data using the SADIST-2 V320 processing suite. However, discrepancies between SSTs calculated using the two and three-channel algorithms have shown an error in the coefficients used to calculate the three-channel algorithm (C.J. Merchant, M.J Murray, personal communication 2000). The ATSR-2 data are currently still processed with these coefficients but updated coefficients have been released (C.J. Merchant, personal communication, 16th March 2000) and have been used along side the original coefficients (where time has permitted) in this thesis. A.R. Birks is currently working to upgrade the radiative transfer model used by RAL. Part of this work has involved trying to reproduce the brightness temperatures that C.J. Merchant used to derive his coefficients. Some discrepancies emerged in the course of his work that were traced to problems with C.J. Merchant's modelling of tropospheric aerosol component. C.J. Merchant states that the numerical effects of correcting his model on dual-view SST retrievals for ATSR-2 are on average -0.015 K (rms 0.02 K) for the 3-channel algorithm and -0.017 K (rms 0.06 K) on average for the 2-channel algorithm (A.R Birks, personal communication 5th June 2000). These problems have a similar effect on ATSR-1 data. This effect is quite small however.

A.R. Birks is currently working to resolve these issues and it is likely that new coefficients will be issued. This chapter uses the most up to date coefficients available (SADIST-2 V320) at the time of writing. It is likely that in the future this work will have to be re-done using any new coefficients published. It is, as far as the author is aware, the first time ATSR-2 data has been validated.

6.3 MUBEX Validation Results – Direct Comparison

6.3.1 Early MUBEX'96 Data (SADIST-1 V600 & SADIST-2 V200)

This section is a summary of the work published in Parkes *et al.* 2000. Initially, after the MUBEX'96 campaign the only ATSR-2 data available were brightness temperature images processed with the SADIST-2 V200 suite and ATSR-1 data processed with the SADIST-1 V600 suite. No GSST product was available. These data were obtained for each overpass of Mutsu Bay and processed by I.M. Parkes to generate SSTs. I.M. Parkes employed an identical method to that being used at that time to generate the GSST product at RAL. The SSTs were generated with nadir only and dual-look algorithms using ASST coefficients provided by A.M. Závody at RAL. For each overpass, SSTs were generated using a three-pixel and eleven-pixel smoothing kernel for the atmospheric correction. An SST for the one ATSR-1 pass was also calculated using a set of image coefficients. These are coefficients appropriate to the 1km product and assume pre-launch estimated NEdT values. In an attempt to account for the spatial variation of SST in the Bay the satellite SST value presented in Table 8 is a nine-pixel mean with each pixel weighted ($1/d^2$) depending on its distance from the boat at overpass. The author's contribution to this paper was to collect, process and analyse the *in situ* data. As mentioned in Chapter 5.4.1 the *in situ* radiometer (SISTeR) suffered from two types of noise during the MUBEX'96 campaign, a cyclic noise of order 1 K and white noise of order 0.5 K. The cyclic noise was filtered by fast Fourier transforming the data, removing the appropriate spikes in frequency space, and transforming back. The white noise was reduced by using a running mean to smooth the data. This method was shown to reduce the error to the order of 0.1 K (See Chapter 5.4.1). The *in situ* radiometric brightness temperatures were corrected for down-welling sky radiation following the method described in Appendix 2 to generate an *in situ* SST. The *in situ* SST data were then averaged three minutes either side of overpass and compared to the satellite SST. Six minutes was taken as a compromise between getting a reasonable spatial average and being close enough to overpass time to have constant meteorological conditions (i.e. avoid the effects of diurnal warming, changing cloud cover, etc.).

Table 8 shows the initial results of the early processing of the ATSR data. These results were submitted to the IJRS and published in Parkes *et al.* 2000.

Date	Time UT	SISTeR SST	SISTeR σ_m	SISTeR-Air T	Cloud flag	ATSR SST (K) Dual-channel algorithm [Three-channel algorithm]		ATSR-SISTeR (K)	
						Nadir	**Dual**	**Nadir**	**Dual**
ATSR-1									
29/7/96	01:28	294.18K	0.02K	-1.92K	Forward	(i) 294.25 (3) 294.24 (11) 294.18	293.97 293.62 293.46	0.10 -0.08 0.02	-0.18 -0.54 -0.70
ATSR-2									
5/08/96	01:40	293.96K	0.02K	-0.21K	Nadir	(3) 294.25 (11) 294.21	294.05 293.96	0.29 0.25	-0.09 0.00
6/08/96	12:28	293.51K	0.02K	0.05K	Nadir and forward	(3) 294.13 (11) 294.13 [(3) 294.10 [(11) 294.13	293.74 293.81 293.90 294.14	0.61 0.61 0.58 0.61	0.22 0.29 0.38] 0.62]

Table 8: Table showing the initial match-ups between satellite and *in situ* SST data. The three different ATSR SSTs are calculated using image coefficients (i), ASST coefficients and a three pixel smoothing (3), and ASST coefficients with an eleven pixel smoothing (11). The values in square brackets were calculated using the three-channel algorithm for the night-time pass on the 6th August, 1996. These data are published in Parkes et. al 2000.

Using the distinctive features of Mutsu Bay's coastline as a guide, the geolocation of each ATSR image was checked by overlaying the land-sea border with each image. An offset was measured by moving the image in the across-track and along-track directions until the image lined up with the bay outline. The error associated with matching the bay's outline with the image is of the order ±1 pixel, due to the nearest neighbour georeferencing of the image. The ATSR-1 image was found to be one pixel (1.1 km) away from the land mask. The ATSR-2 images showed offsets of up to 3.6 km from the land mask particularly in the along-track direction. This larger error is probably due to the ERS-2 platform pointing not being as accurate as the ERS-1 pointing (C.T. Mutlow – personal communication, 1997).

These geolocation errors mean that extreme care must be taken when interpreting SST data especially in areas where thermal gradients exist. Unfortunately, due to the sheltered nature of Mutsu Bay, strong temperature gradients across the bay were often observed. This is further investigated in the next two sections.

The data presented in Table 8 have been corrected for geolocation errors. The initial results showed that the ATSR-2 dual-view SSTs (processed with SADIST V200) were within the instruments design accuracy specifications (Smith et. al, 1994) but these SSTs were not as accurate as those processed with the newer SADIST V320 processing presented in chapters 6.3.2 and 6.5.

This represents the first *in situ* validation results for ATSR-2 and the first ATSR-1/ATSR-2 intercalibration.

The single ATSR-1 dual-view SST was found to measure cool. This is in agreement with previous studies (summarised in Merchant *et al.* 1999) where a significant cool bias was found. Merchant states that this bias is due mainly to two causes of error. The first error is the effect of contamination from stratospheric aerosol from the Mount Pinatubo eruption in 1991 (up to ~ 1.5K). However, by the time these data were taken the stratospheric aerosol had dissipated. The second cause of error arose from the inadequate parameterisation of the water vapour continuum absorption in the 10-13 μm window region. This would lead to errors of the order 0.4 K but these would be present throughout the mission. This is in agreement with the cool bias shown in Table 8. Merchant derived new coefficients (Merchant *et al.*, 1999) that reduced these errors. The ATSR-1 data was later re-processed by RAL using these new coefficients and these data are presented in the next section.

6.3.2 MUBEX'96 and '97 – Direct Comparison with Reprocessed data (SADIST-2 V320)

The SADIST-2 processing suite is from time to time upgraded. The ATSR data of Mutsu Bay had been processed using a variety of SADIST versions depending on when the data were requested/generated. Currently a detailed review of available coefficients is underway with respect to their accuracy and traceability. This review has not yet been completed so this chapter includes all the coefficients available to the author. At the time of writing this thesis, the most up to date version of SADIST-2 was version 320 and all the validation data were reprocessed in February 2000 using this version in order to give an up-to-date and like-for-like comparison. The SADIST-2 manual (Bailey, 1995) and ATSR-1/2 Users Guide (Mutlow *et al.*, 1999) stated that the data were processed using regional coefficients and ten across-track bands for the interpolation of these coefficients (Závody, 1995). However personal communications with various persons (especially A.R. Birks, 2000) stated that this was no longer the case and that 38 across-track bands were now being used. There was some uncertainty as to whether the Merchant global ASST coefficients were now being used to process ATSR-2 as well as ATSR-1 data. In order to check this, and to test the accuracy of different coefficients, the brightness temperature images provided by RAL were processed using a variety of coefficients to generate satellite SSTs. These coefficients were provided by C.J. Merchant (personal communication, 2000 and Merchant *et al.*, 1999). The processing method for converting brightness temperatures to SSTs follows the method described on C.J. Merchant's web site (Merchant, 1999). As stated in section 4.2.2, the ATSR SST is calculated using the following formula to correct for atmospheric effects:

$$SST = a_0 + \sum_{i=1}^{n} a_i T_i$$

Where, SST is the Sea Surface Temperature of a given pixel

a_0 is the offset coefficient

a_i is the coefficient for channel i

i is the channel number

n is the number of channels available

T_i is the brightness temperature of channel i

ATSR has three channels that can be used to calculate an SST – the 3.7μm, the 11μm and the 12μm. During the night all three channels can but used but during the day the 3.7μm channel cannot be used as it detects reflected sunlight. The ATSR instrument also views Earth at two angles – a forward look at 55° and a nadir view straight down at the sub-satellite point. Therefore, there are six brightness temperatures that can be used to calculate a night-time SST (three-channel algorithm) and four to calculate a daytime SST (two-channel algorithm). The 3.7μm channel on the ATSR-1 instrument failed in May 1992 so from this date onwards only a two-channel SST can be generated from ATSR-1 data. The ATSR instrument has a swath width of 512 km. Pixels at the edge of the swath are viewed through a longer atmospheric path than pixels directly beneath the satellite. This means that a different atmospheric correction has to be applied to each pixel. C.J. Merchant provides coefficients for each channel (forward and nadir) and the offset coefficient (forward and nadir) for a sub-satellite pixel and for an edge pixel. The coefficients for pixels between the edge and sub-satellite pixels are interpolated from these two values. C.J Merchant gives sets of coefficients for both the two and three-channel algorithms. The original SADIST-2 processing divided the image into 10 across-track bands and used a set of coefficients for each band (Bailey 1995). The version 320 method uses 38 across track bands (A.R. Birks – personal communication, 2000). The Merchant method does not use bands and interpolates the coefficients for each pixel. It also accounts for the conical scanning mechanism of ATSR. It does this by weighting each pixel coefficient in terms of its path length relative to nadir using a table provided by A.R. Harris. This interpolation method was first applied by Harris and Saunders (1996) who showed that the choice between using the nadir and forward view for the correction makes negligible difference to the retrieval. The SST for a given across-track pixel (d) using the C.J. Merchant method is summarised by the equations below:

$$SST(d) = \left(\frac{l(d) - l(d_c)}{l(d_e) - l(d_c)} \right) \left(a_{0e} + \mathbf{a}_e \cdot \mathbf{T} \right) + \left(\frac{l(d_e) - l(d)}{l(d_e) - l(d_c)} \right) \left(a_{0c} + \mathbf{a}_c \cdot \mathbf{T} \right)$$

Where,

d is the across-track pixel number (0 – 511)

$l(d)$ is the relative atmospheric path length for that pixel number (from A.R. Harris' table)

a_0 is the offset coefficient

a is the **vector** of the coefficients for each brightness temperature

T is the **vector** of the brightness temperature

the subscripts *e* and *c* denote values associated with the edge or centre pixels respectively.

It is important to note that both **a** and **T** are vectors and that **a·T** is a scalar dot product – i.e.

$$\mathbf{a}_e\mathbf{T} = \begin{pmatrix} a_{e11\mu m} & a_{e12\mu m} \end{pmatrix} \begin{pmatrix} T_{11\mu m} \\ T_{12\mu m} \end{pmatrix} = \left(a_{e11\mu m}T_{11\mu m}\right) + \left(a_{e12\mu m}T_{12\mu m}\right)$$

for the daytime two-channel algorithm.

This method is applied to each pixel in the ATSR scene of 512x512 pixels to generate an initial SST image. The SST data generated this way are then smoothed using the SST-11μm BT method described in the ATSR-1/2 User Guide (Bailey, 1995). The method is to generate an SST (using either method described above) and then subtract the 11 μm nadir brightness temperature from this SST. This difference is then smoothed using a 9-pixel box and added back to 11μm brightness temperature to generate the new smoothed SST. The reasoning behind this smoothing is that it reduces atmospheric noise. This is because with no atmosphere the 11 μm nadir view BT would be a good approximation of the SST (differing only due to the non-unity of the emissivity of the ocean). Therefore, the difference between the original SST and this BT is a good measure of the atmospheric attenuation in the 11μm channel. It is assumed that this does not change much over distances of a few kilometres. Thus by smoothing this difference and adding it back to the 11μm BT, an SST with less noise is obtained. This approach is valid in the open ocean, but in the small and highly variable bay, it may not always be a valid assumption. This smoothing method is tested in section 6.3.4.

6.3.3 The Coefficients

Five different sets of coefficients were used to generate SSTs to be compared with the standard product. The first two sets are very similar. The first set were the standard ASST coefficients (published in Merchant *et al.*, 1999) used to generate the ATSR-1 standard GSST product. These were used to process the ATSR-1 BT data in order to check that the method for generating SSTs was satisfactory. The second set were an equivalent set for ATSR-2 BTs that were thought to be generating the ATSR-2 standard GSST product in a similar way. These are called the CM original coefficients in this thesis. In March 2000, after most of this work had been done, C.J. Merchant issued new sets of coefficients for the ATSR-2 processing. This was due to an error in calculating the coefficients. There is little difference to the two-channel algorithm but there is a significant change to the three-channel algorithm of typically –0.4 K (C.J. Merchant – personal communication, 2000). This is the third set and they are called the CM New coefficients. At the time of writing, the three-channel coefficients were under investigation. The last two sets are so called 'image coefficients' designed to generate an SST with a lower noise level than the ASST product and are aimed at the high-resolution product. One of these was robust to stratospheric aerosols (CM Low Noise – robust) and the other (CM Low Noise – Non Robust) was not. The ASST coefficients assume negligible instrument noise contamination whereas the image coefficients assume a NEdT value of 0.07 K. These SST values were then compared to the standard GSST product and to the *in situ* radiometric SISTeR data. Table 9 shows these results. Table 10 shows similar comparisons for data not smoothed using the SST-11μm method.

These data have not been corrected for geolocation errors as the accuracy of the standard GSST product and processing method was being assessed at this stage. The effect of local thermal gradients on the accuracy of the products was also of interest, so a closer look at each validation point and an attempt to correct for geolocation errors is made in section 6.4.

Date	Ascending or Descending Pass	Nadir Cloud Flags	Forward Cloud Flags	ATSR SST (K)	SISTeR SST (K)	ATSR SST - 6 minute SISTeR SST (K)									
						Standard Product	SD of 9 pixel box	CM Original	SD of 9 pixel box	CM New	SD of 9 pixel box	CM Low Noise – Robust	SD of 9 pixel box	CM Low Noise – Non Robust	SD of 9 pixel box
MUBEX'96															
ATSR-1															
29/07/96	D	0	0	294.25	294.18	0.07	0.28	-0.02	0.32	N/A	N/A	N/A	N/A	N/A	N/A
ATSR-2															
05/08/96	D	4	10	294.38	293.96	0.42	0.24	0.33	0.25	0.32	0.24	0.51	0.24	0.51	0.26
06/08/96	A 2-channel	0	0	294.42	293.51	0.91	0.47	0.92 0.71	0.47 0.34	0.52 0.78	0.45 0.34	0.90 0.67	0.46 0.34	0.88 0.73	0.23 0.34
MUBEX'97															
21/07/97	D	4	10	296.65	295.46	1.19	0.33	0.93	0.26	0.97	0.27	1.47	0.41	1.77	0.68
24/07/97	D	4	10	295.11	294.99	0.12	0.39	-0.09	0.41	-0.07	0.40	0.33	0.39	-0.06	0.38
25/07/97	A 2 – Channel	0	0	296.44	296.37	0.07	0.20	0.06 -0.09	0.20 0.20	-0.29 -0.08	0.20 0.20	0.08 0.17	0.20 0.19	0.57 -0.01	0.15 0.20
31/07/97	A 2 – Channel	0	0	298.01	298.22	-0.21	0.27	-0.24 0.13	0.28 0.24	-0.58 0.12	0.27 0.24	-0.19 -0.03	0.27 0.22	0.28 0.16	0.16 0.22
03/08/97	D	0	0	300.85	300.42	0.43	0.18	0.61*	0.17	0.57	0.17	0.23	0.19	0.30	0.24
25/08/97	D	4	0	295.68	295.26	0.42	0.16	0.59	0.18	0.55	0.18	0.21	0.15	0.07	0.12

Table 9: Table showing the difference between ATSR SSTs calculated using various coefficients described 6.3.3 and the *in situ* radiometric SST (measured using the SISTeR radiometer) during the MUBEX campaigns. The standard deviation of a 9-pixel box centred on each satellite SST is given as an indication of the variation of the surrounding pixels. Ascending (night) overpasses are marked with an 'A', descending (day) passes with a 'D'. In the case of night-time overpasses a 2-channel SST has also been calculated. All temperatures are in degrees Kelvin. These data have been smoothed with the SST-11μm method.

Table 9 shows the results of all potential validation points from the MUBEX campaign. The ATSR SST is simply the value of the ATSR pixel in which the *in situ* radiometer was located during overpass. The SISTeR SST is the six-minute average of the SST measured three minutes either side of overpass. Again, a six-minute average was taken as a compromise between getting a reasonable spatial average and being close enough to overpass time. The cloud flag values are also included for completeness (see chapter 4.2 for a detailed description of the cloud flags).

The ATSR-1 data for the standard product and CM original coefficients are very similar as expected. The small difference is because in the standard product 38 across-track bands have been used to interpolate the coefficients instead of the nadir path-length weighting that C.J. Merchant's method uses. This confirmed that the method used for generating SSTs from BT images was correct.
For the ATSR-2 data, the standard product and CM original values are almost identical for cloud free overpasses. This is what would be expected if the same coefficients were used, the small difference again being due to the different coefficient interpolation methods used. This would appear to confirm that for the V320 processing C.J. Merchant's global ASST coefficients are being used. Note that the standard product and CM Original values do not agree for the 3rd August 1997 as one of the forward pixels was flagged as cloudy so the SADIST-2 processing generates a nadir only SST whereas the method used in this thesis still calculates a dual-view SST. This gives a different SST value for this pixel that then affects the centre pixel during the smoothing process.

The results imply that the new ATSR-1 coefficients are more accurate than the original ones but only limited conclusions can be drawn from one data point. There is a large range in the SST of the surrounding eight pixels of about 1 K. The apparent accuracy could be due to chance despite the fact that the pointing of ATSR-1 is more accurate than ATSR-2 (C.T. Mutlow – personal communication, 1997).
The ATSR-2 results do not match the *in situ* data closely on initial inspection. The 5th August 1996 pass has been flagged as possibly suffering from sunglint (cloud

flag 4) and this could be artificially raising the ATSR temperature. The situation for the 21st July and 25th August 1997 is similar. The night-time pass on the 6th August 1996 is not close to the *in situ* data but the surrounding eight ATSR pixels show a large range in temperatures of about 1.5 K (SD of 0.47 K). With the geolocation errors, it could be that the *in situ* data were actually taken in the bottom left pixel that is a lot closer to the *in situ* data – this is further investigated in section 6.4.3. The remaining validation points show a wide range in offsets from the *in situ* data. These could be due to noise, local temperature variations, or geolocation errors. Each validation point is investigated in more detail in section 6.4.

6.3.4 The Validity of the SST-11µm smoothing method

In order to assess whether the SST-11µm smoothing method was still valid for reducing the level of noise in the highly variable bay, SSTs were generated in the same way to those in Table 9 but without applying the SST-11µm smoothing method. The results are given in Table 10. The CM Original results are equivalent to the unsmoothed standard product as the same coefficients are used.

Date	Ascending or Descending Pass	Nadir Cloud Flags	Forward Cloud Flags	ATSR SST (K)	SISTeR SST (K)	ATSR SST - 6 minute SISTeR SST (K)					
						CM Original	SD of 9 pixel box	CM Low Noise – Robust	SD of 9 pixel box	CM Low Noise – Non Robust	SD of 9 pixel box
MUBEX'96											
ATSR-1											
29/07/96	D	0	0	*294.25*	294.18	-0.28	0.97	N/A	N/A	N/A	N/A
ATSR-2											
05/08/96	D	4	10	*294.38*	293.96	0.37	0.33	0.55	0.29	0.57	0.31
06/08/96	A 2 – Channel	0	0	*294.42*	293.51	1.03 0.63	0.74 0.55	1.02 0.69	0.72 0.51	0.93 0.81	0.30 0.49
MUBEX'97											
21/07/97	D	4	10	296.65	295.46	1.21	0.38	1.81	0.57	2.24	0.95
24/07/97	D	4	10	295.11	294.99	-0.31	0.50	0.22	0.47	-0.11	0.47
25/07/97	A 2 – Channel	0	0	296.44	296.37	0.08 0.19	0.22 0.40	0.11 0.40	0.22 0.34	0.54 0.20	0.32 0.14
31/07/97	A 2 – Channel	0	0	298.01	298.22	-0.15 0.17	0.33 0.35	-0.13 -0.03	0.32 0.31	0.34 0.14	0.16 0.30
03/08/97	D	0	0	300.85	300.42	0.56	0.26	0.21	0.23	0.30	0.28
25/08/97	D	4	0	295.68	295.26	0.71	0.34	0.29	0.26	0.11	0.20

Table 10: Table showing the comparison between ATSR SST calculated using various coefficients described in 6.3.3 and the *in situ* radiometric SST (measured using the SISTeR radiometer) during the MUBEX campaigns. The standard deviation of a 9-pixel box centred on each satellite SST is given as an indication of the variation of the surrounding pixels. Ascending (night) overpasses are marked with an 'A', descending (day) passes with a 'D'. All temperatures are in degrees Kelvin. These data are similar to that presented in Table 9 but these data have not been smoothed with the SST-11μm method.

Overall, these data give similar results but there is a lot more noise. This implies that the SST-11μm method does reduce the noise in the SST measurements of the bay but there is still a large noise component mainly due to natural thermal variations in the bay. There is a need to study data taken from areas of uniform temperature, probably in the deep ocean, and compare it to these data, to investigate this further. Unfortunately, no validation points were obtained from the CHAOS'98 cruise where such conditions occurred so this was not possible in this thesis.

6.3.5 Summary of Direct Comparison Validation Results

Table 11 shows the average ΔT between the *in situ* SST and the satellite SST calculated using the various coefficients described in 6.3.3. The average has been calculated using all potential validation points and only validation points flagged as cloud free.

	SST-11μm Smoothing Method				No Smoothing		
	Standard Product	**CM Original**	**CM Low Noise – Robust**	**CM Low Noise – Non Robust**	**CM Original**	**CM Low Noise – Robust**	**CM Low Noise – Non Robust**
Mean (All)	0.42 ±0.45	0.30 ±0.45	0.44 ±0.52	0.54 ±0.58	0.44 ±0.55	0.51 ±0.62	0.61 ±0.73
Mean (cloud free)	0.30 ±0.48	0.34 ±0.52	0.25 ±0.46	0.51 ±0.28	0.38 ±0.53	0.30 ±0.50	0.53 ±0.29

Table 11: Table showing the mean ΔT between the satellite SST (calculated using the coefficients described in section 6.3.3) and *in situ* radiometric SST for the non-geocorrected MUBEX data. The mean values are for all potential match-ups and all match-ups flagged as cloud free.

These results show that overall the SST-11μm smoothing method is more accurate than the non-smoothed method. This confirms that the SST-11μ smoothing method is still valid for Mutsu Bay. The standard deviation of the mean was expected to be higher in the non-smoothed method than the smoothed method but this is not always the case. This could be due to the low number of data points affecting the statistics. The CM low noise, aerosol robust coefficients appear to be the most accurate coefficients with the lowest noise. The standard product and data processed using the CM original coefficients are very similar, as expected, and are slightly less accurate than the low noise coefficients. The non-robust coefficients are the least accurate. The rms error associated with the validation of each set of coefficients is very large. It was suspected that geolocation errors could be causing a significant part of this noise. Each validation point is investigated in more detail in the next section and an attempt made to correct for geolocation errors. It can be said however that the non-geocorrected, standard product is accurate to 0.30±0.48 K in the Mutsu Bay region.

If the new coefficients, released by C.J. Merchant in March 2000, are used the mean ΔT for all potential validation points is 0.25±0.52 K and for cloud free overpasses is 0.05±0.58 K. These new coefficients give more accurate values but with a slightly higher uncertainty.

6.4 Detailed Look at each Validation Point and Geolocation errors

This section looks at each potential validation point in detail. For each point, the surrounding eight pixels and cloud flags are studied to give a better understanding of the surrounding area. The *in situ* SISTeR data taken during each validation transect are also presented so that the variation of the *in situ* data can be studied.

6.4.1 Daytime Descending ATSR-1 Pass on the 29th July 1996

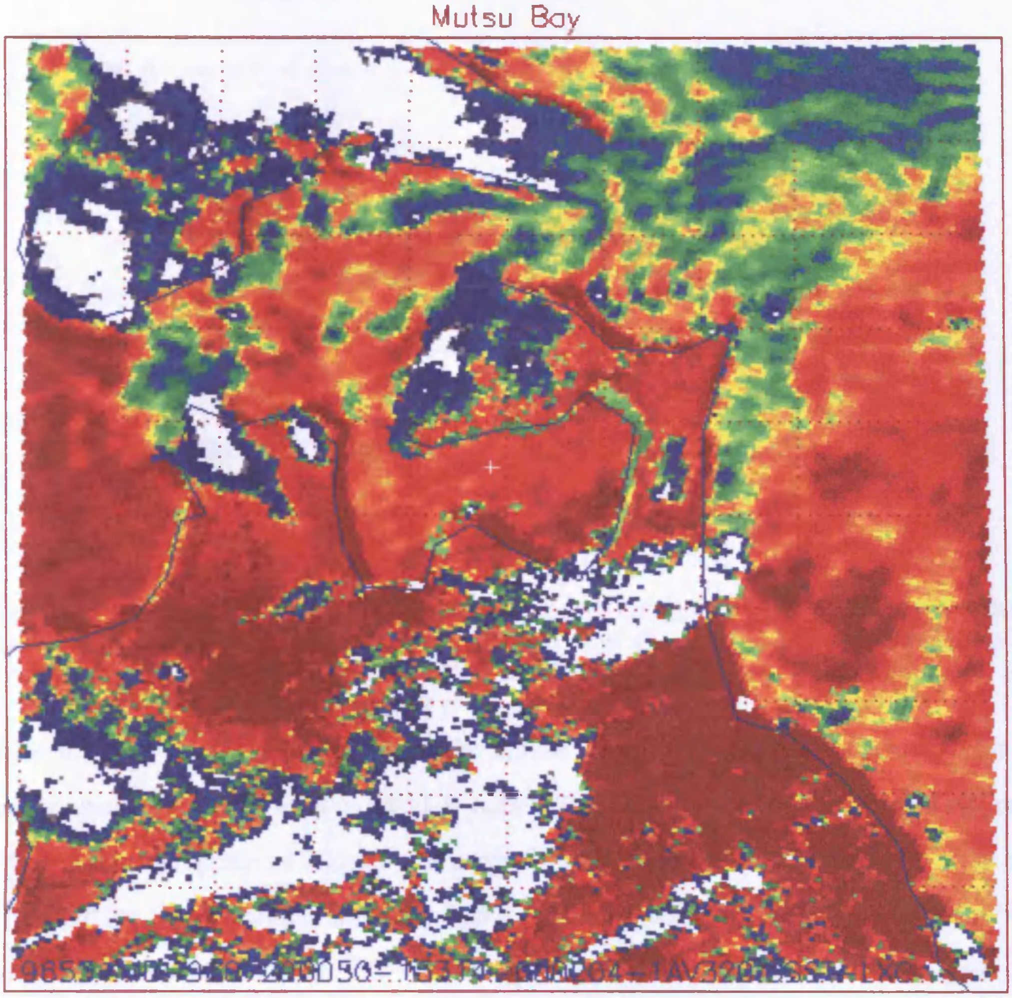

Figure 27: A sub-section (140 - 142° Longitude and 40-42° Latitude) of the ATSR image from the daytime pass on the 29th July 1996. The blue outline shows the ATSR land mask and the white cross the position of the Dai-Ni-Misago at overpass.

293.71	294.21	294.53
293.96	294.25	294.63
294.09	294.40	294.17

0 0	0 0	0 0
0 0	0 0	0 0
0 0	0 0	0 0

Table 12: Left –Table showing the standard GSST pixel in which the *in situ* data were taken (centre) and the surrounding eight pixels. These data have not been corrected for geolocation errors. Right – Table showing the forward (top) and nadir (bottom) cloud flags associated with each of these pixels. Note: as this is a descending pass the top left pixel is to the southeast and the bottom right is to the northwest.

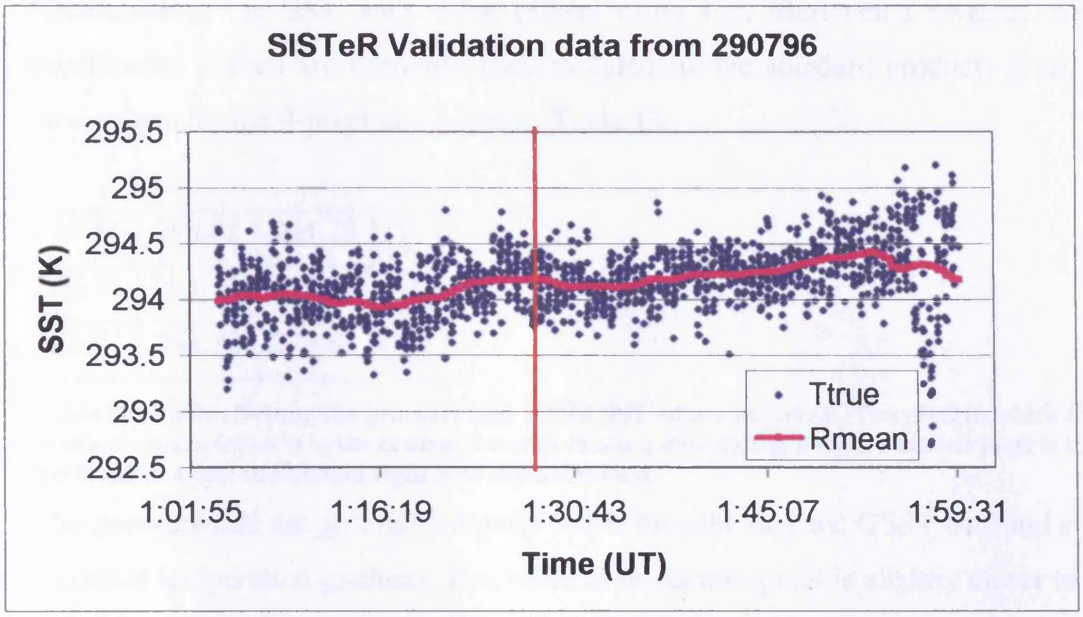

Figure 28: Graph showing the *in situ* radiometric (SISTeR) SST against universal time for the validation transect on the 29th July 1996. The dots show the individual data (with the cyclic noise removed but still with the white noise) and the solid line shows the running mean. The vertical red line is the time of overpass of the satellite.

The weather conditions for the only ATSR-1 overpass were clear overhead with some cumulus cloud over land (1/8 octa). The wind speeds were in the region 5-7 ms^{-1} with a sea state of 3 and increasing. The surface humidity was 85%. The ship's transect for this overpass lasted roughly one hour and was along the bearing WNW with the sun to stern. The Dai-Ni-Misago was at buoy number 6 at overpass (buoy to starboard). The original data from earlier versions of the SADIST-2 processing had nadir cloud flags but in the latest V320 processing the data were flagged as cloud free in agreement with the *in situ* observations. The surrounding pixels show a rising temperature gradient from the southeast to the northwest with the temperature rising roughly 0.8K. The *in situ* radiometric SISTeR data are relatively constant rising slightly from roughly 294 K to 294.5 K over the hour. The SISTeR SST three minutes either side of overpass is 294.18±0.23 K. This matches the centre satellite pixel value of 294.25 K closely (ΔT 0.07 K).

By lining each image up with a land mask, the geolocation error of each image was found. The forward view was found to have across-track and along-track offsets of 0 and –1 pixel respectively. The nadir view was found to have offsets of –1 and –1. This means (as the pass is descending) the forward image had to be moved one pixel south and the nadir image had to be moved one pixel south and one pixel west.

Recalculating the SST with these offsets using C.J. Merchant's original ASST coefficients (which are currently used to calculate the standard product) gives the new values for the 9-pixel box given in Table 13.

293.56	293.82	294.28
293.76	294.15	294.20
293.87	294.22	293.87

Table 13: Table showing the geocorrected ATSR SST values in Kelvin. The pixel in which the *in situ* data are taken is in the centre. Note: as this is a descending pass the top left pixel is to the southeast and the bottom right is to the northwest.

The geocorrected are generally slightly lower than the original GSST data and show a similar temperature gradient. The value of the centre pixel is slightly closer to the *in situ* value (ΔT -0.03 K) but not significantly so. This is the only ATSR-1 validation point obtained and it implies that the new processing (V320) is more accurate than the earlier V200 processing (see section 6.3.1). This is only one validation point however, so care must be taken when drawing conclusions.

6.4.2 Daytime Descending ATSR-2 Pass on the 5th August 1996

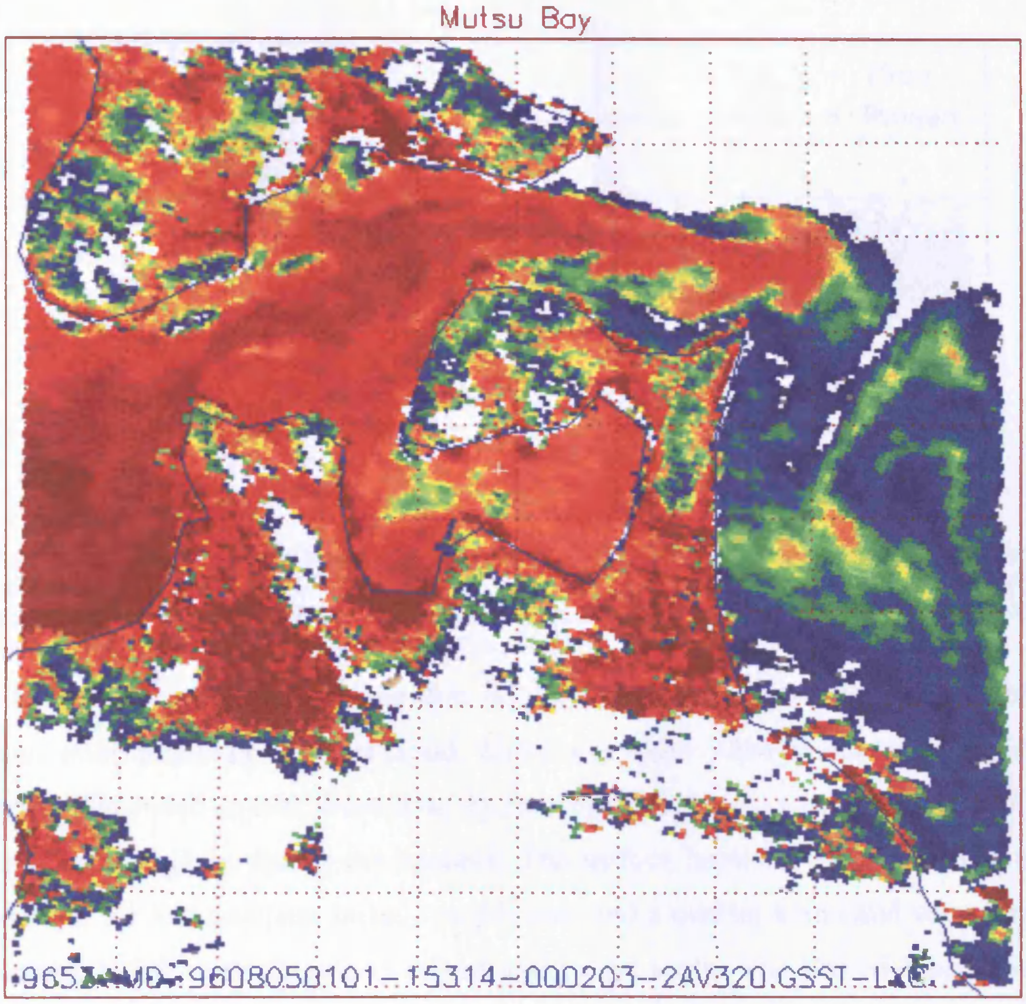

Figure 29: A sub-section (140 - 142° Longitude and 40-42° Latitude) of the ATSR image from the daytime pass on the 5th August 1996. The blue outline shows the ATSR land mask and the white cross the position of the Dai-Ni-Misago at overpass.

294.58	294.25	293.93
294.57	294.38	294.15
294.69	294.42	294.23

10 4	10 4	10 4
10 4	10 4	10 4
10 4	10 4	10 4

Table 14:Left –Table showing the standard GSST pixel in which the *in situ* data were taken (centre) and the surrounding eight pixels. These data have not been corrected for geolocation errors. Right – Table showing the forward (top) and nadir (bottom) cloud flags associated with each of these pixels. Note: as this is a descending pass the top left pixel is to the southeast and the bottom right is to the northwest.

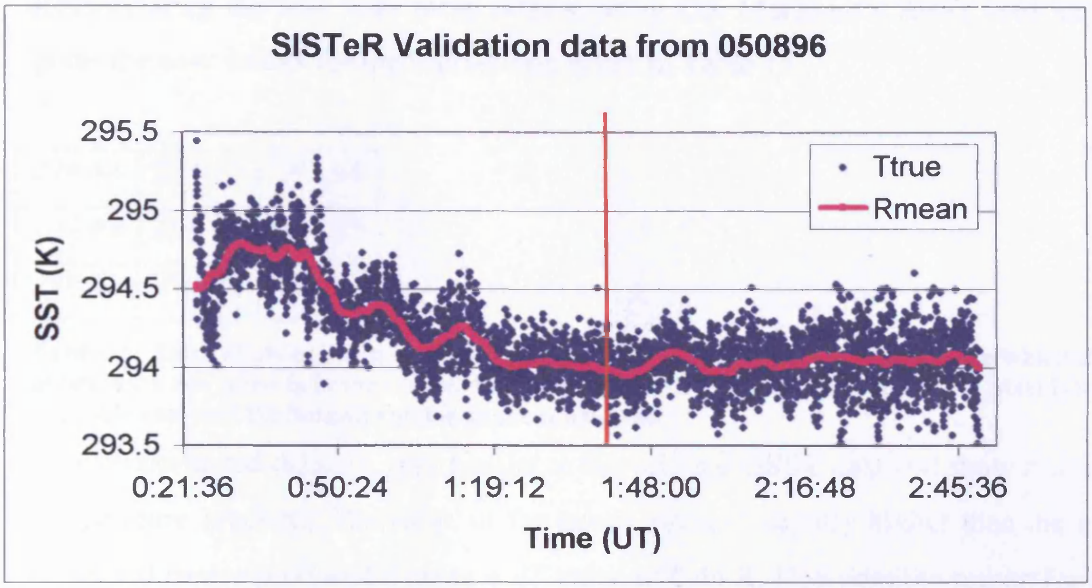

Figure 30: Graph showing the *in situ* radiometric (SISTeR) SST against universal time for the validation transect on the 5th August 1996. The dots show the individual data (with the cyclic noise removed but still with the white noise) and the solid line shows the running mean. The vertical red line is the time of overpass of the satellite.

The weather conditions for the first ATSR-2 overpass were a light haze overhead with small amounts of cirrus cloud. There was some cumulus cloud over land (1/8 octa). The wind-speeds were low, in the region 3-5ms^{-1}, with a sea state of 1-2, increasing slightly during the transect. The surface humidity was 65%. The ship's transect for this overpass lasted roughly two and a quarter hours and was along the bearing WSW with the sun overhead and to the south. The Dai-Ni-Misago was at buoy number 6 at overpass.

The forward ATSR-2 data are flagged with cloud flag 10. This means the data have failed the 1.6μm reflectance histogram test. This might be due to the small amounts of cirrus clouds observed. The nadir pixels are flagged as possibly suffering from sun glint. The surrounding pixels show a rising temperature gradient from the southwest to the northeast with the temperature rising roughly 0.8K. The *in situ* radiometric SISTeR data fall initially from roughly 294.75 K to 294 K and then remain relatively constant. The SISTeR SST three minutes either side of overpass is 293.96±0.17 K. The centre satellite pixel has a value of 294.38 K (ΔT 0.42 K).

The forward view was found to have no offsets and the nadir view was found to have no across-track offset but an along-track offset of –1. This means (as the pass is descending) that the nadir image had to be moved one pixel south.

Recalculating the SST with these offsets, using C.J. Merchant's ASST coefficients gives the new values for the 9-pixel box given in Table 15.

294.44	294.13	293.94
294.49	294.40	294.29
294.61	294.45	294.32

Table 15: Table showing the geocorrected ATSR SST values in Kelvin. The pixel in which the *in situ* data are taken is in the centre. Note: as this is a descending pass the top left pixel is to the southeast and the bottom right is to the northwest.

The geocorrected data are very similar to the original GSST data and show a similar temperature gradient. The value of the centre pixel is slightly higher than the non-corrected centre pixel and it gives a ΔT value of 0.44 K. One possible reason for this offset is that the ATSR-2 data are suffering from sunglint and this is artificially raising the ATSR-2 SST relative to the *in situ* data. The *in situ* data show a similar thermal structure to the satellite data. As the Dai-Ni-Misago travelled WSW the SST dropped from roughly 294.5 K to 294 K. This is consistent with the vessel moving from the region of the centre pixel to the region of the top right (Southwest) pixel. This could also explain the offset. Due to the large number of cloud flags however, this validation point must be considered suspect.

6.4.3 Night-time Ascending ATSR-2 Pass on the 6th August 1996

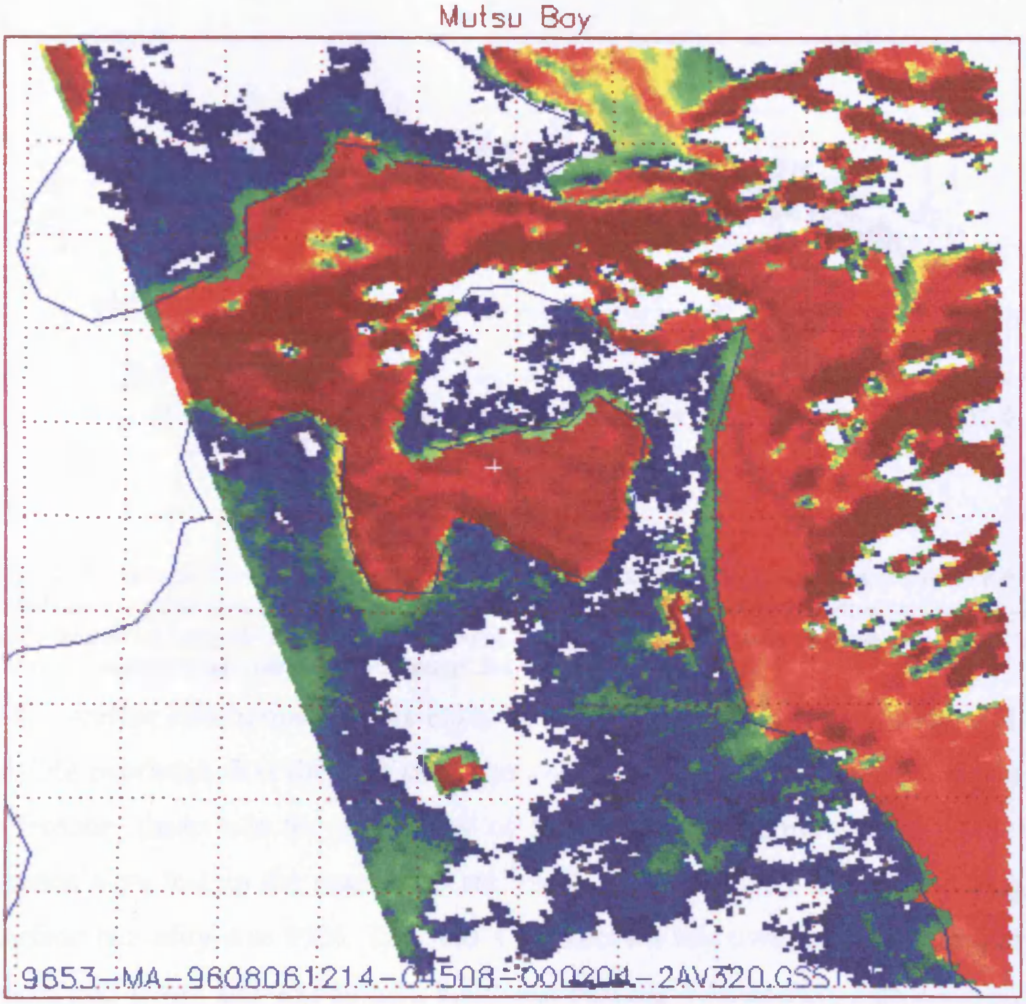

Figure 31: A sub-section (140 - 142° Longitude and 40-42° Latitude) of the ATSR image from the night-time pass on the 6th August 1996. The blue outline shows the ATSR land mask and the white cross the position of the Dai-Ni-Misago at overpass.

294.36	294.78	294.96
293.87	294.42	294.84
293.54	294.20	294.65

0 0	0 0	0 0
0 0	0 0	0 0
0 0	0 0	0 0

Table 16: Left –Table showing the standard GSST pixel in which the *in situ* data were taken (centre) and the surrounding eight pixels. These data have not been corrected for geolocation errors. Right – Table showing the forward (top) and nadir (bottom) cloud flags associated with each of these pixels. Note: as this is an ascending pass the top left pixel is to the northwest and the bottom right is to the southeast.

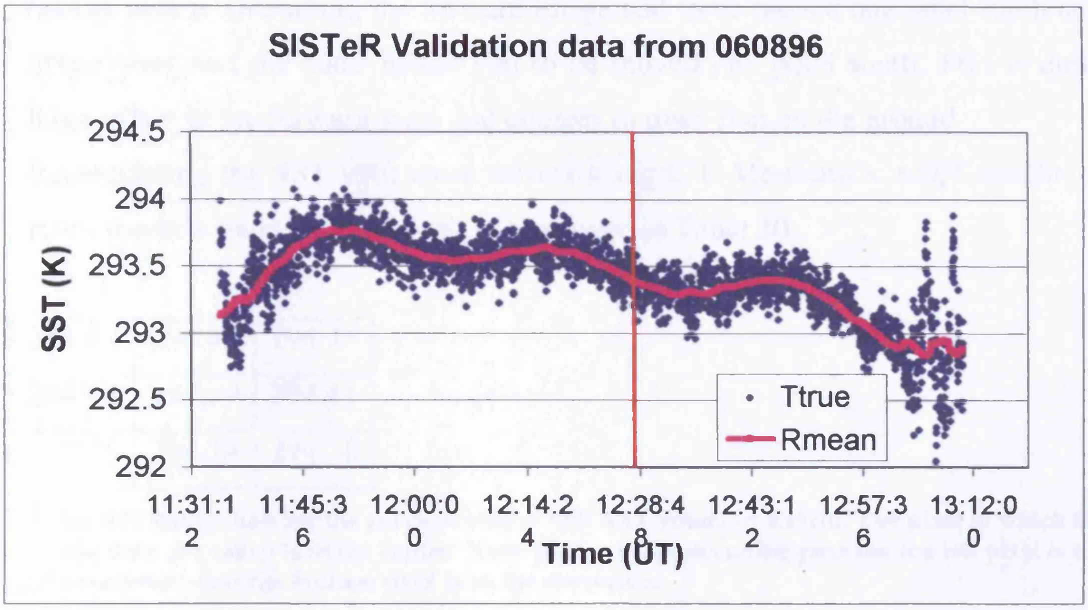

Figure 32: Graph showing the *in situ* radiometric (SISTeR) SST against universal time for the validation transect on the 6th August 1996. The dots show the individual data (with the cyclic noise removed but still with the white noise) and the solid line shows the running mean. The vertical red line is the time of overpass of the satellite.

The weather conditions for this night-time ATSR-2 overpass were clear with stars visible overhead. It is difficult to assess cloud cover at night but using the stars as a reference, there was the possibility of haze or cloud on the horizon. The wind-speeds were low in the region 3-5 ms^{-1} with a sea state of 2-3 and increasing. The surface humidity was 85%. The ship's transect for this overpass lasted roughly one and a half hours and was along a southeast bearing. The satellite data are flagged as cloud free as are the surrounding eight pixels. The surrounding pixels show a strong rising temperature gradient from the southwest to the northeast with the temperature rising roughly 1.5K. The *in situ* radiometric SISTeR data start at roughly 293 K rising to 294 K and then gradually falling back to below 293K. As this is a night-time overpass, there is no diurnal warming of the sea. This means that the warming seen in the *in situ* data is probably due to the research vessel moving across a thermal gradient. The later cooling is probably it moving back across the gradient again although some of the cooling could be due to the natural cooling of the ocean surface at night. The SISTeR SST three minutes either side of overpass is 293.51±0.12 K. This does not match the centre satellite pixel value of 294.42 K (ΔT 0.91 K).

The forward view was found to have across-track and along-track offsets of 1 and 3 pixel respectively. The nadir view was found to have offsets of 0 and 1. This means (as the pass is ascending) the forward image had to be moved one pixel south and 3 pixels west and the nadir image had to be moved one pixel south. This is quite a large offset in the forward view and equates to over 3km on the ground.

Recalculating the SST with these offsets using C.J. Merchant's ASST coefficients gives the new values for the 9-pixel box given in Table 30.

294.33	294.45	294.45
294.04	294.29	294.41
293.55	294.14	294.38

Table 17: Table showing the geocorrected ATSR SST values in Kelvin. The pixel in which the *in situ* data are taken is in the centre. Note: as this is an ascending pass the top left pixel is to the northwest and the bottom right is to the southeast.

The geocorrected data show a similar temperature gradient to the original GSST data but the magnitude of the gradient has been reduced. The value of the centre pixel is closer to the *in situ* value (ΔT 0.78 K) but there is still a large difference between the satellite and *in situ* data. The *in situ* data are much closer to the value of the ATSR pixel southwest of the centre pixel. The ATSR and *in situ* data show large thermal gradients and this implies that the *in situ* data are taken in an area of high thermal gradient between the southwest and central pixel (there is a ΔT of roughly 0.75 K). The *in situ* data vary between 293 and 294 K, which is consistent with the ATSR data. The Dai-Ni-Misago was moving in a southeast direction perpendicular to this gradient. This large thermal gradient and large geolocation errors make this a very difficult validation point to use. As stated earlier, the *in situ* data at overpass appears to be more representative of the southwest pixel rather than the centre pixel and the maximum *in situ* data are representative of a temperature roughly halfway between these two pixels. If the southwest pixel is used for the validation instead of the central pixel, a ΔT value of 0.04 K is obtained. This value is also used in the summary statistics, given in Table 31 and Table 32, but is highlighted in italics as this data point is considered suspect and needs to be treated with care.

6.4.4 Daytime Descending pass on the 21st July 1997

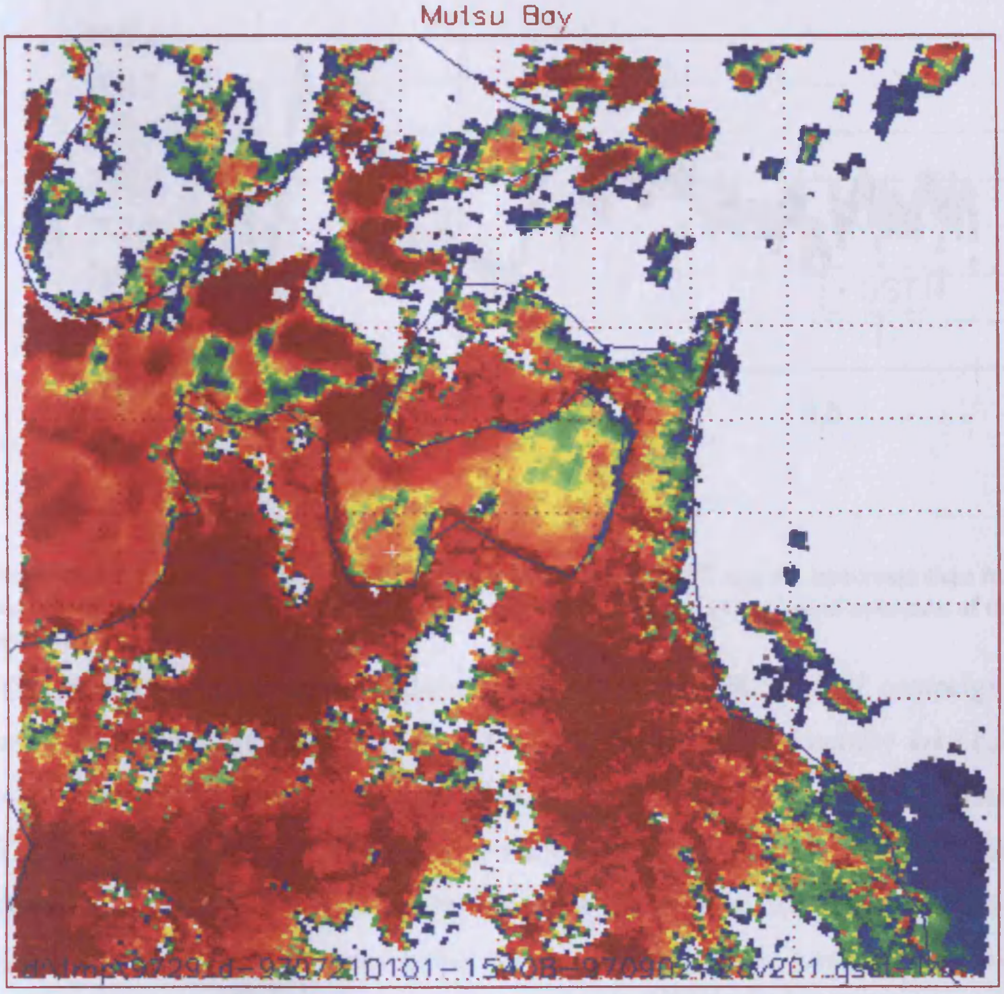

Figure 33: A sub-section (140 - 142° Longitude and 40-42° Latitude) of the ATSR image from the daytime pass on the 21st July 1997. The blue outline shows the ATSR land mask and the white cross the position of the Dai-Ni-Misago at overpass.

296.08	296.48	296.95
296.32	296.65	296.93
296.17	296.61	296.93

0 4	34 4	34 4
0 4	10 4	0 4
0 4	10 4	10 4

Table 18: Left –Table showing the standard GSST pixel in which the *in situ* data were taken (centre) and the surrounding eight pixels. These data have not been corrected for geolocation errors. Right – Table showing the forward (top) and nadir (bottom) cloud flags associated with each of these pixels. Note: as this is a descending pass the top left pixel is to the southeast and the bottom right is to the northwest.

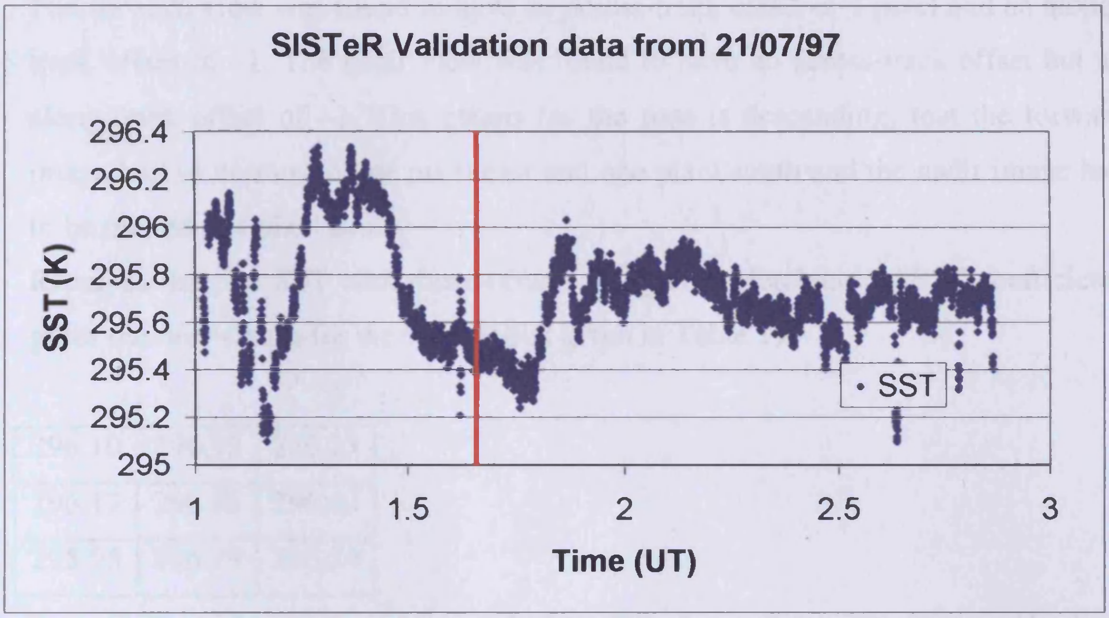

Figure 34: Graph showing the *in situ* radiometric (SISTeR) SST against universal time for the validation transect on the 21st July, 1997. The vertical red line is the time of overpass of the satellite.

This was the first potential validation point from the MUBEX'97 campaign. The weather conditions for this daytime ATSR-2 overpass were generally very calm. It was clear overhead with some wispy cloud off nadir and cumulus cloud overland. The wind speeds were low (3-4ms^{-1}) with a sea state of 0-1 increasing slightly during the transect. The relative humidity at the surface was 85% to 90%. The ship's transect for this overpass lasted roughly two hours and was along the bearing 260° with the sun overhead and to port. The Dai-Ni-Misago was at buoy number 4 at overpass.

Three of the forward ATSR-2 pixels are flagged with cloud flag 10 (1.6μm reflectance histogram test) and two others are flagged with cloud flag 34 (11μm spatial coherence test). The thin wispy cloud observed off nadir could have triggered these flags. The nadir pixels are flagged as possibly suffering from sun glint.

The surrounding pixels show a rising temperature gradient going from east to west with the temperature rising roughly 0.7 K. The *in situ* radiometric SISTeR data vary from roughly 295.2 K to 296.2 K. Roughly 10 minutes either side of overpass the *in situ* data are lower than during the rest of the transect. The SISTeR SST three minutes either side of overpass is 295.46 K. The centre satellite pixel has a value of 296.65 K (ΔT 1.19 K).

The forward view was found to have an across-track offset of 1 pixel and an along-track offset of –1. The nadir view was found to have no across-track offset but an along-track offset of –1. This means (as the pass is descending) that the forward image had to be moved one pixel east and one pixel south and the nadir image had to be moved one pixel south.

Recalculating the SST with these offsets using C.J. Merchant's ASST coefficients gives the new values for the 9-pixel box given in Table 19.

296.10	296.31	296.23
296.17	296.45	296.40
295.95	296.29	296.24

Table 19: Table showing the geocorrected ATSR SST values in Kelvin. The pixel in which the *in situ* data are taken is in the centre. Note: as this is a descending pass the top left pixel is to the southeast and the bottom right is to the northwest.

The geocorrected data are very similar to the original GSST data and show a similar east-west temperature gradient. The value of the centre pixel is still much higher than the *in situ* value (ΔT 0.99 K). One possible reason for this offset is that the ATSR-2 data are suffering from sunglint and this is artificially raising the ATSR-2 SST relative to the *in situ* data. Another more probably reason for the offset is sub pixel variations in the diurnal thermocline. The *in situ* data roughly 10 minutes before the satellite overpass are roughly 296.1 K. These data are in much closer agreement with the satellite data. It could be speculated that the Dai-Ni-Misago was in a region of cooler water from roughly 10 minutes before the time of overpass. It could be that the Dai-Ni-Misago passed into a region where the diurnal thermocline had been broken down by either another boat or natural processes mixing the water. If the majority of the satellite pixel had the diurnal thermocline still present, this would explain the discrepancy between the *in situ* and satellite data. Figure 35 shows data that support this. It shows the bulk CTD temperature, measured at roughly 0.75m, and the radiometric temperature measured from the Dai-Ni-Misago during the overpass transect. The data show a strong warm diurnal thermocline, of order 1K, until about 1.30 UT when the skin data fall rapidly and match the 0.75m temperatures much more closely. There is still a small warm thermocline, of order 0.2 K, so some diurnal warming is still present. It could be that a disturbance mixed the water earlier and that the small warm skin seen is the diurnal thermocline building up again.

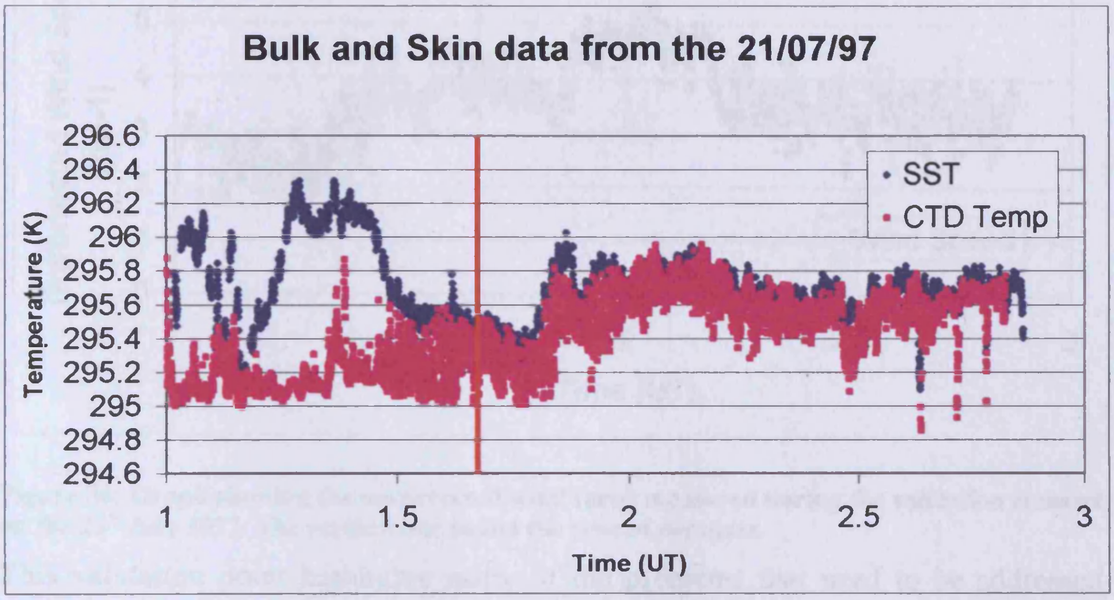

Figure 35: Graph showing the *in situ* bulk (approximately 0.75m depth) and skin sea surface temperatures during the validation transect on the 21st July 1997. The vertical line is the time of overpass.

Figure 36 shows the wind speed measured during the transect. It shows a slight increase in the wind speed (of order $2ms^{-1}$) at about 1.20 UT that could have led to increased mixing of the surface water and so reduced the diurnal thermocline. This increase in wind speed is not conclusive however and the mixing could have been caused by a small local wind burst or a ship passing by earlier.

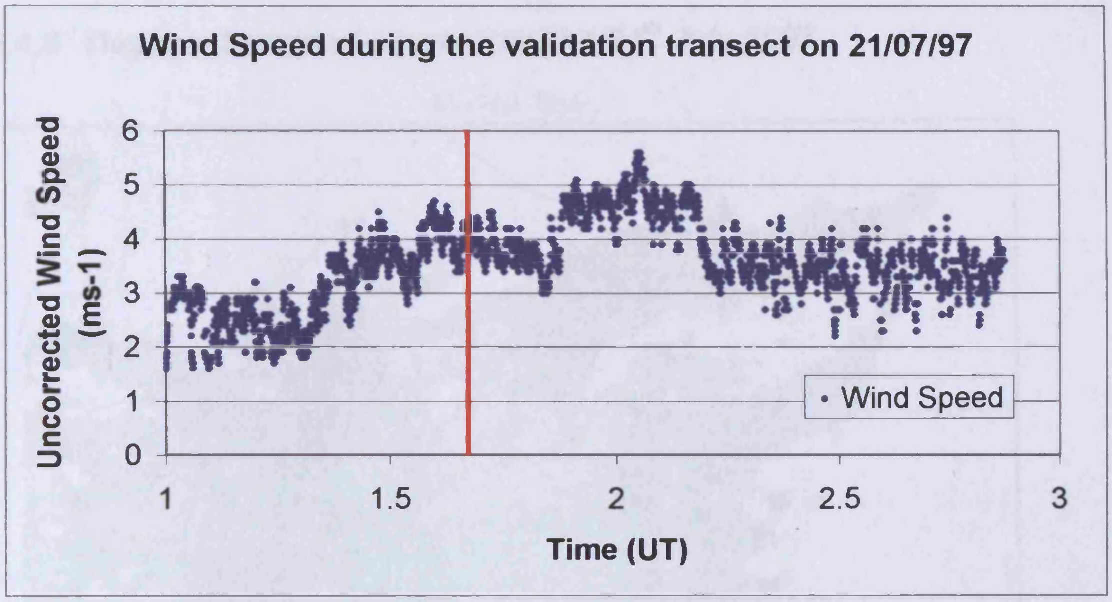

Figure 36: Graph showing the uncorrected wind speed measured during the validation transect on the 21st July 1997. The vertical line shows the time of overpass.

This validation point highlights many of the problems that need to be addressed when validating in a sheltered area. The geolocation errors, thermal gradients, and the diurnal thermocline all combine to reduce the confidence in this validation point.

6.4.5 Daytime Descending pass on the 24th July 1997

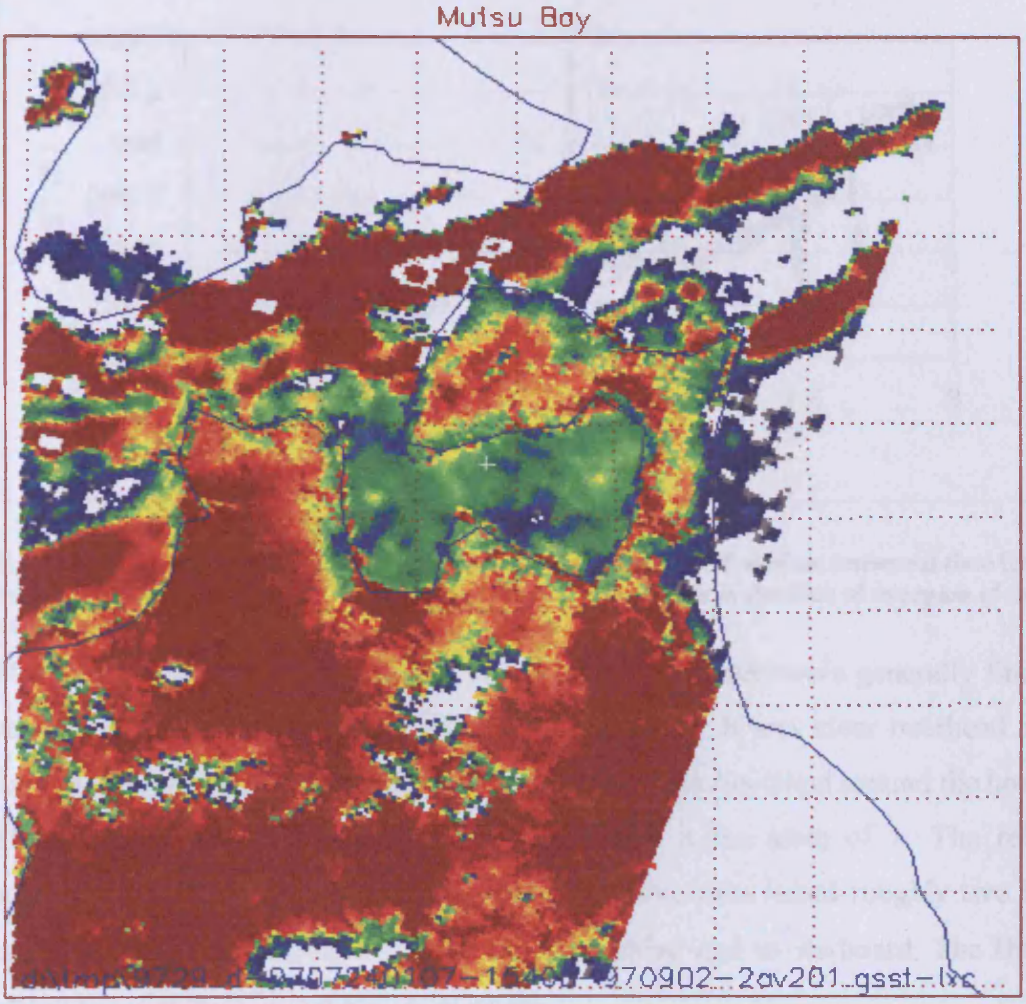

Figure 37: A sub-section (140 - 142° Longitude and 40-42° Latitude) of the ATSR image from the daytime pass on the 24th July 1997. The blue outline shows the ATSR land mask and the white cross the position of the Dai-Ni-Misago at overpass.

294.97	295.21	295.76
294.81	295.11	295.74
294.73	295.15	295.65

10 22	10 4	10 34
10 4	10 4	0 4
10 4	10 4	10 4

Table 20: Left –Table showing the standard GSST pixel in which the *in situ* data were taken (centre) and the surrounding eight pixels. These data have not been corrected for geolocation errors. Right – Table showing the forward (top) and nadir (bottom) cloud flags associated with each of these pixels. Note: as this is a descending pass the top left pixel is to the southeast and the bottom right is to the northwest.

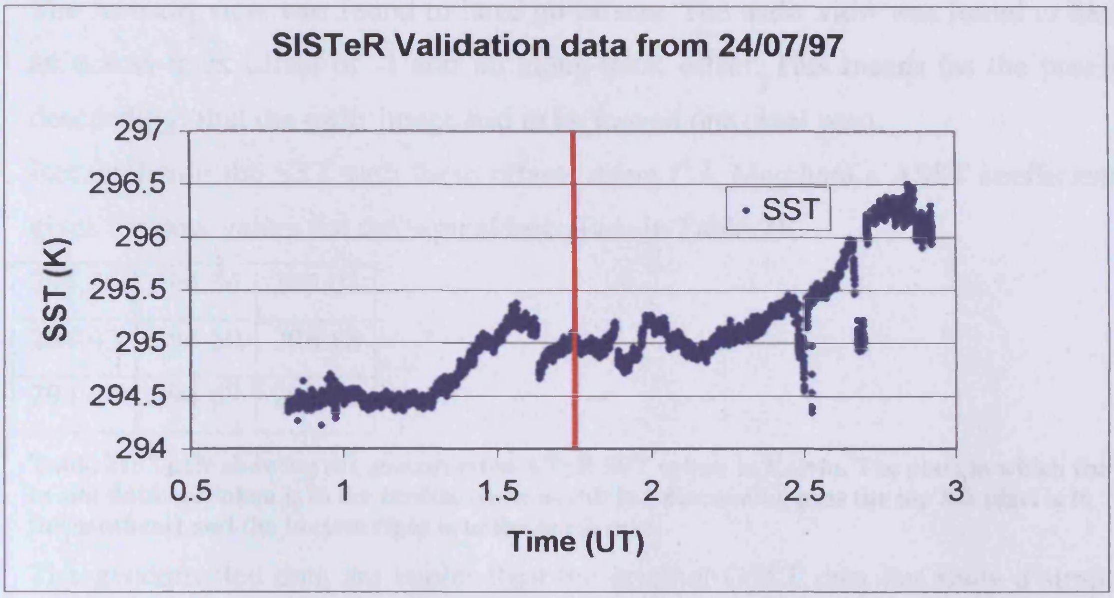

Figure 38: Graph showing the *in situ* radiometric (SISTeR) SST against universal time for the validation transect on the 24th July, 1997. The vertical red line is the time of overpass of the satellite.

The weather conditions for this daytime ATSR-2 overpass were generally fine and very calm but with the amount of cloud building up. It was clear overhead at the time of overpass but with 3/8 octas of stratus and cumulus cloud around the horizon. The wind speeds were very low (0-2ms^{-1}) with a sea state of 1. The relative humidity was 90%. The ship's transect for this overpass lasted roughly two hours and was along the bearing 50° with the sun behind and to starboard. The Dai-Ni-Misago was at buoy number 6 at overpass.

All but one of the forward ATSR-2 pixels are flagged with cloud flag 10 which means they have failed the 1.6μm reflectance histogram test. This is probably the off-nadir cloud that was observed from the ground. The nadir pixels are flagged as possibly suffering from sun glint. The southwest and southeast nadir pixels are also flagged as cloudy with cloud flags 34 (11μm spatial coherence test) and 22 (1.6μm special coherence test and sunglint) respectively.

The surrounding pixels show a rising temperature gradient going from east to west with the temperature rising roughly 0.9 K. The *in situ* radiometric SISTeR temperature rises slowly over the time of the transect from 294.5 K to 296.5 K. This is due to a strong diurnal thermocline building up due to the calm conditions. The SISTeR SST three minutes either side of overpass is 294.99 K. The centre satellite pixel has a value of 295.11 K (ΔT 0.12 K).

The forward view was found to have no offsets. The nadir view was found to have an across-track offset of -1 and no along-track offset. This means (as the pass is descending) that the nadir image had to be moved one pixel west.

Recalculating the SST with these offsets using C.J. Merchant's ASST coefficients gives the new values for the 9-pixel box given in Table 21.

294.26	294.36	295.03
294.42	294.50	295.18
294.64	294.67	295.10

Table 21: Table showing the geocorrected ATSR SST values in Kelvin. The pixel in which the *in situ* data are taken is in the centre. Note: as this is a descending pass the top left pixel is to the southeast and the bottom right is to the northwest.

The geocorrected data are cooler than the original GSST data but show a similar east-west temperature gradient. The value of the centre pixel is lower than the *in situ* value (ΔT –0.49 K). The three centre pixels are roughly 0.7 K cooler than the western three pixels. This strong temperature gradient is probably the cause of the offset as the *in situ* data fall between these values and the geolocation is really only accurate to ±1 pixel. The amount of cloud flags rule this point out as a good candidate for a validation point.

6.4.6 Night-time Ascending pass on the 25th July 1997

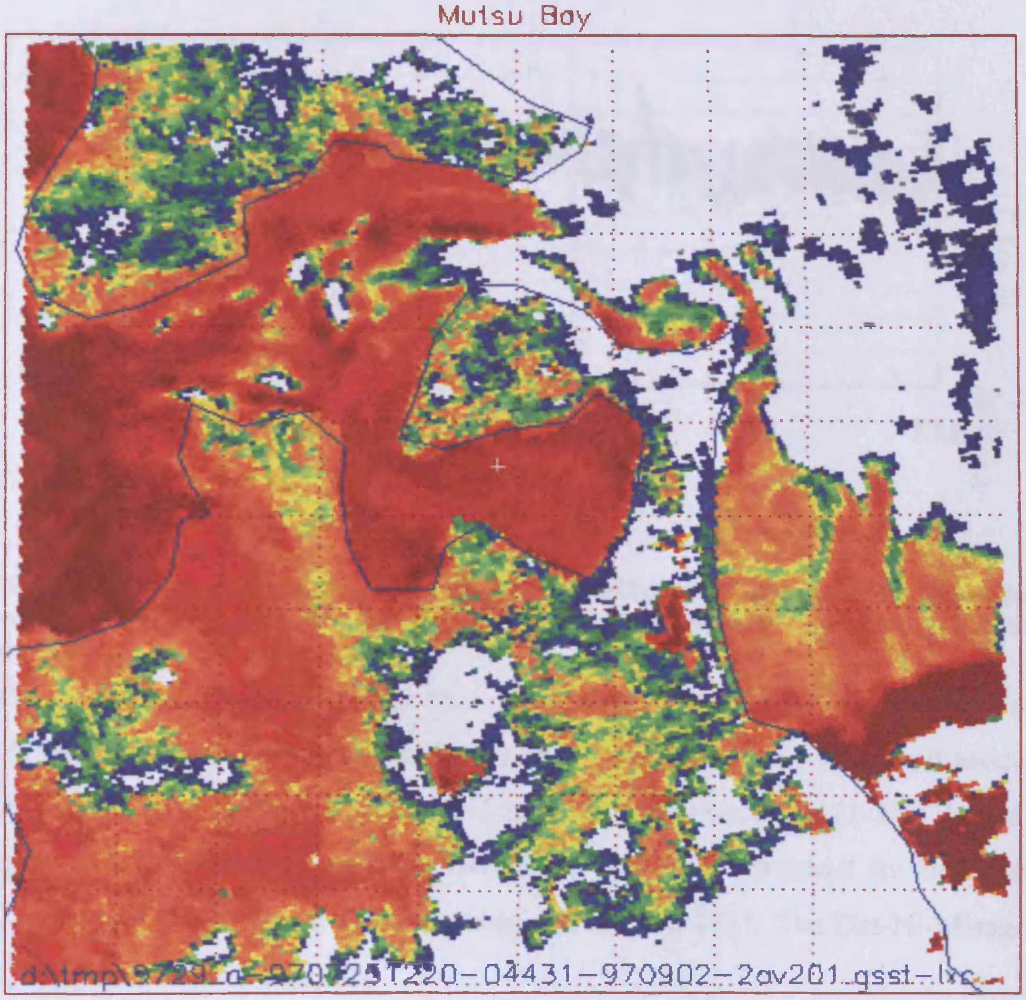

Figure 39: A sub-section (140 - 142° Longitude and 40-42° Latitude) of the ATSR image from the night-time pass on the 25th July 1997. The blue outline shows the ATSR land mask and the white cross the position of the Dai-Ni-Misago at overpass.

296.30	296.31	295.98
296.56	296.44	296.14
296.50	296.31	296.04

0 0	0 0	0 0
0 0	0 0	0 0
0 0	0 0	0 0

Table 22: Left –Table showing the standard GSST pixel in which the *in situ* data were taken (centre) and the surrounding eight pixels. These data have not been corrected for geolocation errors. Right – Table showing the forward (top) and nadir (bottom) cloud flags associated with each of these pixels. Note: as this is an ascending pass the top left pixel is to the northwest and the bottom right is to the southeast.

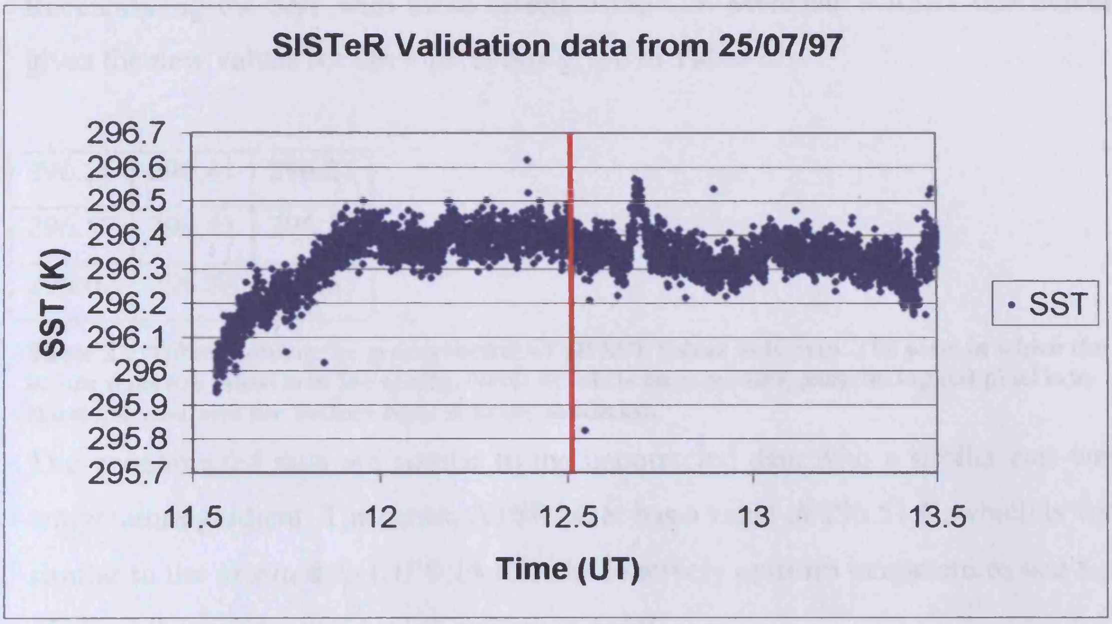

Figure 40: Graph showing the *in situ* radiometric (SISTeR) SST against universal time for the validation transect on the 25th July, 1997. The vertical red line is the time of overpass of the satellite.

The weather conditions for the first night-time ATSR-2 overpass during MUBEX'97 were generally clear and calm. There were stars visible all around the sky, which implies clear conditions. The wind speeds were low (1-3ms^{-1}) with a sea state of 2. The relative humidity was 93%. The ship's transect for this overpass lasted roughly two hours and was along the bearing 145°. The Dai-Ni-Misago was at buoy number 6 at overpass.

All the forward and nadir ATSR pixels are flagged as cloud free (flag 0).

The surrounding pixels show a rising temperature gradient going from east to west with the temperature rising roughly 0.4 K. The *in situ* radiometric SISTeR temperature rises initially by 0.4 K over the first half hour then remains relatively constant at roughly 296.4 K. The SISTeR SST three minutes either side of overpass is 296.37 K. The centre satellite pixel has a value of 296.44 K (ΔT 0.07 K).

The forward view was found to have an across-track offset of 2 and an along-track offset of 1. The nadir view was found to have no across-track offset and an along-track offset of 1. This means (as the pass is ascending) that the forward image had to be moved west by 2 pixels and south by one pixel and the nadir image had to be moved one pixel south.

Recalculating the SST with these offsets using C.J. Merchant's ASST coefficients gives the new values for the 9-pixel box given in Table 23.

296.36	296.41	296.21
296.57	296.51	296.35
296.62	296.58	296.45

Table 23: Table showing the geocorrected ATSR SST values in Kelvin. The pixel in which the *in situ* data are taken is in the centre. Note: as this is an ascending pass the top left pixel is to the northwest and the bottom right is to the southeast.

The geocorrected data are similar to the uncorrected data with a similar east-west temperature gradient. The centre ATSR pixel has a value of 296.51 K, which is very similar to the *in situ* data (ΔT 0.14 K). The relatively uniform temperatures and lack of cloud flags make this a good validation point.

6.4.7 Night-time Ascending pass on the 31st July 1997

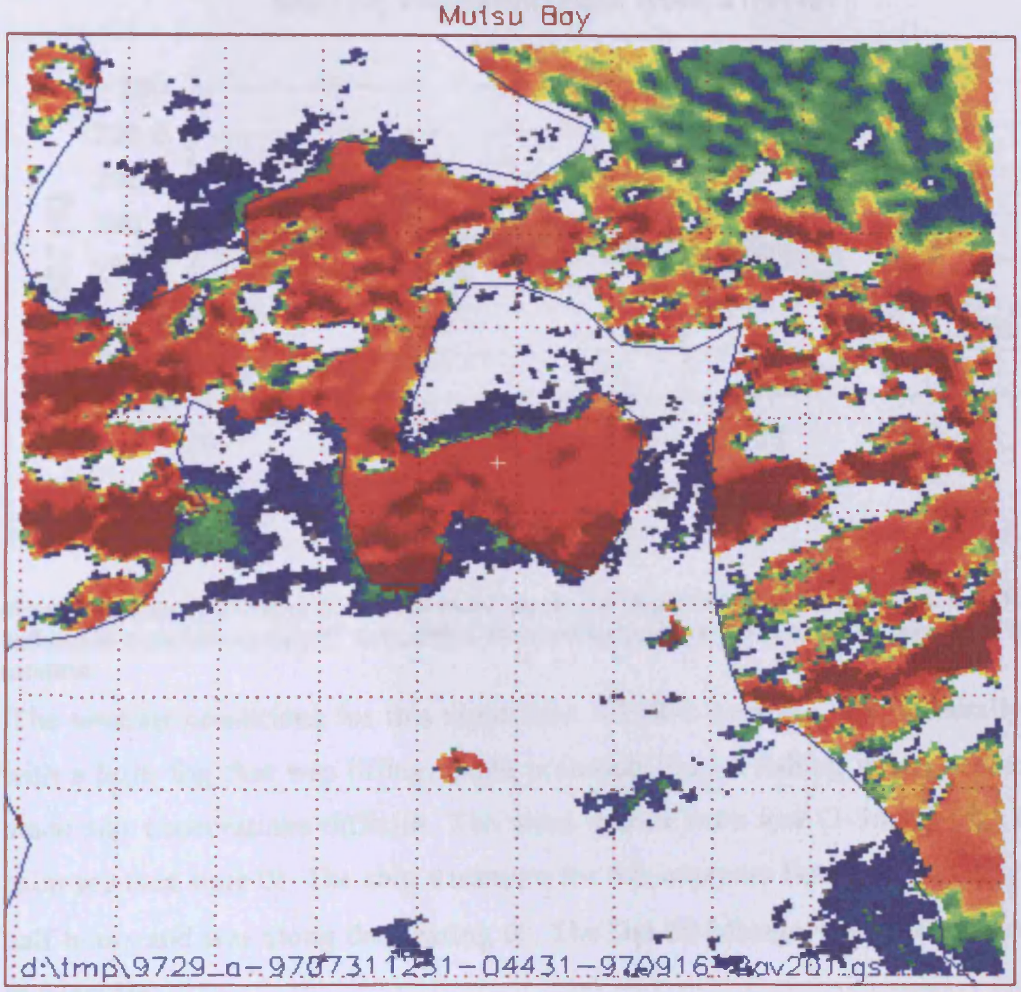

Figure 41: A sub-section (140 - 142° Longitude and 40-42° Latitude) of the ATSR image from the night-time pass on the 31st July 1997. The blue outline shows the ATSR land mask and the white cross the position of the Dai-Ni-Misago at overpass.

298.20	297.90	297.76
298.42	298.01	297.76
298.40	297.99	297.70

0 0	0 0	0 0
0 0	0 0	0 0
0 0	0 0	0 0

Table 24: Left –Table showing the standard GSST pixel in which the *in situ* data were taken (centre) and the surrounding eight pixels. These data have not been corrected for geolocation errors. Right – Table showing the forward (top) and nadir (bottom) cloud flags associated with each of these pixels. Note: as this is an ascending pass the top left pixel is to the northwest and the bottom right is to the southeast.

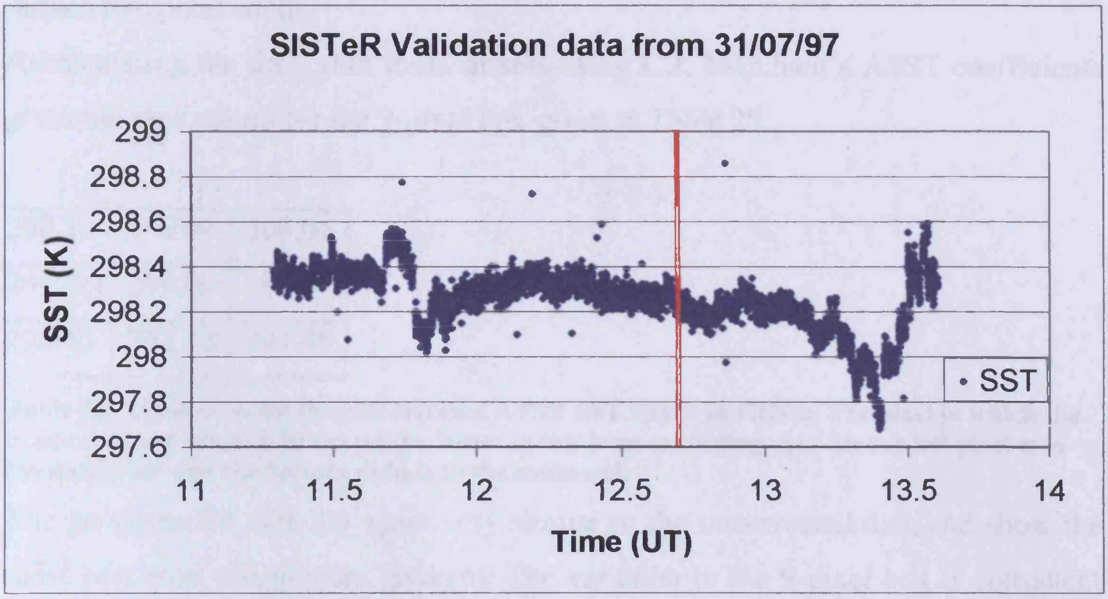

Figure 42: Graph showing the *in situ* radiometric (SISTeR) SST against universal time for the validation transect on the 31st July, 1997. The vertical red line is the time of overpass of the satellite.

The weather conditions for this night-time ATSR-2 overpass were generally calm with a light fog that was lifting. Light pollution from a fishing vessel to the south made star observations difficult. The wind speeds were low (1-3ms^{-1}) with a very calm sea (sea state 0). The ship's transect for this overpass lasted roughly two and a half hours and was along the bearing 0°. The Dai-Ni-Misago was at buoy number 6 at overpass.

All the forward and nadir ATSR pixels are flagged as cloud free (flag 0).

The surrounding pixels show a rising temperature gradient going from east to west with the temperature rising roughly 0.6 K. The *in situ* radiometric SISTeR temperature varies between 298.4 K and 297.8 K during the transect. This is consistent with the surrounding ATSR pixels. The SISTeR SST three minutes either side of overpass is 298.22 K. The centre satellite pixel has a value of 298.01 K (ΔT –0.21 K).

The forward view was found to have an across-track offset of 2 and an along-track offset of 2. The nadir view was found to have no across-track offset and an along-track offset of 1. This means (as the pass is ascending) that the forward image had to be moved west by 2 pixels and south by 2 pixels and the nadir image had to be moved one pixel south.

Recalculating the SST with these offsets using C.J. Merchant's ASST coefficients gives the new values for the 9-pixel box given in Table 25.

298.13	298.04	298.04
298.38	298.06	297.97
298.52	298.13	297.98

Table 25: Table showing the geocorrected ATSR SST values in Kelvin. The pixel in which the *in situ* data are taken is in the centre. Note: as this is an ascending pass the top left pixel is to the northwest and the bottom right is to the southeast.

The geocorrected data are again very similar to the uncorrected data and show the same east-west temperature gradient. The variation in the 9-pixel box is consistent with the variation seen in the *in situ* data. The centre pixel has a value of 298.06 K, which differs from the *in situ* data by a ΔT of –0.16 K.

6.4.8 Daytime Descending pass on the 3rd August 1997

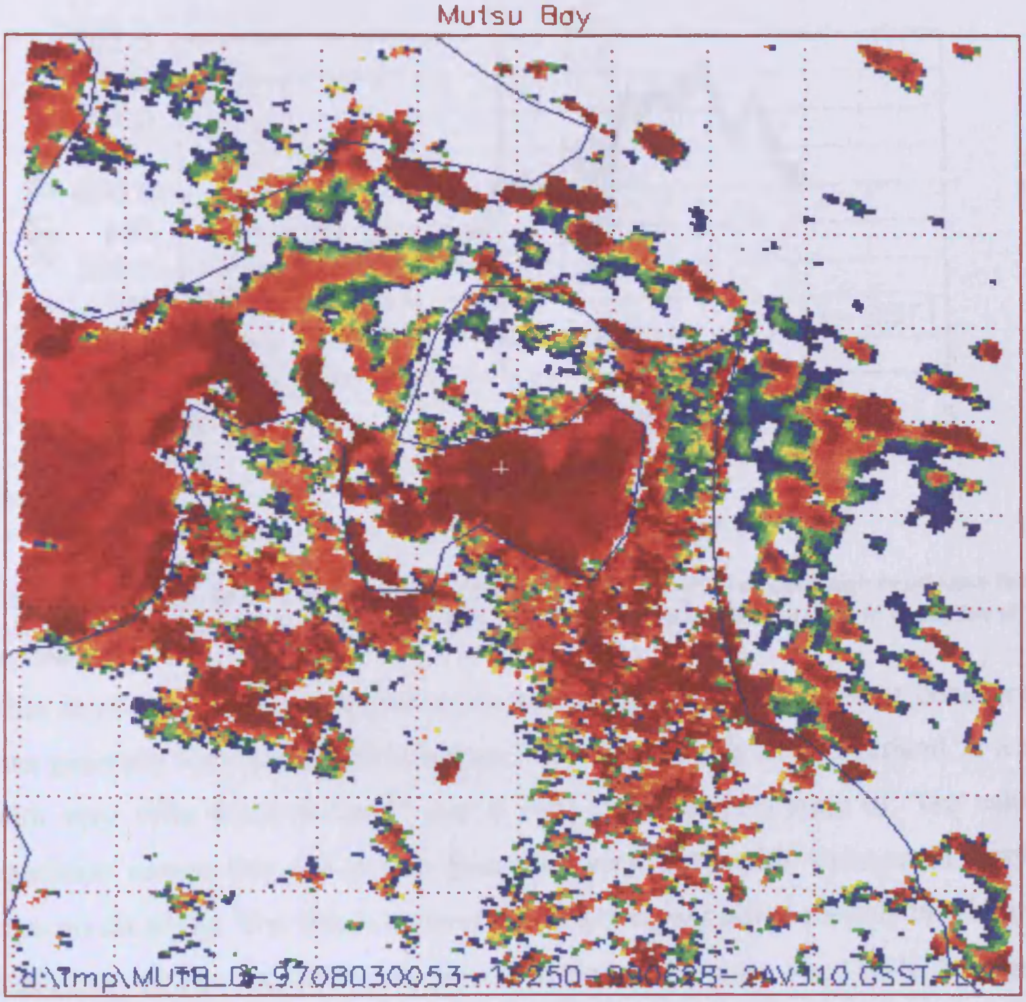

Figure 43: A sub-section (140 - 142° Longitude and 40-42° Latitude) of the ATSR image from the daytime pass on the 3rd August 1997. The blue outline shows the ATSR land mask and the white cross the position of the Dai-Ni-Misago at overpass.

301.14	300.86	300.55
300.95	300.85	300.60
300.94	300.90	300.81

0 0	0 0	0 0
0 0	0 0	0 0
10 0	0 0	0 0

Table 26: Left –Table showing the standard GSST pixel in which the *in situ* data were taken (centre) and the surrounding eight pixels. These data have not been corrected for geolocation errors. Right – Table showing the forward (top) and nadir (bottom) cloud flags associated with each of these pixels. Note: as this is a descending pass the top left pixel is to the southeast and the bottom right is to the northwest.

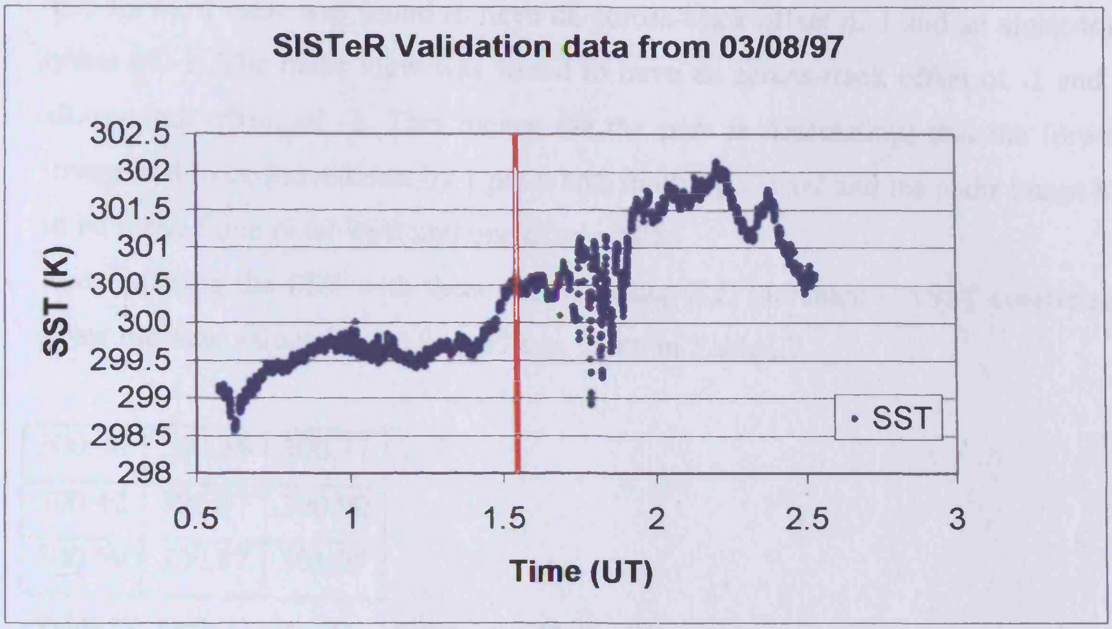

Figure 44: Graph showing the *in situ* radiometric (SISTeR) SST against universal time for the validation transect on the 3rd August, 1997. The vertical red line is the time of overpass of the satellite.

This daytime ATSR-2 overpass occurred during very calm weather conditions. It was generally very clear with less than 1 octa of cumulus cloud overland. It was hot with very little wind (0-1ms^{-1}) and a very calm sea (sea state 0). The calm sea condition meant that the sea surface was very dirty with widespread (probably natural) oil slicks. The ship's transect for this overpass lasted roughly two hours and was along the bearing 280° with the sun behind and to port. The Dai-Ni-Misago was roughly 500m from buoy number 6 at overpass.

All but one of the forward pixels are flagged as cloud free. The northeast pixel is flagged with cloud flag 10 (1.6μm reflectance histogram test). All the nadir ATSR pixels are flagged as cloud free (flag 0).

The surrounding pixels show a relatively uniform temperature with slightly cooler temperatures to the southwest. The *in situ* radiometric SISTeR temperature rises almost 3 K as a strong diurnal thermocline builds up during the day due to the calm conditions. The rapidly changing temperatures at about 1.40 UT are due to another ship passing in front of the Dai-Ni-Misago, breaking up the thermocline and mixing the surface waters. The SISTeR SST three minutes either side of overpass is 300.42 K. The centre satellite pixel has a value of 300.85 K (ΔT 0.43 K).

The forward view was found to have an across-track offset of 1 and an along-track offset of -1. The nadir view was found to have an across-track offset of -1 and an along-track offset of -1. This means (as the pass is descending) that the forward image had to be moved east by 1 pixel and south by 1 pixel and the nadir image had to be moved one pixel west and one pixel south.

Recalculating the SST with these offsets using C.J. Merchant's ASST coefficients gives the new values for the 9-pixel box given in Table 27.

300.36	300.56	300.77
300.42	300.67	300.90
300.59	300.87	301.27

Table 27: Table showing the geocorrected ATSR SST values in Kelvin. The pixel in which the *in situ* data are taken in is the centre. Note: as this is a descending pass the top left pixel is to the southeast and the bottom right is to the northwest.

The geocorrected data show a different situation to the non-corrected data. They show a strong rising temperature gradient, of roughly 1 K, going from southeast to northwest. The centre pixel has a value of 300.67 K that is closer to the *in situ* data than the non-corrected data (ΔT 0.25 K). This is reasonably close considering the rapidly rising SST and the high spatial variation.

6.4.9 Daytime Descending pass on the 25th August 1997

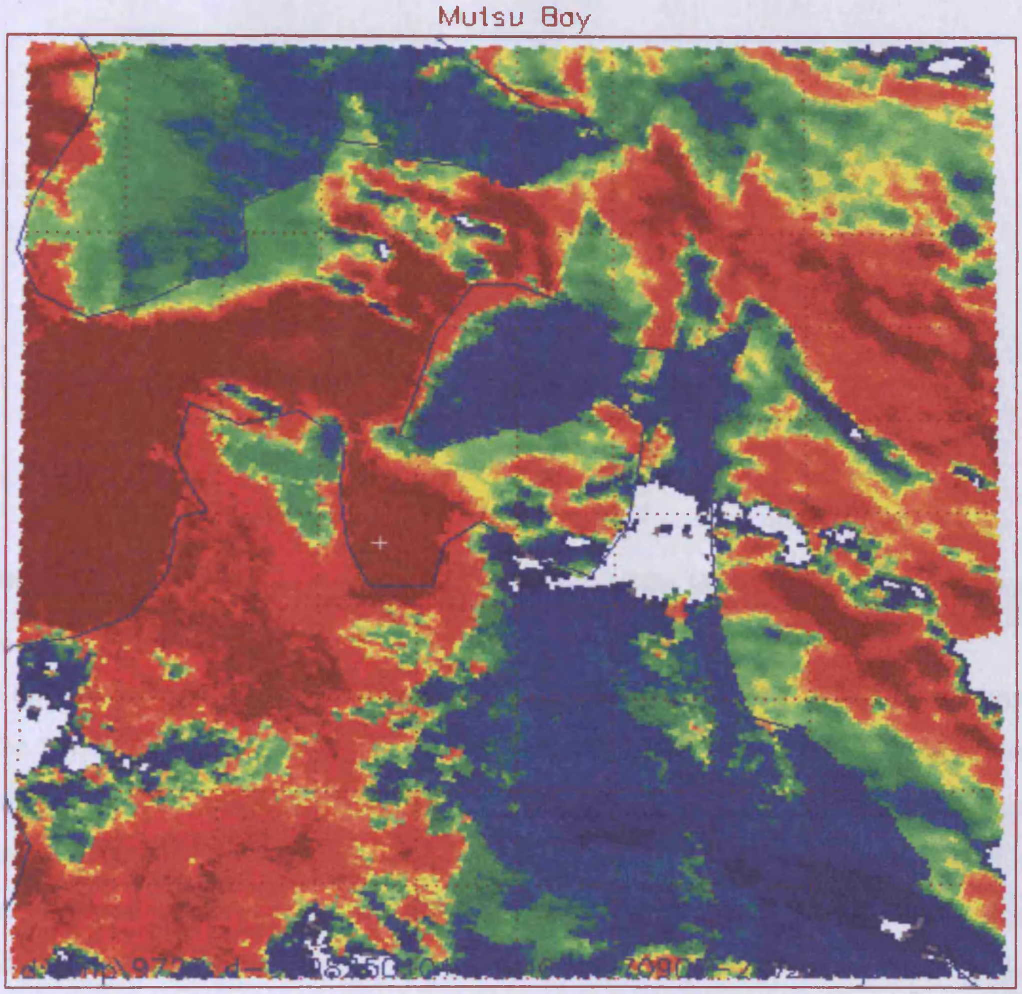

Figure 45: A sub-section (140 - 142° Longitude and 40-42° Latitude) of the ATSR image from the daytime pass on the 25th August 1997. The blue outline shows the ATSR land mask and the white cross the position of the Dai-Ni-Misago at overpass.

295.69	295.80	295.77
295.55	295.68	295.82
295.34	295.50	295.50

0 4	0 4	0 4
0 4	0 4	0 4
0 4	0 4	0 4

Table 28: Left –Table showing the standard GSST pixel in which the *in situ* data were taken (centre) and the surrounding eight pixels. These data have not been corrected for geolocation errors. Right – Table showing the forward (top) and nadir (bottom) cloud flags associated with each of these pixels. Note: as this is a descending pass the top left pixel is to the southeast and the bottom right is to the northwest.

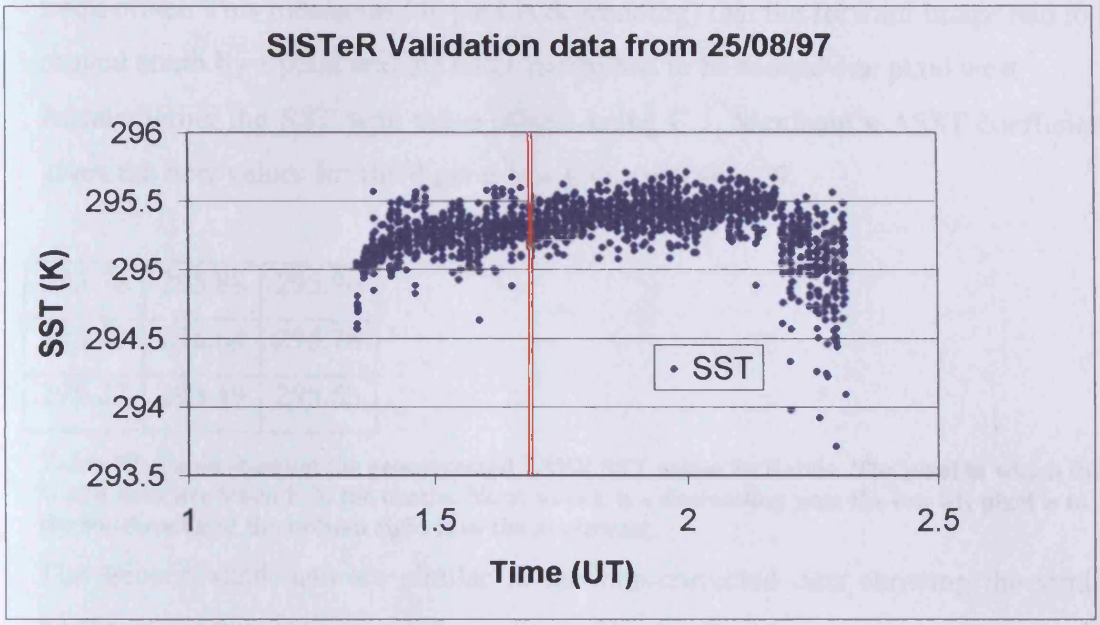

Figure 46: Graph showing the *in situ* radiometric (SISTeR) SST against universal time for the validation transect on the 25th August, 1997. The vertical red line is the time of overpass of the satellite.

The eastern side of Mutsu Bay was cloudy for this daytime ATSR-2 overpass but the western side of the bay was clear. For this reason the Dai-Ni-Misago was not near any of the buoys at overpass. It was clear overhead with cirrus and altocumulus cloud on the horizon. It was relatively rough with a sea state of 4 and a wind speed at buoy number six of 9 ms^{-1}. The ship's transect for this overpass was relatively short due to the time spent getting to the clear skies in the west. It lasted roughly an hour and was along the bearing 250-270° with the sun overhead and to port. Unfortunately, the meteorological station was not working at this time and there is a lack of meteorological data.

All the forward pixels are flagged as cloud free and all of the nadir ATSR pixels are flagged as possibly suffering from sunglint (flag 4).

The surrounding pixels show a relatively uniform temperature with a small temperature gradient going from northeast to southwest. The *in situ* radiometric SISTeR temperature slowly rises 0.5 K, from 295 K to 295.5 K, during the transect. The SISTeR SST three minutes either side of overpass is 295.26 K. The centre satellite pixel has a value of 295.68 K (ΔT 0.42 K).

The forward view was found to have no across-track offset and an along-track offset of -1. The nadir view was found to have an across-track offset of -1 and no along-track offset. This means (as the pass is descending) that the forward image had to be moved south by 1 pixel and the nadir image had to be moved one pixel west. Recalculating the SST with these offsets using C.J. Merchant's ASST coefficients gives the new values for the 9-pixel box given in Table 29.

295.78	295.88	295.96
295.48	295.64	295.78
295.27	295.49	295.53

Table 29: Table showing the geocorrected ATSR SST values in Kelvin. The pixel in which the *in situ* data are taken is in the centre. Note: as this is a descending pass the top left pixel is to the southeast and the bottom right is to the northwest.

The geocorrected data are similar to the non-corrected data showing the similar northeast-southwest temperature gradient. The *in situ* data seem to match these data as the *in situ* SST slowly increased as the ship went westwards. The centre ATSR pixel is slightly lower than the non-corrected data (295.64), but not significantly so, and this gives a ΔT of 0.38 K.

6.4.10 Summary of geolocation

Table 30 shows a summary of the geocorrection (in pixels) that had to be applied to each BT image. The exact value of the offset is a subjective value as often the offset is not exactly 'to the pixel' and a judgement has to be made as to which offset fits more closely. For this reason the offsets must be considered accurate to ±1 pixel.

Date	Forward View		Nadir View	
	Across-track	Along-track	Across-track	Along-track
MUBEX'96				
ATSR-1				
29/07/96	0	-1 (-1)	-1 (0)	-1 (-1)
ATSR-2				
05/08/96*	0 (0)	0 (-1)	0 (0)	-1 (-1)
06/08/96*	1 (-1)	3 (-3)	0 (0)	1 (-1)
MUBEX'97				
21/07/97	1	-1	0	-1
24/07/97	0	0	-1	0
25/07/97	2	1	0	1
31/07/97	2	2	0	1
03/08/97	1	-1	-1	-1
25/08/97	0	-1	-1	0

Table 30: Table showing the offset, in pixels, of the geolocation of the forward and nadir BT images of the validation points during the MUBEX campaign. The figures in brackets are those published in Parkes *et al.* 2000.

Note: The published Parkes *et al.* 2000 offsets are in terms of latitude and longitude whereas the offsets in Table 30 are in terms of image pixels. This is the reason for the difference in sign for the ascending pass on the 6th August 1996.The offsets for the MUBEX'96 ATSR-2 overpasses appear to be the opposite way round to those published in Parkes *et al.* 2000. This is a typographic error and has been printed the correct way round in this table.

There does not appear to be any pattern to the size or nature of the offsets. The largest offset in the forward view, on the 6th August, equates to an error of about 3km on the ground. This highlights the need for extreme care when validating in areas of high thermal variation. In the case of Mutsu Bay, the distinctive shape of the bay could be used to geolocate each ATSR view but this might not always be possible, especially in open ocean, and this could lead to large errors.

6.4.11 Geocorrected Data

Table 31 shows similar data to Table 10 but for geocorrected data. It shows the satellite SST calculated using the original and new (March 2000) C.J. Merchant coefficients, the *in situ* SST and the ΔT between the satellite and *in situ* SSTs. It also gives the nadir and forward cloud flags associated with each validation pixel. The data have been geocorrected by aligning each forward and nadir image with a land mask, measuring the offset and then applying this offset when recalculating the SST following the method described in section 6.3.2.

Overall, the geocorrected data match the *in situ* data more closely than the non-corrected data as expected. This implies that some of the 'noise' seen in the non-corrected data is due to geolocation errors and that these errors can be reduced by geolocating each BT image. Average ΔT values are discussed in the next section.

Date	Ascending or Descending Pass	Nadir Cloud Flags	Forward Cloud Flags	ATSR SST (K) (CM Original)	ATSR SST (K) (CM New)	SISTeR SST (K)	ATSR-SISTeR (K) (CM Original)	ATSR-SISTeR (K) (CM New)
MUBEX'96								
ATSR-1								
29/07/96	D	0	0	294.15	N/A	294.18	-0.03	N/A
ATSR-2								
05/08/96	D	4	10	294.40	294.4	293.96	0.44	0.44
06/08/96	A 2 – Channel SW pixel	0	0	294.29 294.34 *293.55**	293.93 294.34 *293.19**	293.51	0.78 0.83 *0.04**	0.42 0.83 *-0.32**
MUBEX'97								
21/07/97	D	4	10	296.45	296.5	295.46	0.99	1.04
24/07/97	D	4	10	294.5	294.44	294.99	-0.49	-0.55
25/07/97	A 2 – Channel	0	0	296.51 296.24	296.14 296.26	296.37	0.14 -0.13	-0.23 -0.11
31/07/97	A 2 – Channel	0	0	298.06 298.21	297.69 298.16	298.22	-0.16 -0.01	-0.53 -0.06
03/08/97	D	0	0	300.67	300.64	300.42	0.25	0.22
25/08/97	D	4	0	295.64	295.61	295.26	0.38	0.35

Table 31: A table showing geocorrected validation data. The table shows for each potential validation overpass, the nadir and forward cloud flags, the SST calculated using the original and new (March 2000) C.J. Merchant coefficients, the *in situ* SST and the ΔT between each satellite and *in situ* SST. Whether a pass is either ascending (A) or descending (D) is also stated and in the case of night-time passes a 2-channel SST is also calculated. These data have been smoothed using the SST-11μm method. * Note: The reprocessed geolocated data for the 6th August 1996 still shows a lot of thermal variation (~1 K) in the eight pixels surrounding the validation point. The pixel to the southwest of the validation point has a value of 293.55 K that is much closer to the *in situ* value. It is possible that the *in situ* data are from an area of mixing between the two pixels and measure an SST that is more representative of the southwest pixel than the validation pixel. This value is given in italics in Table 31.

6.5 Summary of MUBEX Validation points

Table 32 shows average ΔT values between the *in situ* SISTeR SST and the ATSR-2 SST calculated with the V320 coefficients currently being used to process ATSR-2 data. The table includes some of the non-geocorrected data shown in Table 11 for comparison. The column on the far right show values that would be obtained if it assumed that the *in situ* data on the 6th August 1996 is more representative of the southwest pixel than the centre pixel as explained in section 6.4.3.

As only one ATSR-1 pass was obtained, mean ΔT values cannot be calculated. This ATSR-1 overpass had a ΔT of 0.069 with the un-geocorrected data and –0.031 with the geocorrection applied. This implies that the reprocessed ATSR-1 data are more accurate than the original processing (ΔT –0.54 K see chapter 6.3.1) and that the cool bias has been corrected. However, only limited conclusions can be drawn from one data point.

	Non-geocorrected	**Geocorrected**	
	CM Original	**CM Original**	**06/08/96 pixel change**
Mean (all)	0.39 ±0.45	0.29 ±0.48	*0.20 ±0.44*
Mean (Cloud Free)	0.34 ±0.52	0.25 ±0.39	*0.07 ±0.17*
Mean (Cloud Free '97)	0.14 ±0.43	0.08 ±0.21	

Table 32: Table showing the mean ΔT between the ATSR-2 and *in situ* radiometric SST for the geocorrected MUBEX data. The non-geocorrected data (from Table 11) has been included to aid comparison. The mean values are for all match-ups, all cloud free match-ups and the cloud-free MUBEX'97 match-ups respectively. Note: Night-time data have also been processed using the two-channel algorithm for completeness but the three-channel algorithm value has been used to calculate these means. The means using only the two-channel algorithm are presented in Table 34.

The ATSR-2 data show that the instrument is meeting its design accuracy (Smith *et al.*, 1994). The standard product GSST, when cloud cleared, shows a warm bias of 0.30 K with an rms error of 0.48 K in the Mutsu Bay area. This value is unlikely to be representative of the instrument performance as a whole as the bay shows a high degree of local thermal variation and errors in geolocation led to errors in validation. If attempts are made to minimise the errors due to incorrect geolocation, then the error drops to a warm bias of 0.25 ± 0.39 K. The point on the 6th August 1996 appears to be biasing the results. If just cloud-free 1997 data are used, the error is 0.08 ± 0.21 K and if the southwest pixel from the 6th August 1996 is used the error becomes 0.07 ± 0.17 K. This value is likely to be more representative of the instrument performance in general as the majority of data are collected in the open ocean where thermal gradients are usually less steep.

These values are valid for the standard GSST product (SADIST-2 Version 320) produced by RAL at the time of writing (March 2000). Further work is currently underway to improve the coefficients and it is likely that in the future the standard product will use new coefficients. Table 33 presents the results of using the new coefficients (released by C.J. merchant on the 16th March) to calculate ATSR SSTs, using the same geocorrection as in Table 32.

	CM New	**06/08/96 pixel change**
Mean (all)	0.14 ±0.55	*0.05* *±0.56*
Mean (Cloud Free)	-0.03 ±0.43	*-0.22* *±0.32*
Mean (Cloud Free '97)	-0.18 ±0.38	

Table 33: A table showing identical data to Table 32 but for satellite SST values calculated with the new Merchant coefficients. The table shows the mean ΔT between the ATSR-2 and *in situ* radiometric SST for geocorrected MUBEX data.

C.J. Merchant's new coefficients give ambiguous results. They give a smaller offset than the earlier coefficients, if the correction for the 6th August 1996 is not made but they give a larger rms error value and do not help reduce the uncertainty. The coefficients are very new however and more analysis is needed. Unfortunately, they were released too late for a detailed analysis in this thesis. C.J. Merchant and Jo Murray (in late March 2000) suggested that, as the three-channel algorithm is still under investigation, only the two-channel algorithm could be used.

	Geocorrected	
	Two- Channel CM Original	**06/08/96 pixel change**
Mean (all)	0.28 ±0.49	0.19 ±0.44
Mean (Cloud Free)	0.24 ±0.43	0.04 ±0.17
Mean (Cloud Free '97)	0.04 ±0.19	

Table 34: Table showing the mean ΔT between the two-channel ATSR-2 SST and *in situ* radiometric SST for the geocorrected MUBEX data. The non-geocorrected data (from Table 11) has been included to aid comparison. The mean values are for all match-ups, all cloud free match-ups and the cloud-free MUBEX'97 match-ups respectively. Table 32 shows the means calculated using the three-channel algorthm that was considered suspect at the time of writing.

Comparing Table 32 and Table 34 shows that using only the two-channel algorithm (day and night) gives better agreement with the *in situ* data than using the three-channel algorithm at night and the two-channel algorithm during the day. These data show that the three-channel algorithm is causing a warm bias. The effect is small and these data are not conclusive (due to the small number of data points). The work done by M.J. Murray and C.J. Merchant show the warm three-channel algorithm problem more clearly (Murray, 2000).

All the results presented here have a large error associated with them that limits the conclusions that can be drawn. This error is partly due to the high thermal variations of the bay and partly due to the small number of validation points. More validation points, preferably in open ocean, where there is much less local thermal variation, at various latitudes, are needed to verify these results.

6.6 CHAOS'98 Data

Unfortunately, despite being at sea for five and a half weeks, no clear overpasses were obtained during the CHAOS'98 cruise. This highlights the difficulties involved with the validation of satellites using *in situ* radiometers. The cost of dedicated cruises and the amount of ship time needed to obtain a reasonable numbers of validation points makes it very expensive. To this end, C.J. Donlon, with T.J. Nightingale and others, is currently designing and building a cheap, autonomous, self-sealing radiometer that can be deployed on ships of opportunity (oil tankers, freighters etc.). Such a system could greatly increase the number of skin validations of satellite SSTs and reduce the large errors that currently exist.

6.7 The Accuracy of the ASST Product

The accuracy figures stated in section 6.5 are for the high-resolution $1km^2$ product. The ASST product is the main product used for climate change studies and the accuracy of this product is therefore of interest. Each one-degree ASST pixel contains about 2500 $1km^2$ pixels. If the worst-case scenario is taken and the SD error associated with each pixel is of order 0.5 K, and it is assumed that this error is statistical in nature, then the error of an ASST pixel is of order 0.01K. This is well within the design criteria and means that it is important to calculate the absolute accuracy of the ATSR ASST product, as this is now the limiting error. The data presented here have a large uncertainty associated with the offset (due to the reasons described above) and so the absolute accuracy of the ASST product can only be stated as 0.07±0.17 K.

6.8 Cross-Calibration

ATSR-1 operated until June 1996. Data is available from ATSR-2 from May 1995. This gives a potential overlap period of 13 months. Unfortunately, due to a scan mirror malfunction ATSR-2 was not operational from January to June 1996. This leaves 7 months of coincident data that can be used for cross-calibration purposes. The cross-calibration between instruments is important because of the need for a continuous data set (spanning at least 10 years) for climate change studies and to check that both instruments are functioning correctly. In the case of climate change studies, any discontinuity in the data sets will lead to an artificial warming or cooling of global temperatures. In order to cross-calibrate the ATSR instruments, average global SSTs are calculated for each month in the two overlapping data sets. Unfortunately, at the time of writing this thesis, errors in the current coefficients used to generate both ATSR data sets (see chapter 6.2) mean that this work cannot be done with the currently available data.

Once the ATSR-1 data has been reprocessed to take into account the detector warming and the ATSR-2 data reprocessed to eliminate the current errors this work will need to be done to compare the relative performance of both instruments using the new processing.

6.9 Summary

The results presented in this chapter indicate that both the ATSR instruments are working accurately and to specification although care must be taken when making statements about both instruments as there are only a few data points and this is only one geographical area. There are currently however, known problems with both the ATSR-1 and 2 datasets that are being addressed. It can be said however, that in areas of low thermal variation, for the Mutsu Bay area, the standard ATSR-2 GSST product processed with the SADIST-2 V320 suite is accurate to 0.07±0.17 K. These numbers are likely to change as the SADIST-2 processing suite is upgraded in the future and this work will need to be repeated using the new data. Table 35 presents a summary of the validation points from this chapter.

Date and time	**Satellite SST (K)**	***In Situ* SST (K)**	**Weather Summary**	**Comments**
ATSR-1				
29/07/96 AM	294.15	294.18	Clear O/H, sea state 3 increasing, wind speed 5-7 ms^{-1}	Included
ATSR-2				
05/08/96 AM	294.40	293.96	Light haze O/H, sea state 1-2, wind speed 3-5ms^{-1}	Rejected due to cloud flags
06/08/96 PM	294.29	293.51	Haze on horizon, sea state 2-3 increasing, wind speed 3-5 ms^{-1}	Suspect – see 6.4.3
21/07/97 AM	296.45	295.46	Clear O/H, calm, sea state 0-1, wind speed 3-4 ms^{-1}	Rejected due to cloud flags
24/07/97 AM	294.50	294.44	Clear O/H, cloud building, sea state 1, wind speed 0-2 ms^{-1}	Rejected due to cloud flags
25/07/97 PM	296.51	296.37	Clear, calm, sea state 2, wind speed 1-3 ms^{-1}	Included
31/07/97 PM	298.06	298.22	Calm, light lifting fog, sea state 0, wind peed 1-3 ms^{-1}	Included
03/08/97 AM	300.67	300.42	Clear, hot, calm, sea state 0, wind speed 0-1 ms^{-1}	Included
25/08/97 AM	295.64	295.68	Clear O/H - cloud to the East, sea state 4, wind speed 9 ms^{-1}	Rejected due to cloud flags

Table 35: A summary of the validation points from the MUBEX'96 and '97 campaigns

7 Observations of the Skin Effect

7.1 Introductions

7.1.1 General

This section looks at the wind speed dependence of the skin effect (introduced in section 3.2.3) from data taken during the MUBEX'97 campaign (see section 4.3.2) and the CHAOS'98 cruise (see section 4.3.3). The aim of this chapter is to study the results obtained from these campaigns and to compare them with similar data sets from other authors. The implications of these results on the validation of satellite SSTs are then discussed. These results from this chapter were published along with data from two ROSSA-AMT cruises in Donlon *et al.* 1999c (See section 9.3).

7.1.2 Previous Work

There is a range of published data on the skin effect. Table 36 shows a selection of the range of values found by various authors.

Author	**Date**	**Mean ΔT (K)**	**Range of ΔT (°K)**	**Comments**
Woodcock and Stommel	1947		-0.5 to -1.0	Special mercury in glass thermometer used.
Ewing and McAlister	1960		-0.6	Night observations
Hasse	1963		-0.1 to -0.3	
Saunders	1967		-0.2 to -0.35	
Hill	1972		-0.1 to -2.0	Laboratory experiment
Paulson and Parker	1972		-1.14 to - 1.81	Laboratory experiment
Grassl	1976		-0.17 to - 0.21	
Katsaros	1977		-0.25 to -0.4	Laboratory experiment
Schooley	1977		-0.2	
Nicholls	1979	~ -0.5 ± 0.3		
Simpson and Paulson	1980		-0.15 to - 0.30	
Paulson and Simpson	1981		0.3 to -0.4	
Schluessel *et al.*	1987		0.6 to -0.3	
Emery	1989		2.0 to -2.0	
Hepplewhite	1989	-0.3 ± 0.3	0.6 to -1.4	
Coppin *et al.*	1991	-0.3 ± 0.14	1.0 to -1.5	
Schluessel *et al.*	1992		1.0 to -1.0	

Jessup	1992		0.0 to -0.5	
Emery *et al.*	1993-94		1.0 to -1.0	
Donlon	1994	-0.4 ± 0.31	0.5 to -1.8	
Sheasby (MUBEX'97)	*1997*	*0.39 ±0.80*	*3.45 to -1.87*	*Very calm conditions*
Sheasby (CHAOS'98)	*1998*	*-0.15 ±0.13*	*1.73 to -0.96*	

Table 36: Table of previously published ΔT data. The values in italics are from the data presented in this thesis. (from Robinson et. al 1984 and Donlon 1994)

The previous work shows a wide variety in the magnitude and range of ΔT. This variety is due to:

- the different methods of measuring the 'skin' SST
- the different accuracy of the radiometric measurements (and sky corrections)
- the different depths and accuracy of the bulk measurements
- the wide variety of conditions under which the data were taken (e.g. day/night measurements, thermoclines forming etc.).

Data taken only at night eliminate a lot of the variation due to environmental conditions. Table 37 shows data from two previous PhD theses (Donlon 1994 and Wick 1995) that has been separated into day and night values. The last two rows are the MUBEX'97 and CHAOS'98 data sets collected as part of this thesis.

Data Set	**Author**	**Day and Night Data**		**Daytime only data**		**Night-time only data**	
		Mean (K)	**SD (K)**	**Mean (K)**	**SD (K)**	**Mean (K)**	**SD (K)**
Meteor	Wick	-0.15	0.28	0.04	0.30	-0.31	0.14
Valdivia	Wick	-0.24	0.21	-0.20	0.18	-0.27	0.08
Malcolm Baldrige	Wick	0.00	0.22	0.09	0.28	-0.10	0.10
TOGA COARE	Wick	-0.15	0.19	-0.08	0.18	-0.23	0.08
CEPEX	Wick	-0.21	0.16	-0.21	0.09	-0.21	0.05
Flip	Wick	-0.17	0.29	-0.06	0.26	-0.28	0.24
JCR'92	Donlon	-0.4	0.31	-0.48	0.38	-0.30	0.31
MUBEX'97	*Sheasby*	*0.39*	*0.80*	*0.51*	*0.83*	*-0.17*	*0.07*
CHAOS'98	*Sheasby*	*-0.15*	*0.12*	*-0.14*	*0.13*	*-0.16*	*0.11*

Table 37: Table showing mean values of the skin-bulk *(ΔT)* difference obtained from a variety of campaigns. The standard deviation of the data is also shown. The day and night only values are shown as well.

The day only data show a large variation in ΔT but the night-time data are much more consistent. This shows that the processes that occur during the day greatly increase the variation in ΔT. The night-time data show a consistently cool ΔT of about 0.2 K.

7.1.3 Wind Speed Dependence

Previous work (e.g. Schlüssel 1990, Wick 1995, Donlon 1994, Donlon and Robinson 1997) has shown wind speed dependence (among other factors) of the skin effect. Previous studies have mainly used data from less accurate radiometry and from deeper bulk SST thermometers (typically 2-5 metres). Donlon and Robinson 1997 conclude that at high wind speeds (high u) the value of ΔT has a mean value of approximately –0.1 K with no evidence of a wind speed dependence above 10 ms^{-1}. They state that their data was limited by the accuracy of the radiometer, the accuracy of the BSST measurements and scarcity of data in some wind regimes. These problems were eliminated in the data sets from the three cruises presented in Donlon *et al.* 1999c and in the MUBEX'97 results. The CHAOS'98 data set is one of the data sets used in Donlon *et al.* 1999c. Unfortunately due to the noise problem with the SISTeR radiometer during MUBEX'96 (see chapter 5.4.1) the data was not accurate enough to use here.

7.2 Results

7.2.1 MUBEX'97

7.2.1.1 The data

A detailed description of the MUBEX campaigns is given in chapter 4.3.2. All data collected during MUBEX was logged with the time (UT) at which it was taken in order to aid later processing and comparisons. The radiometric data collected during MUBEX'97 were taken using the SISTeR radiometer (see Chapter 5). The radiometer was on a platform on the bow of the ship five metres above the surface and looking forward at an angle of 18°. A sky brightness temperature was also measured at the complimentary angle (162°). The brightness temperatures were converted to a sea surface temperature using a suite of IDL programs using the method described in Appendix 2. The bulk temperature used here is from the CTD instrument that was deployed over the side of the research vessel at a depth of approximately 0.75 m. This depth tended to vary as the ship rolled depending on the sea state. The CTD data was logged every second. There was a temperature profiler deployed by the Japanese side but unfortunately, the calibration of the thermometer chain was considered suspect (S. Tamba – personal communication 1999) so the CTD temperature measurement was used as it was calibrated before and after the campaign. The calibrated meteorological station, provided by the UK side, logged all data every second. Unfortunately, the meteorological station stopped working on the 30th July 1997. After this time, a spare SSO, provided by the Japanese side, was attached to the rear of the research vessel as a back up measure to give meteorological measurements. As it could only be placed at the rear of the vessel due to physical limitations, it was not in clear air and data from this instrument has not been used. The weather conditions during this period were generally quite calm and (aided by the sheltered and shallow nature of the bay) quite strong diurnal thermoclines often built up during the day.

7.2.1.2 Data Processing Method

The CTD and meteorological data were interpolated to each SISTeR data point. The wind speeds were corrected for ship speed during transects by assuming a speed of 1 knot. They were then also corrected to a standard 10m height following Smith 1988. A skin-bulk temperature *(ΔT)* was then generated for each SISTeR data point. There were a total of 35884 data points collected.

7.2.1.3 The Distribution of ΔT

Figure 47 is a histogram of all ΔT values calculated from the data collected during MUBEX'97.

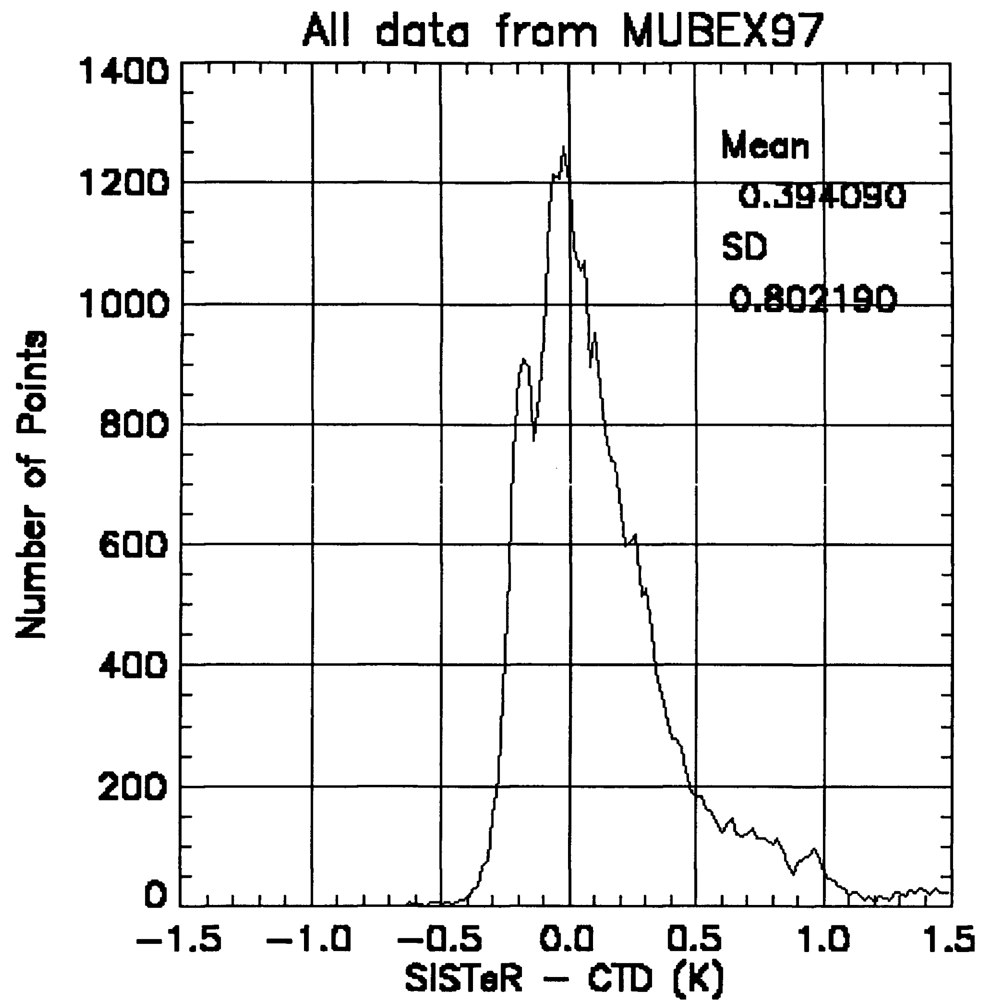

Figure 47: Histogram of all available ΔT measurements taken during the MUBEX'97 campaign.

The mean value of ΔT is 0.394 K with a large standard deviation of 0.802 K. These values agree with those found by previous authors (see Table 36) although the variation is larger than previously published data. The large variation in ΔT (-1.87 to 3.45 K) is due to the sheltered nature of the bay and the calm conditions. These lead to strong diurnal thermoclines forming during the day. As the CTD was at a depth of 0.75 metres it often measured a much cooler 'bulk' temperature than what the 'bulk' temperature at the surface actually was. This gives the impression of there being a strong 'warm skin' when in fact there is usually still a cool skin across the ocean-atmosphere interface. This is one of the problems of studying the skin effect. Care must be taken (especially in calm conditions such as these) to define exactly where the 'bulk' measurement is made. At night, the thermocline breaks down and so the 0.75 metre bulk is more representative of a surface bulk temperature. Figure

48 and Figure 49 show the data separated into day and night data only. There were 29960 daytime points and 5924 night-time points.

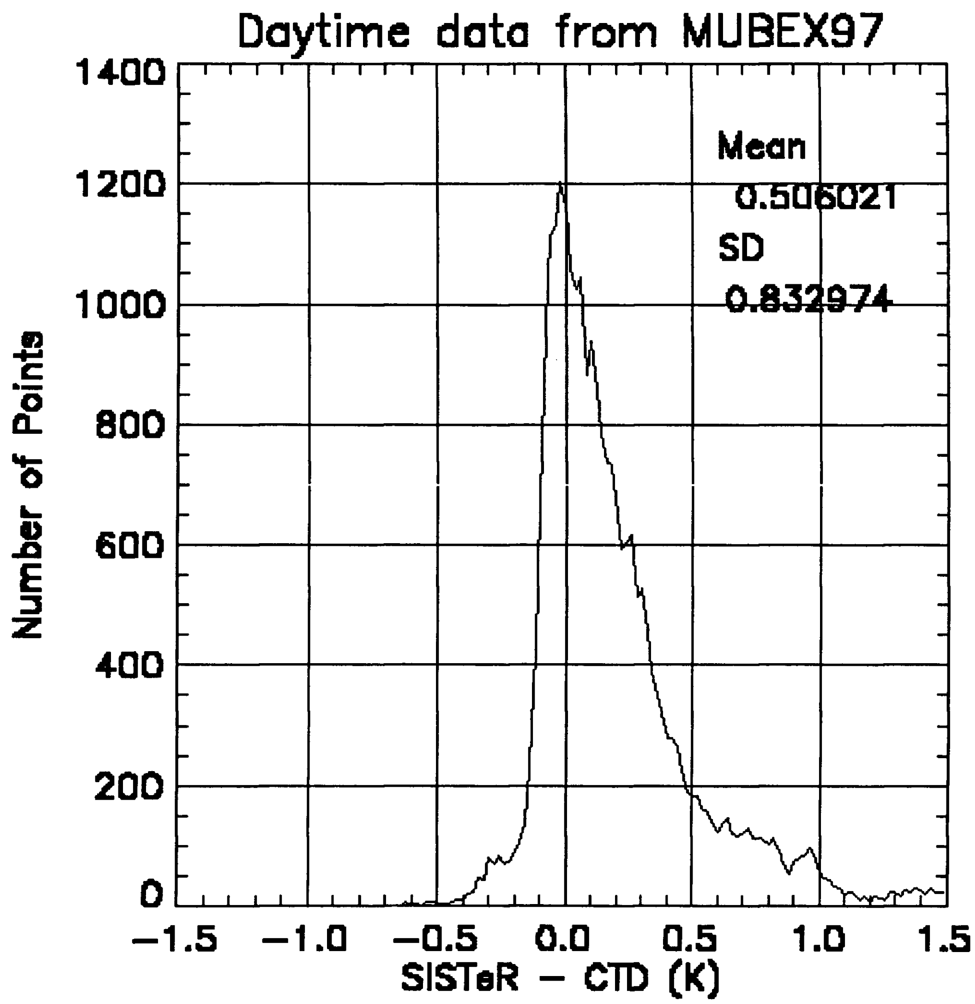

Figure 48: Histogram of all available daytime ΔT measurements taken during the MUBEX'97 campaign.

The daytime data show a warmer mean ΔT of 0.506 K with a similar standard deviation (0.833 K) to the complete data set. This is to be expected as the night-time data will give a cool bias to the data and most of the variation comes from the daytime data. The daytime data peaks at about –0.1 K showing that a cool skin of this magnitude is still very common. These daytime only data presented here show a larger range of ΔT values than previously published data (see Table 37). This is due to the sheltered nature of Mutsu Bay and the calm condition encountered that led to strong thermoclines forming. These large extremes are less common in data sets from the open ocean and are not seen in the CHAOS'98 data set (section 7.2.2).

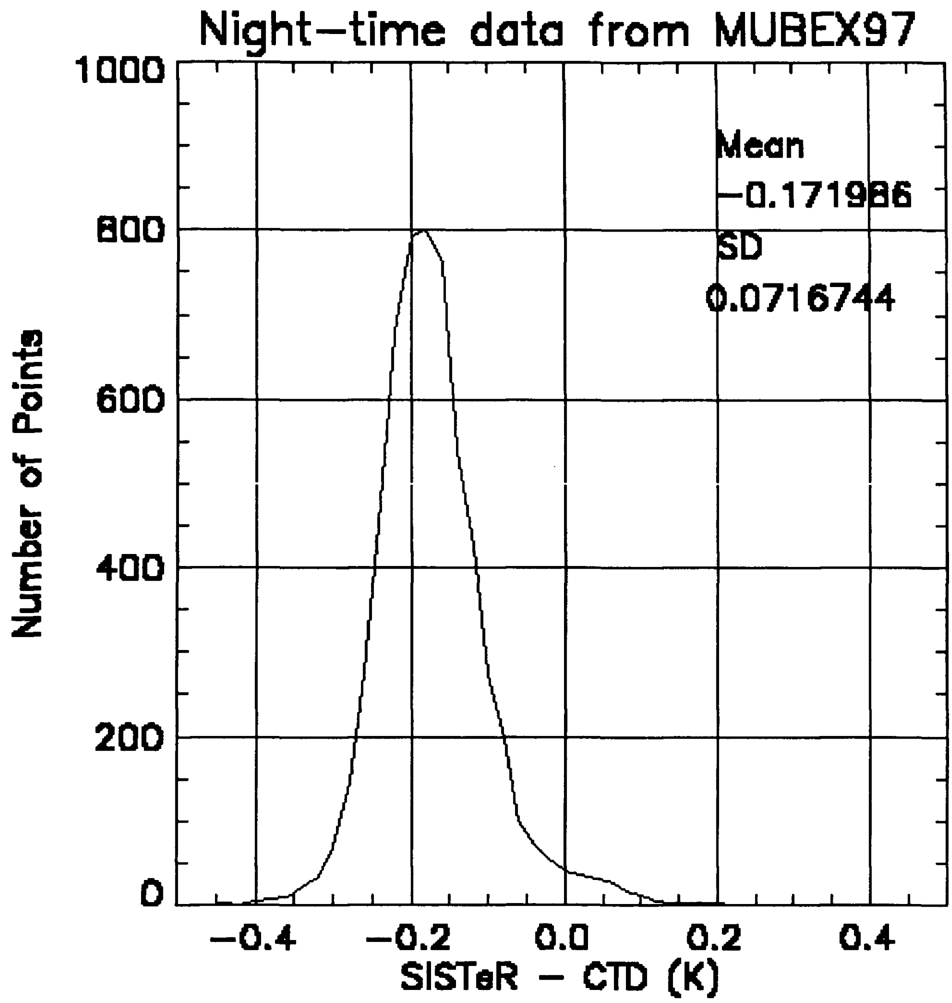

Figure 49: Histogram of all available night-time ΔT measurements taken during the MUBEX'97 campaign.

The night-time data has a mean value of –0.172 K and a much smaller standard deviation of 0.072 K. This is because the night-time data does not suffer from the problem of diurnal warming seen in the daytime data. This value of ΔT is in close agreement with the values found during the CHAOS'98 cruise (see chapter 7.2.2) and published in Donlon *et al.* 1999c.

7.2.1.4 Wind Speed Dependence

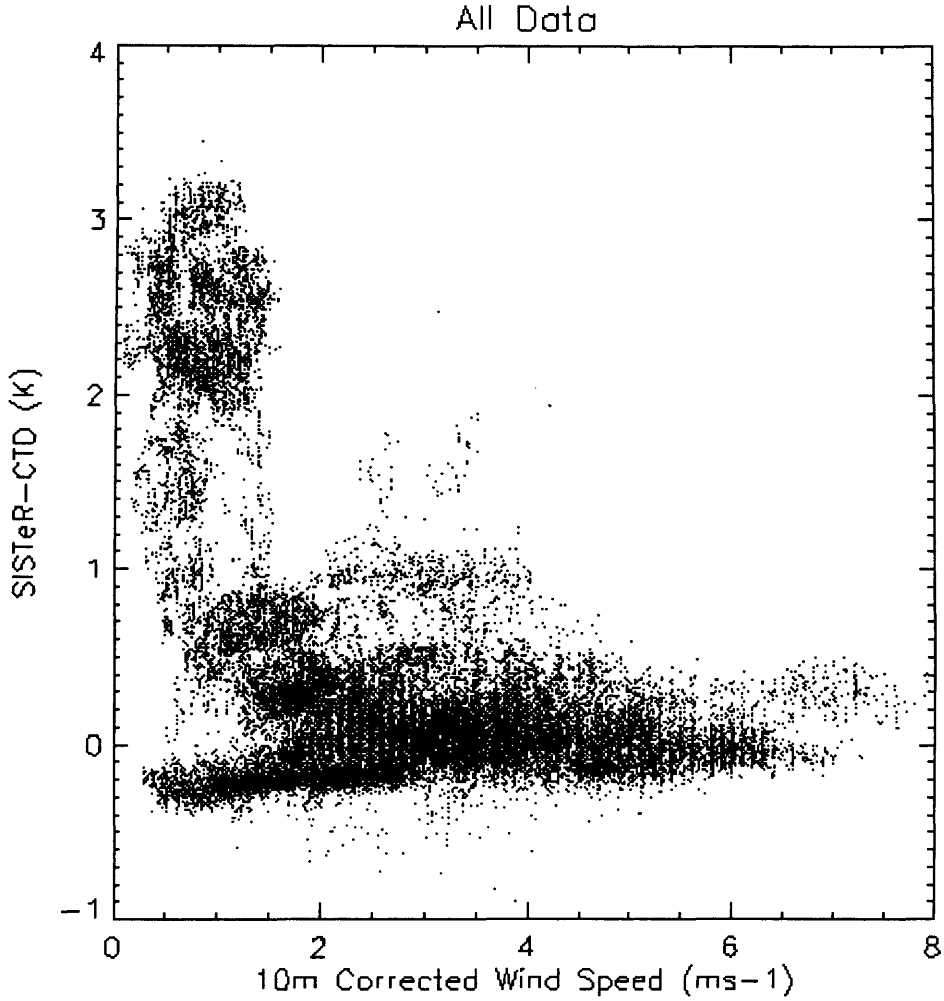

Figure 50: Graph showing all calculated ΔT values from the MUBEX'97 UK data as a function of wind speed. The wind speed has been corrected to a standard 10m height following Smith 1988.

Figure 50 shows all the ΔT values collected during the MUBEX'97 campaign as a function of the corrected 10-metre wind speed. The data show that the variation of ΔT decreases as the wind speed increases. The large variation at low wind speeds is because the diurnal thermocline tends to be strongest at low wind speeds. The mean ΔT has been calculated for one ms^{-1} wind speed intervals and separated into day and night values. These mean ΔT values have been plotted in Figure 51.

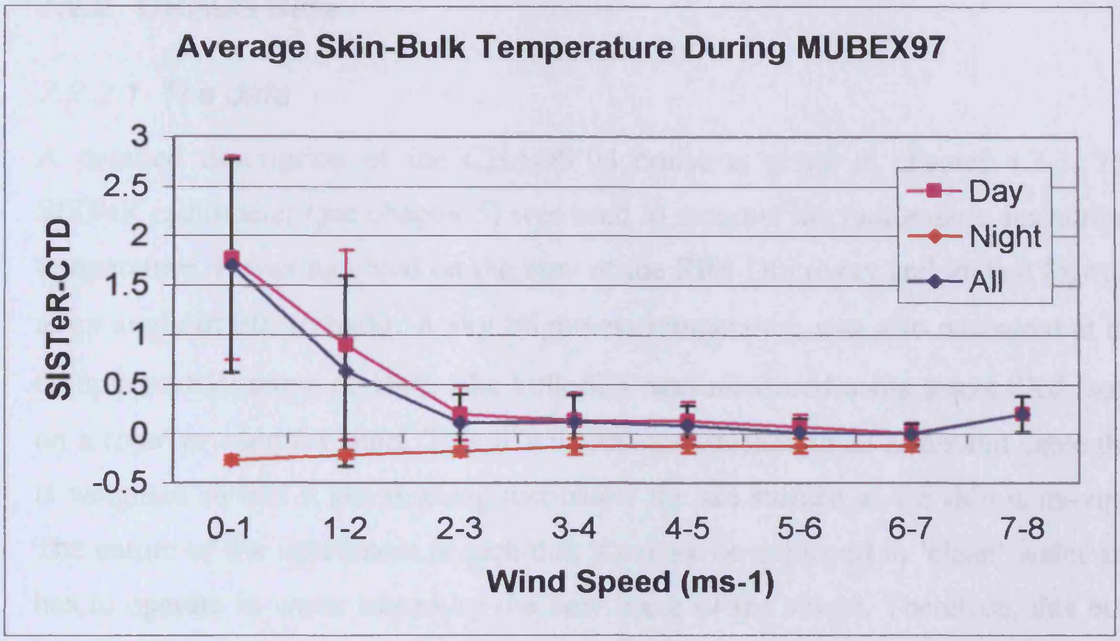

Figure 51: Graph of the average SISTeR-CTD temperatures *(ΔT)* for various wind speed ranges during the MUBEX'97 campaign. The three lines show all data, daytime only data and night-time only data.

The night-time data shows a relatively small amount of scatter and a constantly cool skin that tends to a value of about -0.12 K at higher wind speeds. This is similar to the results published in Donlon *et al.* 1999c.

The daytime data shows a large amount of scatter as stated above. These data do not tend to the values published in Donlon *et al.* 1999c. This is probably due to the shallow and sheltered nature of the bay that allows a thermocline to build up even at reasonably high wind speeds. The Donlon *et al.* 1999c data were taken in the open ocean where the almost unlimited fetch and much deeper water lead to more mixing of surface waters. The bulk data (CTD data) presented here are taken at a deeper depth than that published in Donlon *et al.* 1999c and so will not be directly comparable.

The data from MUBEX'97 are a very from very limited conditions. They come from a small range of latitudes and are in a sheltered bay. These data compliment and are complimented by the data collected during the CHAOS'98 cruise that covered a wide range of latitudes (20° N to 60° N) and a wide range of weather conditions in open ocean.

7.2.2 CHAOS Data

7.2.2.1 The data

A detailed description of the CHAOS'98 cruise is given in chapter 4.3.3. The SISTeR radiometer (see chapter 5) was used to measure the radiometric sea surface temperature. It was mounted on the bow of the RRS Discovery and looked forward at an angle of 30° to nadir. A sky brightness temperature was also measured at the complimentary angle of 150°. The bulk SST was measured using a so-called 'soap on a rope' or soap for short. This is a thermistor attached to an armoured cable that is weighted so that it skims along just below the sea surface as the ship is moving. The nature of the instrument is such that it cannot be deployed in 'clean' water and has to operate in water mixed by the bow wave of the vessel. Therefore, this bulk temperature is an 'average' of about the top metre of the ocean. There was also a temperature measurement available from a thermosalinograph (TSG) mounted at a depth of 5 metres below the surface on the ship's hull. Unfortunately, this instrument was not always working properly and these data were considered too suspect to use here. Comparisons of the temperature measured by the TSG (when working correctly) and the soap showed that in all but the calmest of conditions the two temperatures were identical. This implies that at least the top 5 metres of ocean were well mixed for most of the cruise. The soap and meteorological instruments were operated by S.A. Josey and R.W. Pascal of the SOC. The wind speed data were measured using two sonic anemometers mounted at a height of 20 metres. The wind speeds were automatically corrected for the ship's movement using the ship's navigational data. The data were collected over large geographical area ranging from roughly 20° N to 60°N and over a wide range of weather conditions. There was relatively little data from calm conditions during the CHAOS'98 cruise and the MUBEX'97 data compliments the CHAOS'98 data in this respect.

7.2.2.2 Data Processing Method

The SISTeR data was converted from brightness temperatures to SSTs using a similar suite of IDL programs to those used for the MUBEX campaign. The theory behind this is described in Appendix 2. The wind speed data were also corrected to the 10 metre standard height following Smith 1998 to aid comparison with the MUBEX'97 and other data sets (e.g. Donlon *et al.* 1999c).

The meteorological and soap data were automatically averaged and logged at one-minute intervals. It was therefore necessary to transform the SISTeR data onto the same time scale. This was done by averaging all SISTeR SST data 30 seconds either side of each meteorological data point. The soap tended to sink whilst the ship was stationary (on station) so all data was rejected from when the ship's speed was less than 2 knots. An array of data was then generated of radiometric SST (SISTeR), bulk SST (soap) and the various meteorological parameters. The array was then screened for any data flagged as 'bad' and those data points were discarded. There were a total of 11344 points of which 7281 were during the day and 4063 during the night. The skin-bulk temperature difference (ΔT) was generated by subtracting the bulk (soap) temperature from the skin (SISTeR) temperature.

7.2.2.3 The Distribution of ΔT

Figure 52 shows a histogram for all ΔT values calculated from the data taken during the CHAOS'98 cruise.

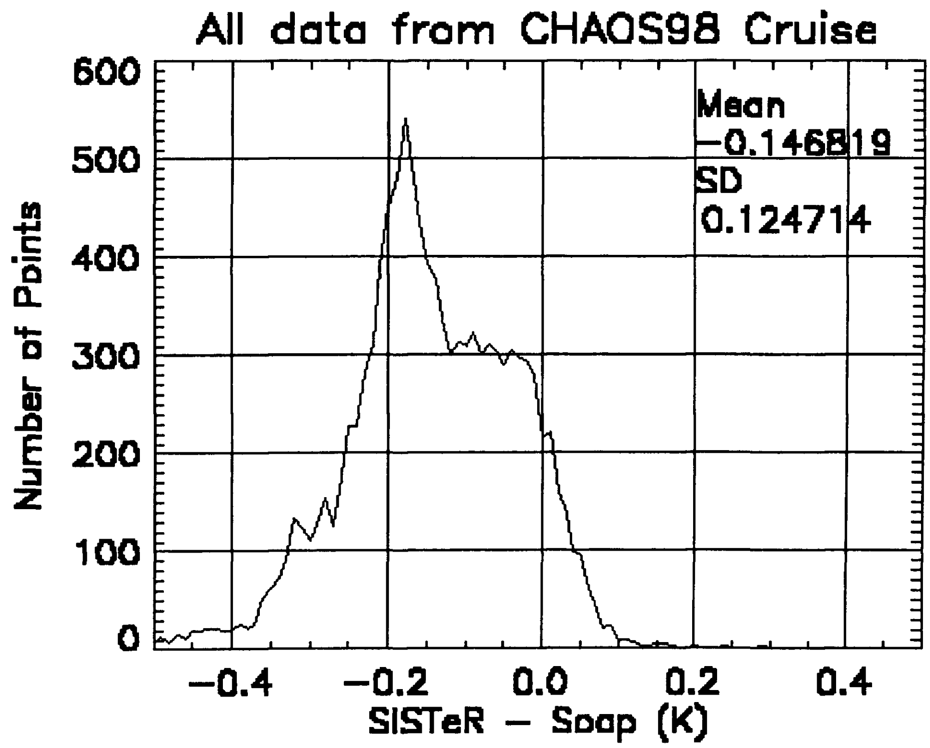

Figure 52: Histogram of all valid ΔT measurements taken during the CHAOS'98 cruise

The mean value of ΔT during the cruise was -0.147 K with a standard deviation of 0.125 K. This is very different to the MUBEX'97 data and shows the difference between sheltered calm water and rougher open ocean. The maximum and minimum values for ΔT recorded were 1.73 K and -0.96 K respectively. This shows that the majority of the data collected during the CHAOS'98 cruise were from conditions with no (or very little) diurnal warming but that there were a few cases that give the extreme range seen. Figure 53 and Figure 54 show the histograms of the data split into daytime and night-time only data.

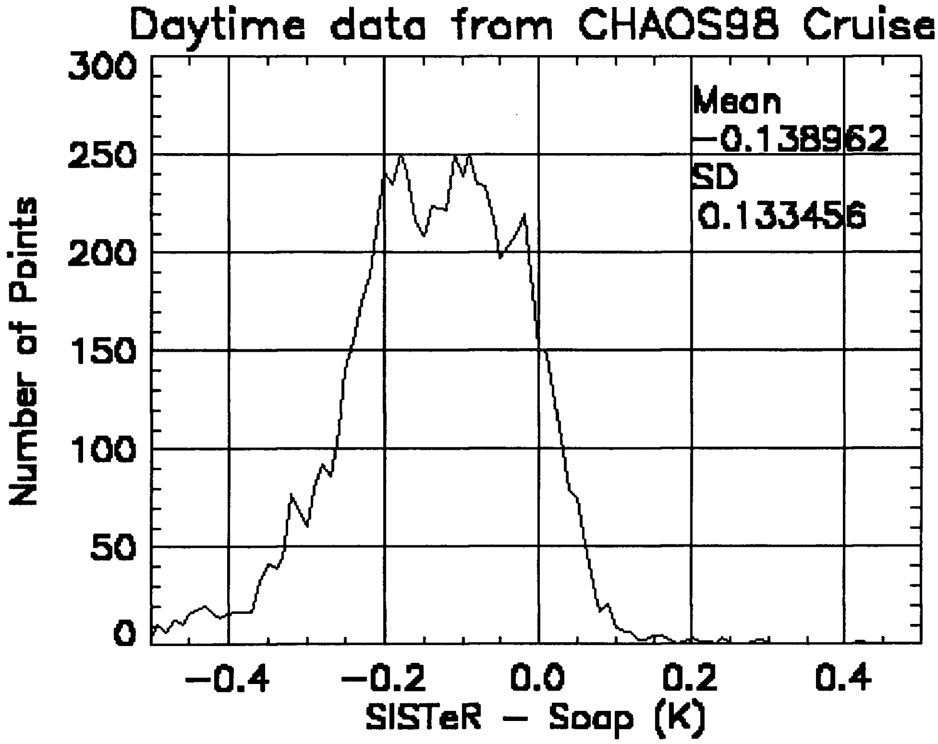

Figure 53: Histogram of all valid daytime ΔT measurements taken during the CHAOS'98 cruise

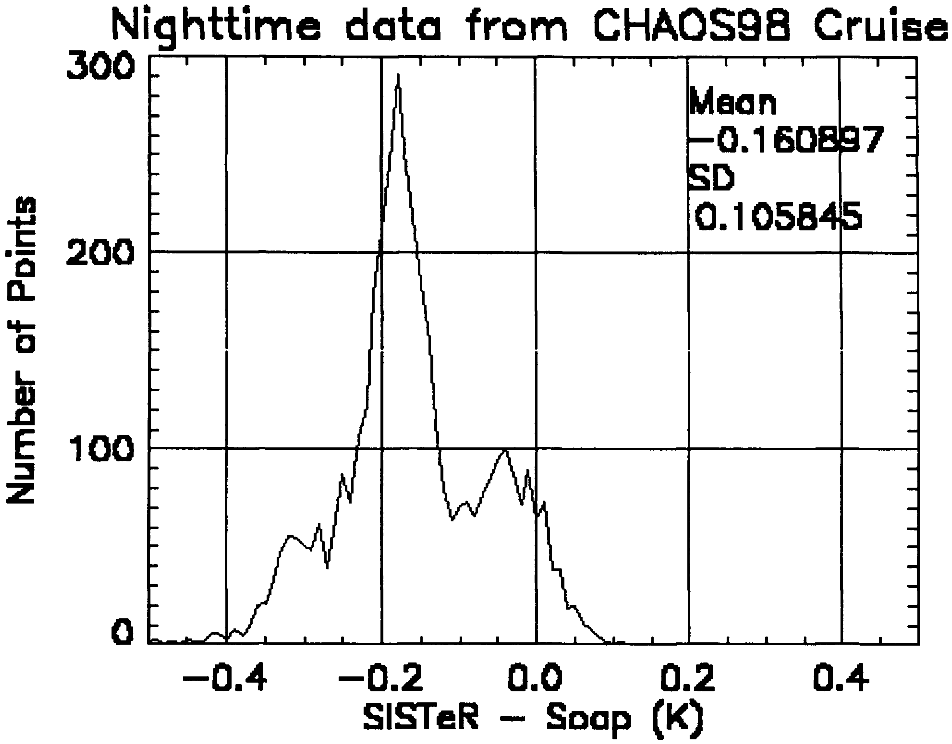

Figure 54: Histogram of all valid night-time ΔT measurements taken during the CHAOS'98 cruise

The average daytime value of ΔT was -0.139 K with a standard deviation of 0.133 K and the night-time value was slightly cooler at -0.161 K with a slightly smaller standard deviation of 0.106 K as expected. The daytime histogram is broader than the night-time histogram which shows the wider variety of ΔT values that occur during the day. These values agree with the previously published data summarised in Table 36 and Table 37.

7.2.2.4 Wind Speed Dependence

Figure 55 shows all the valid ΔT data taken during the CHAOS cruise as a function of wind speed. It shows a high level of scatter but there is a general trend of larger ΔT's at lower wind speeds and more scatter at these lower wind speeds. The high level of scatter is because the wind speed is not the sole factor in determining the skin effect. Other factors such as the humidity and solar radiation also play a role. The data from the CHAOS cruise was taken from a wide range of climatic zones, from sub-tropical to polar. This wide range of conditions contributes to the scatter.

Graph of Wind Speed against ΔT during the CHAOS Cruise

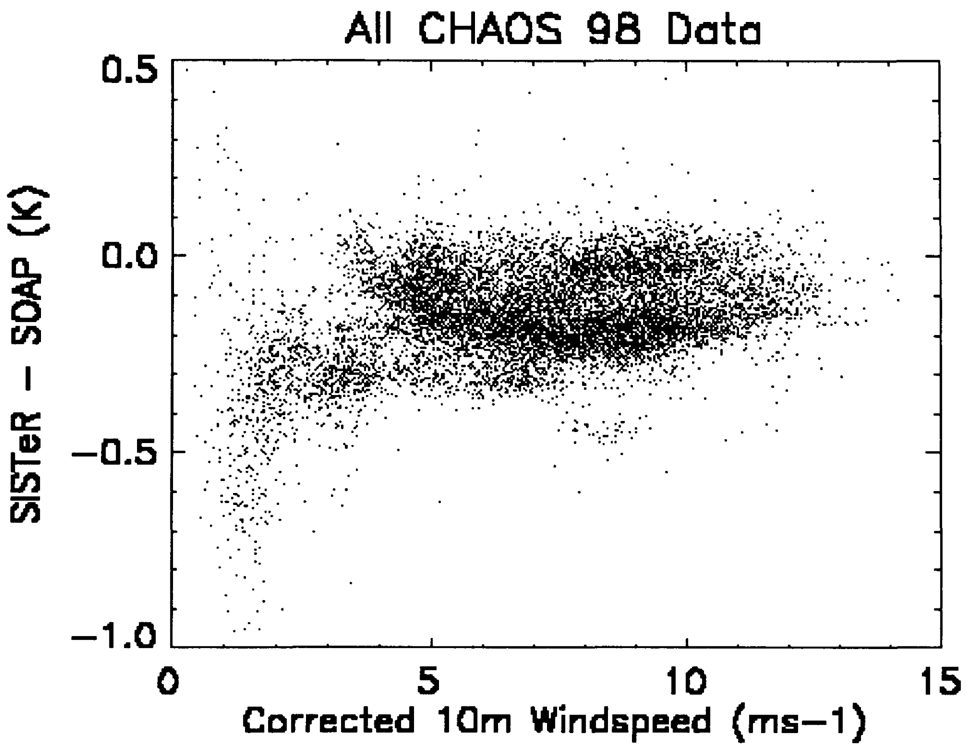

Figure 55: Graph showing all calculated ΔT values from the CHAOS cruise as a function of wind speed. The wind speed has been corrected to a standard 10m height following Smith 1988.

The data were then split into wind speed intervals of one ms^{-1} and into day and night data. The mean and standard deviation for each wind speed range was then calculated. Figure 56 shows the variation of the average ΔT with wind speed. Each point has error bars of the standard deviation associated with each point.

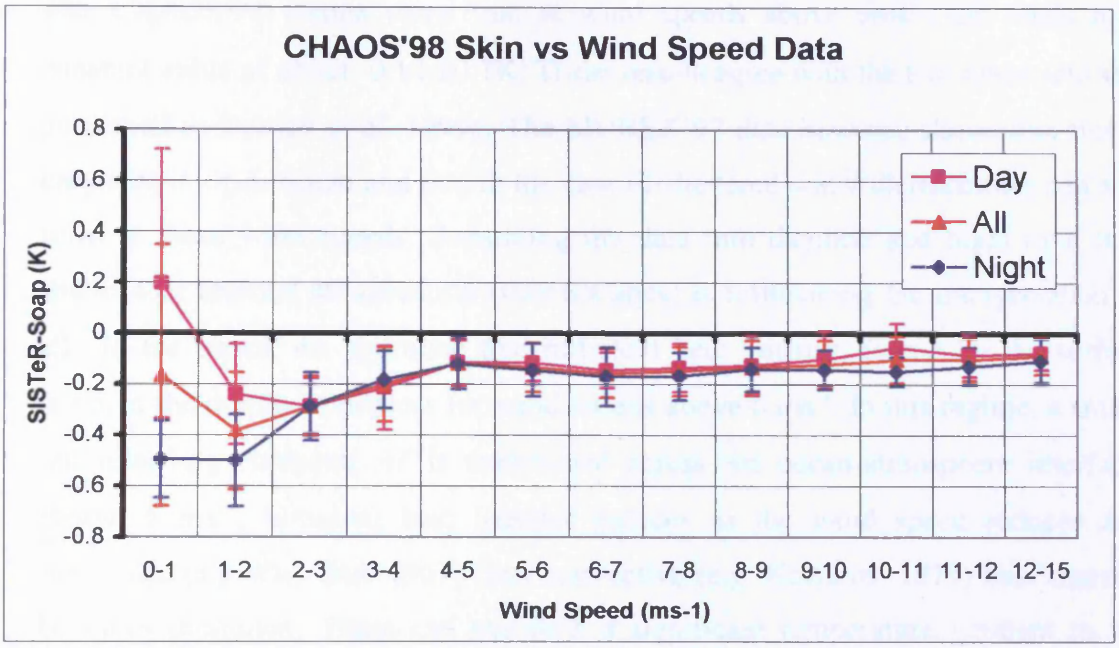

Figure 56: Graph of the average SISTeR-soap temperatures (*ΔT*) for various wind speed ranges during the CHOAS'98 cruise. The three lines show all data, daytime only data and night-time only data.

The graph shows that at low wind speeds the day and night data behave differently with the day data showing much more variation. As the wind speed increases above about 4 ms^{-1} the day and night data become coupled. At larger wind speeds (above 6 to 7 ms^{-1}), ΔT tends to a constant value of about –0.15 K. This agrees with similar work done by C.J. Donlon and others and these data are published in a GRL paper by C.J. Donlon, T.J. Nightingale, T.N. Sheasby, J. Turner, I.S Robinson and W.J Emery in 1999. The night-time data from MUBEX'97 (section 7.2.1) also agrees with these results but the daytime data does not. The daytime MUBEX'97 data does not become coupled to the night-time data and tends to a higher value of ΔT. As stated earlier, this is due to the sheltered nature of Mutsu Bay and the deeper bulk measurement.

7.2.3 Discussion

Previous work on the wind speed dependence of the skin effect suffered from a lack of accurate radiometric and bulk data. The data presented here are accurate to better than 0.05 K and so the scatter seen in the measurements is mostly due to the natural variability of the skin-bulk difference. There is however, some variability due to the contribution of the reflected radiation from a non-uniform sky. This is an area currently under research.

The CHAOS'98 results show that at wind speeds above 6ms^{-1}, ΔT tends to a constant value of about -0.14 ±0.1K. These results agree with the two other data sets published in Donlon *et al.* 1999c. The MUBEX'97 data however shows that this is only true in open ocean and that in the case of sheltered water thermoclines can still form at these wind speeds. Separating the data into daytime and night-time data shows that thermal stratification (thermoclines) is influencing the interpretation of ΔT. In the paper, we speculate that turbulent heat transfer, forced by the surface wind, is the dominant process for wind speeds above 6 ms^{-1}. In this regime, a small, but relatively constant, ΔT is maintained across the ocean-atmosphere interface. Below 6 ms^{-1}, turbulent heat transfer reduces as the wind speed reduces and molecular (e.g. Saunders 1967) then convective (e.g. Katsaros, 1977) heat transfer becomes dominant. These can maintain a significant temperature gradient in the skin layer. Thermal stratification during periods of low wind speeds and high solar insolation can complicate the study of the skin effect. In such cases a warm ΔT does not necessarily rule out a cool skin, much depends on measurement techniques. In highly stratified conditions, such as those experienced during MUBEX'97, ΔT more often depends on the depth at which the bulk data were taken. If the bulk temperature is measured too deep, then it can measure a bulk temperature much cooler than the real bulk temperature just below the surface and so give a 'false' warm skin. Only in wind speeds greater than 6 ms^{-1} and in open water can the bulk SST be considered well coupled to the skin SST. This has implications for satellite validations, as at high wind speeds, well-calibrated bulk temperature measurements could be used to validate satellite SST measurements. Satellite SST data sets can be considered valid if they are found to have an average ΔT of -0.14±0.1 K compared with bulk data taken at high wind speeds. The reader is referred to Appendix 3: Donlon *et al.*, 1999c for a full discussion. Any validation has to be done on an average basis not an individual basis, as this is an average correction not an exact correction. Individual points cannot be corrected in this way, so that using various models (e.g. Wick 1995, Saunders 1967, etc.) may be a better way to do this. Murray *et al.* 2000, found a similar bias between buoy data and (ATSR) satellite skin SST data. They used the Tropical Atmosphere Ocean (TOA) moored buoy array in the equatorial Pacific Ocean and state that a bias of about –0.2 K is seen at wind speeds above about 7 ms^{-1} during the day and 4 ms^{-1} at night.

There is still a need to validate satellite SST measurements in low wind speed conditions with an *in situ* skin SST due to the highly variable nature of ΔT in these conditions.

8 Conclusions and Further Work

8.1 The Accuracy of ATSR

Unfortunately, only one validation point for the ATSR-1 instrument was obtained from the data used in this thesis. The data from this one point imply that the new global coefficients derived by C.J. Merchant give better results in the Mutsu Bay area than the original set of regional coefficients. The new coefficients give a value for ΔT of 0.07 with the un-geocorrected data and –0.03 with the geocorrection applied. This is in comparison to the original coefficients that gave a ΔT of –0.54 K. Four cloud-free validation points were obtained for the ATSR-2 instrument. Using the most up-to-date coefficients available at the time of writing (V320) gives a mean value for ΔT of 0.30±0.48 K for the standard un-geocorrected product. The value for ΔT and the error are reduced after geocorrecting the data and careful analysis of the data to reduce the effects of local thermal gradients to 0.07±0.17 K. There is a known error in the dual-look coefficients that is currently being investigated. If the nadir-only SST is used the errors drop to 0.24±0.43 K for the standard uncorrected data and 0.04±0.17 K for the corrected data. The high levels of noise in the data are due to two main causes. The first is the low number of validation points and can be reduced if more validation data are collected. The second reason for the noise is the environment of Mutsu Bay. The SST in the bay shows a high degree of thermal variation on sub-pixel spatial scales. This is a major limitation of the data from Mutsu bay. There is a need for many more validation points, especially obtained in thermally uniform waters, to confirm these results. The results for the 1km^2 product translate into an error of order 0.01 K in the ASST product if the noise is assumed to be statistical in nature. At the time of writing, there is a review of the currently available coefficients underway and it is expected that new coefficients will be released when this has been completed. It will be necessary to redo this work in order to assess the accuracy of any new coefficients.

8.2 The Characterisation of the skin effect

The data collected during this thesis confirm that ΔT is highly variable depending on a number of factors. Data collected during the night show much less variation. This implies that solar insolation is a major cause of the variation, especially at low wind speeds. The data presented here, and along with other data sets in Donlon *et al* 1999c, show that at wind speeds greater than 6ms^{-1}, ΔT tends to a constant value of about -0.14 ±0.1K. This has implications for the validation of satellite-derived skin SSTs with bulk SSTs from accurately calibrated buoys (such as the TOA moored array). Applying a constant offset to correct individual skin SST values is not valid but the offset can be applied to compare average values however.

8.3 The Accuracy of the SISTeR Radiometer

Data collected from external calibration of the SISTeR radiometer during the period of this thesis chart the development of the instrument. The instrument was constantly being improved between the data collection phases of this PhD. The data from the last campaign in 1998 (CHAOS'98) show that SISTeR is now meeting its design criteria and has an absolute accuracy of better that 0.025 K and an rms error (with a clean scan mirror) of less than 0.03 K. The data also show that as the scan mirror is degraded by external contaminants during a campaign, the absolute accuracy does not change significantly and the rms noise increases. This is what was expected and shows the advantage of using this style of radiometer, as its absolute accuracy is not affected by external factors. The SISTeR radiometer is however limited by the fact that it needs to be constantly manned and by its high unit cost. There is a need for a low cost, autonomous version that can be deployed on ships of opportunity for periods of many months that do not need human intervention.

8.4 Further Work

8.4.1 Validation Points

During the period of this PhD, the author spent a total of almost 20 weeks at sea. During this time, only five validation points were obtained (one for ATSR-1 and four for ATSR-2). This is clearly a limited data set and highlights the difficulty of validating satellite SSTs with *in situ* radiometric SSTs. There is a need for more validation points from a variety of latitudes and from differing ocean environments to compare with these data.

8.4.2 Updated coefficients

The validation work presented in this thesis will need to be re-done when the new coefficients for processing ATSR-1 and 2 data are released. The data collected for this thesis could be used to test the accuracy of any new coefficients and this will hopefully improve the accuracy of the SSTs.

8.4.3 Climate Change Studies

The main goal of the ATSR series of instruments was the detection of global climate change. This was one of the main aims of this PhD but unfortunately, due to the errors in the retrieval coefficients no novel work could be done. Hilton 1999 presents a basic methodology that could be followed in order to try to detect any changes once the ATSR data have been reprocessed with new coefficients that eliminate all of the known errors.

9 Appendices

9.1 Appendix 1: Basic Radiometric Heat Transfer Theory

All objects above zero degrees Kelvin emit electromagnetic radiation. A radiometer is a device that is capable of measuring this energy. The amount of energy radiated by an object, its emittance (H), is related to its absolute temperature. For a blackbody, the total energy emitted over all wavelengths is give by the Stefan-Boltzmann law:

$$H=\sigma T^4 \ Wm^{-2}$$

where σ is the Stefan-Boltzmann constant ($5.7\times10^{-8}Wm^{-2}K^{-4}$).

A blackbody is an object that absorbs and re-emits all the electromagnetic energy it receives. They are often used to calibrate radiometers as the radiation leaving a blackbody can be accurately calculated. It is said to have an emissivity (ε) of 1. Everyday objects are not blackbodies and have an emissivity ranging from 0 to 1. For everyday objects the Stefan-Boltzmann law becomes:

$$H=\varepsilon\sigma T^4$$

Planck's Law gives the spectral distribution of the emittance as a function of wavelength:

$$B_\lambda = \frac{2hc^2}{\lambda^5\left(e^{hc/\lambda kT}-1\right)} Wm^{-2}m^{-1}sr^{-1}$$

where, h is the Planck constant (6.626×10^{-34})

c is the speed of light in metres per second (2.997×10^{8})

λ is the wavelength in metres

k is the Boltzmann constant in(1.381×10^{-23})

T is the absolute temperature in Kelvin

Again, for non-blackbodies an emissivity term is added which is also wavelength dependent:

$$B_\lambda = \varepsilon_\lambda \frac{2hc^2}{\lambda^5\left(e^{hc/\lambda kT}-1\right)} Wm^{-2}m^{-1}sr^{-1}$$

This equation can be integrated over a wavelength range to calculate the total energy in that wavelength range.

9.2 Appendix 2: The principle of Radiometric Sea Surface Temperature (SST) Retrieval.

In order to obtain the true sea surface temperature SST from *'in-situ'* radiometric measurements of the sea it is necessary to correct for the effect of reflected sky radiation. Because the emissivity of the sea is not unity, a radiometer looking at the ocean will 'see' a reflected sky signal (see Figure 57). This (lower) initial radiometric temperature or *brightness* temperature (BT) needs to be corrected to obtain the true SST. This is currently done using two radiometers. One looks at the sea and the other looks at the sky at the complimentary angle to the sea radiometer. In the case of SISTeR (see chapter 5.1), it is programmed to look at the sea then at the complementary sky angle. This way a sky temperature is obtained at the same time as, or close to, the sea temperature and a correction can be made.

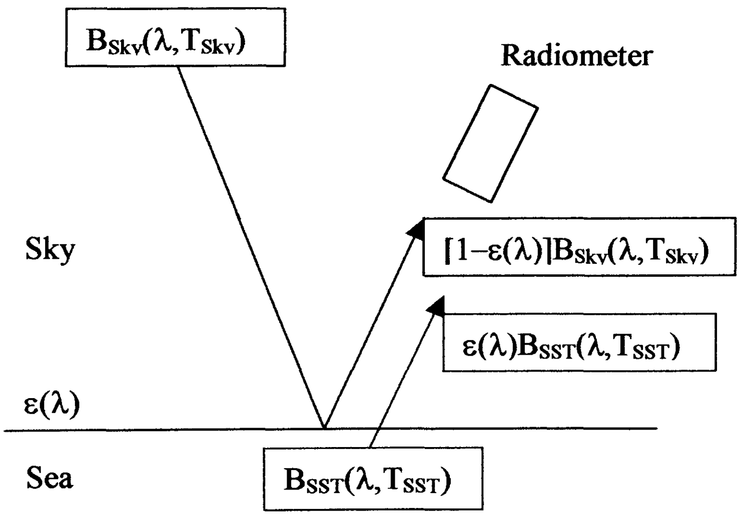

Figure 57: Diagram showing the components of the flux entering a radiometer looking at the ocean surface.

The effect of the sky radiation is corrected for using the equation below:

$$B_{Target}(\lambda, T_{Brightness}) = \varepsilon(\lambda) \times B_{SST}(\lambda, T_{SST}) + [1 - \varepsilon(\lambda)] \times B_{Sky}(\lambda, T_{Sky})$$

where,

B_{Target} is the flux measured by the radiometer

B_{Sky} is the flux from the sky

B_{SST} is the flux from the ocean

$\varepsilon(\lambda)$ is the emissivity of the ocean

The radiometer measures the flux from the target and from the sky. The down-welling flux from the sky is multiplied by (1-ε), to calculate the reflected component, and then subtracted from the target flux. The remaining flux is then the sea component and an inverse Plank function (see Appendix 1) is used to calculate the SST. The value of $\varepsilon(\lambda)$ has been obtained experimentally (Masuda *et al.*, 1998, Sidran, 1981) and varies with wavelength (see Figure 58) and viewing angle (see Figure 59). Generally, if the viewing angle is kept below 40° from nadir, the emissivity is relatively constant. Above 40° it drops off rapidly.

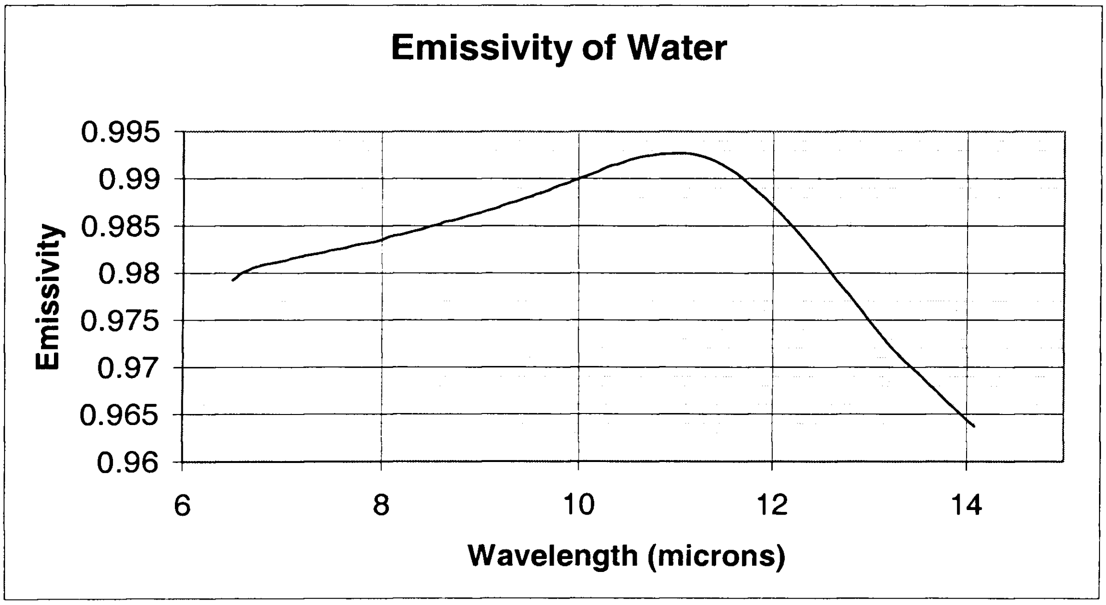

Figure 58: Graph of the emissivity of water as a function of wavelength (following Sidran, 1981)

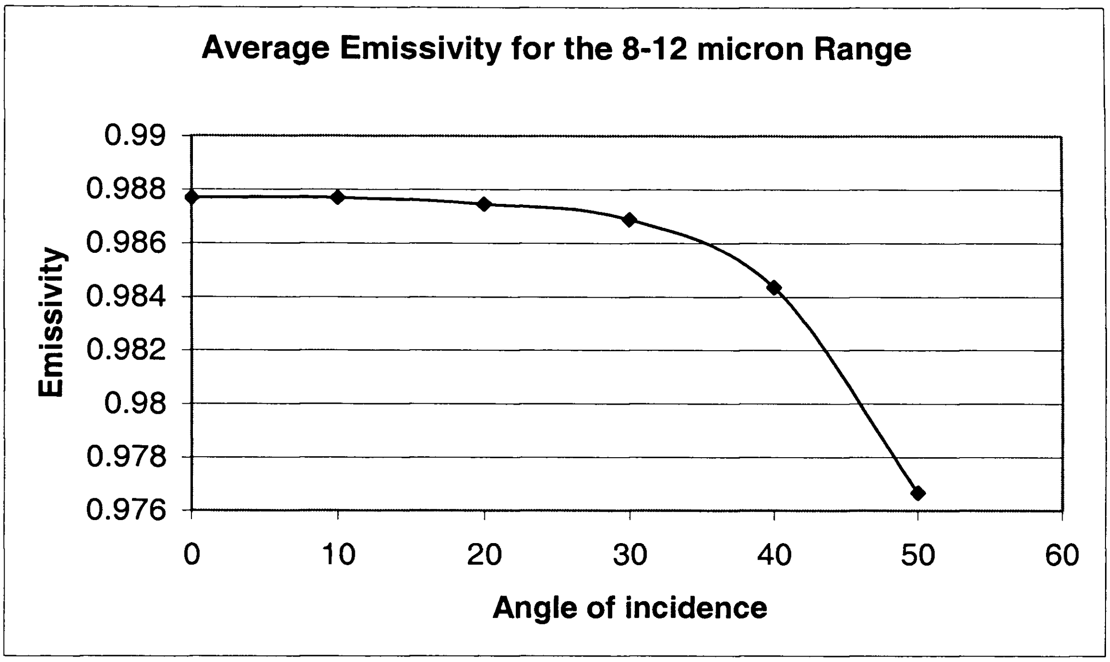

Figure 59: Graph showing the variation of emissivity with viewing angle (from nadir) for the 8-12μm region.

When correcting for the reflected sky radiation it is necessary to allow for the variation of the emissivity with wavelength, especially for broadband radiometers. For narrow band radiometers, it is possible to use a single value for the emissivity (weighted with the filter profile) as the emissivity varies negligibly over very short ranges. This greatly simplifies the maths and reduces computational time.

This is currently the standard way of correcting the brightness temperature but this method assumes that all the reflected sky radiation is from a source at a uniform temperature. This is currently an area under research (e.g. Watts *et al.*, 1996).

The value used for the emissivity of the ocean during this thesis was 0.99246, which is the sea's emissivity (e.g. Masuda *et al.*, 1998, Sidran, 1981) weighted with the SISTeR filter window and detector functions. Because the spectral window of SISTeR is very narrow, it is possible to use a single value for the emissivity.

9.3 Appendix 3: Donlon *et al.*, 1999c

GEOPHYSICAL RESEARCH LETTERS, VOL. 26, NO. 16, PAGES 2505-2508, AUGUST 15, 1999

Implications of the Oceanic Thermal Skin Temperature Deviation at High Wind Speed

C. J. Donlon,[1] T. J. Nightingale,[2] T. Sheasby,[3] J. Turner[4] I. S. Robinson[5] and W. J. Emery[6]

Abstract. Extensive oceanographic and atmospheric observations obtained during three independent experiments in the Atlantic Ocean are used to demonstrate the relationship between wind speed and the temperature deviation ΔT, which is defined as the sea surface skin temperature (SSST) minus the subsurface bulk sea surface temperature (BSST). At wind speeds < 6 m s^{-1}, the variability of ΔT increases because thermal stratification complicates the measurement and interpretation of ΔT: extreme ΔT magnitudes of $>$ 1.5 K are common during periods of high insolation. The variability of ΔT at night is reduced and extreme cool skin temperatures of $<$ -0.5 K are recorded. In all cases, at wind speeds > 6 m s^{-1}, the variability of ΔT is diminished and the mean value of ΔT approximates a cool bias of -0.14 K ± 0.1 K. We conclude that BSST measurements obtained at wind speeds > 6 m s^{-1}, when corrected for a small (- 0.14 K) cool bias, are representative of the SSST and can be used with confidence to validate satellite derived SSST. When the wind speed is < 6 m s^{-1} and the magnitude of ΔT is high, in situ radiometric SSST measurements are mandatory to validate satellite derived SSST.

1. Introduction

At the atmosphere-ocean interface there is a characteristic temperature gradient within the surface micro-layer of the ocean [e.g., *Donlon and Robinson,* 1997]. In general, skin sea surface temperature (SSST) is measured non-invasively using infrared sensors and exhibits increased spatial and temporal variability when referenced to the subsurface bulk sea surface temperature (BSST) measured using a variety of immersion-contact sensors. For many purposes, SSST is a more appropriate ocean surface temperature than the BSST: it represents a physically definable property that exerts significant control on the exchange of heat, gas, and moisture between the atmosphere and the ocean. Perhaps more importantly, it is the temperature that is directly observed by satellite infrared radiometer sensors that form one of the core data sets used to investigate earth climate system dynamics. It is particularly important to define the accuracy and stability of these data within a comprehensive validation programme: a poor validation strategy compromises the integrity of satellite derived data products because of an inability to adequately specify appropriate confidence limits.

Self calibrating satellite radiometers such as the ERS along track scanning radiometer (ATSR) are capable of providing SSST to an accuracy equivalent to the magnitude of ΔT [*Parkes et al.,* 1999]. In the infrared spectral wavebands used by most satellite sensors, seawater has a high emissivity, ϵ, [e.g., *Bertie and Lan,* 1996]. Consequently, the radiance measured by a radiometer viewing the sea surface for a spectral bandwidth of 10-12μm is emitted exclusively from the top $\sim$10μm of the water surface and is therefore only representative of the temperature corresponding to that thin layer. Unfortunately, there are only a small number of in situ SSST measurements available, a fact which has substantially compromised the international satellite SSST validation effort and has perpetuated the use of subsurface BSST for the operational validation of satellite SSST.

In this paper we present new observations obtained in the Atlantic Ocean derived from state of the art instrumentation providing SSST measurements of hitherto unattainable accuracy. We use these data to demonstrate the relationship between the surface wind speed, u, and the SSST-BSST difference, ΔT.

2. Data and Methodology

Three atmosphere - ocean data sets have been selected which have all been obtained in the Atlantic Ocean during 1996 - 1998. Figure 1 shows the extent of ship tracks made during the experiments that include a diversity of ocean-atmosphere conditions from major climatic regions. Collectively, these observations provide a data set well suited to our purpose.

During two joint Radiometric Observations of the Sea surface and Atmosphere (ROSSA) and Atlantic Meridional Transect (AMT) experiments (Sep-Oct, 1996 and 1998 respectively), a scanning infrared sea surface temperature radiometer (SISTeR) mounted to the forward mast of the RRS *James Clark Ross* (JCR) was used to determine the radiometric SSST viewing the sea surface at a 40° zenith angle. The SISTeR is a precise self-calibrating radiometer which relies on two internal radiance sources maintained at different temperatures to derive a continuous calibration. The reader is referred to *Donlon et al.,* [1999] for a description of the SISTeR instrument including independent calibration data. A precision trailing thermistor unit accurate to ± 0.02 K of a similar design to that reported by *Kent et al.* [1996] was used to obtain a BSST at a depth of 0.1 m for the majority

[1]Space Applications Institute, Joint Research Centre, Ispra Italy.
[2]Space Science Department, Rutherford Appleton Laboratory, Chilton, England.
[3]Dept. Earth Observation Science, University of Leicester, Leicester, England.
[4]Ice and Climate division, British Antarctic Survey, Cambridge, England.
[5]School of Ocean and Earth Sciences, University of Southampton, Southampton, England.
[6]Colorado Center for Astrodynamics Research, University of Colorado, Boulder, Colorado.

Paper number 1999GL900547.
0094-8276/99/1999GL900547$05.00

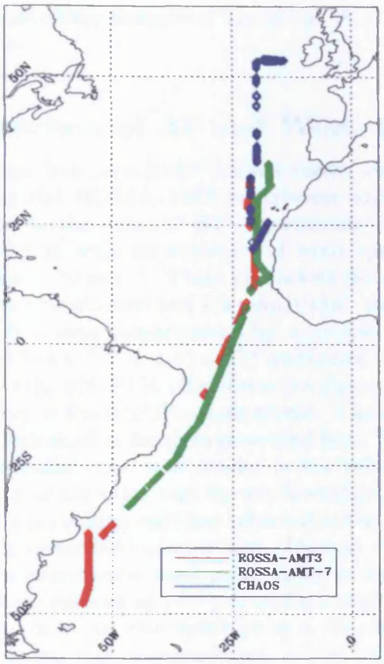

Figure 1. Position of data aquired during the AMT-3 (red), AMT-7 (green) and CHAOS (blue) experiments.

of the experiment. During the ROSSA-AMT96 experiment, when it was not possible to use the thermistor, a SeaBird thermosalinograph (TSG) was used to provide a BSST accurate to ± 0.02K from a depth of 5.5 m. The substitution of 5.5 m TSG data for 0.1 m BSST data was was not used for daytime data because of the complicating effect of surface thermal stratification. Wind speed was measured by a sonic anemometer mounted on the forward mast of the JCR at a height of 23 m.

The third cruise data set used in this study also used a SISTeR radiometer on the UK research vessel RRS *Discovery* during the Chemical and Hydrographic Atlantic Ocean Survey (CHAOS) experiment (May-Jun, 1998). The SISTeR was mounted on the bow of the *Discovery* and viewed the sea surface at a zenith angle of 30°. Throughout the experiment, BSST was determined at a depth of 0.1 m using a trailing thermistor. Wind speed was measured by two sonic anemometers mounted on the *Discovery* fore mast at a height of 20 m.

In all cases, wind speed measurements have been corrected for ship movement using ship's navigation data streams and adjusted to a height of 10m accounting for atmospheric stability following *Smith* [1988]. The processed wind speed data are accurate to better than ± 0.25 m s^{-1}. BSST measurements made by the TSG instruments located within the ship have been corrected for a small warm bias introduced by the ships pumps and internal plumbing using

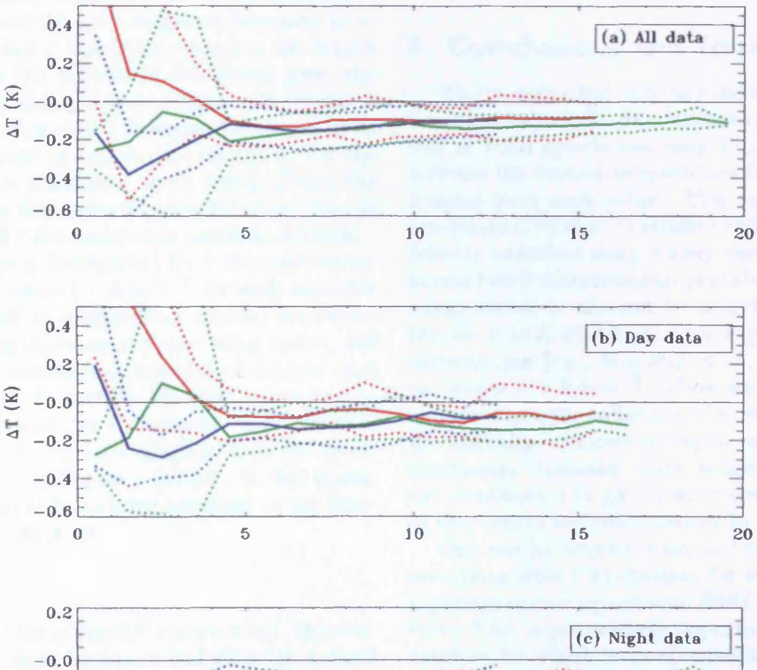

Figure 2. The mean wind speed plotted against the mean thermal skin temperature deviation ΔT (SSST-BSST) for AMT-3 data (red), AMT-7 data (green) and, CHAOS data (blue). The resolution of ΔT is 0.1 K and wind speed is 0.5 m s^{-1}. Dotted lines show $\pm$ 1 standard deviation for each data set.

data from a precision thermistor located at the TSG intake pipe aperture.

3. Comparison of ΔT and Wind speed

Donlon and Robinson [1997] discuss similar observations made during the ROSSA 1992 experiment and conclude that, at high u, the value of ΔT approximates to a mean value of ~-0.1 K with no evidence of wind speed dependency when $u > 10$ m s^{-1}. These characteristics are similar to those shown by *Minnett and Hanafin* [1998]. However, the ROSSA-92 data were compromised by; a scarcity of data in the regime of 7 m s^{-1} $< u <$ 11 m s^{-1} and below 3 m s^{-1}, the calibration of the SIL-STR-100 infrared radiometer and, the poor precision of the BSST measurements. These problems have been eliminated in the data presented here. The critical source of potential error now resides in the values used for the emissivity of seawater and the methodology adopted to account for downwelling radiance reflected at the sea surface into the radiometer field of view [e.g., *Thomas et al.*, 1995]. All SSST measurements were made using a narrow band (<1 μm) filter centered at 10.8 μm and a sample frequency of 1.25 Hz for a 4s sky view followed by a 16s sea view. For each sky and sea view measurement, a two point calibration was obtained resulting in an end-to-end measurement cycle of approximately 40 s. The ϵ of seawater was taken from *Bertie and Lan* [1996] weighted with the combined SISTeR spectral window and detector response functions (ϵ = 0.990434). We note that ϵ has little variation for zenith angles of <50° and for the waveband considered here, the effective ϵ is very weakly dependent on wind speed [*Watts et al.*, 1996]. Changes in ϵ due to the increase of seawater foam associated with high wind speeds is also negligible for the SISTeR spectral window [*Salisbury et al.*, 1993]. Thus, the limiting accuracy of the ΔT measurements for these data is that of the SISTeR SSST determination which is ±0.05K.

The mean ΔT has been determined for wind speed intervals of 1 m s^{-1} over a range 0 - 20m s^{-1} for each separate cruise data set. In order to identify any diurnal characteristics of the relationship between ΔT and wind speed, the data have been further decomposed into day and night time conditions. No attempt to stratify the data according to cloud type or cloud amount has been made. The resulting data have then been plotted to a common axis for interpretation and are shown in Figure 2 (a)-(c). In this figure, separate dotted lines indicate an error envelope of ±1 standard deviation for each data set.

4. Discussion

Given the high accuracy of the ΔT observations, the variance of the ΔT values must be associated with the natural variability of the SSST, although variability in the sky radiance correction could make a contribution to the statistic. Considering the complete data sets shown in Figure 2 (a), we note that for u >6 m s^{-1}, ΔT reduces to an approximate cool bias of - 0.14 K ±0.1K relative to the subsurface BSST. When $u <$ 6 m s^{-1}, ΔT is characterised by a significant increase in variability. We decompose Figure 2 (a) into day time data shown in Figure 2 (b) and night time data in Figure 2 (c). Comparing Figure 2 (b) and (c), it is evident that thermal stratification of the sea surface is influencing the measurement and interpretation of ΔT. Large warm ΔT values are found in the day time although a cool ΔT prevails at night.

From our results, we hypothesise that on the water side turbulent heat transfer forced by the surface wind is the governing heat transfer process for $u >$ 6 m s^{-1}. A small but nearly constant temperature difference is maintained across the air-sea interface by the impedance of the surface layer to the heat flux passing from the ocean to atmosphere [e.g., *Grassl*, 1976]. When $u <$ 6 m s^{-1}, the role of turbulent heat transfer gradually diminishes as wind speed reduces so that molecular [e.g., *Saunders*, 1967] and subsequently convective heat transfer [e.g., *Katsaros*, 1977] become dominant: these processes can maintain a significant temperature gradient in the thin skin layer. Thermal stratification of the sea surface during periods of high insolation and low wind speed complicates the interpretation of ΔT relative to the depth of the BSST measurement. In this respect, a warm ΔT does not necessarily preclude the presence of a cool SSST layer at the air- sea interface because the variability in ΔT at wind speeds < 6 m s^{-1} depends on the measurement techniques used to determine ΔT; for stratified conditions the variability in ΔT is actually a function of the depth at which the BSST is determined. Due to these difficulties, we identify a need for further study of the near-surface ocean thermal structure in these conditions particularly by developing operational multi-spectral sounding techniques [e.g., *Paulson and Simpson*, 1981].

5. Conclusions and Implications

We conclude that only in wind speeds > 6 m s^{-1} should the subsurface BSST be considered well coupled to the SSST and at wind speeds less than this critical value, our data indicate the related temperature fields are increasingly decoupled from each other. This implies that in high wind conditions (> 6 m s^{-1}) satellite SSST retrievals may be confidently validated using widely available, quality controlled in situ BSST measurements provided they are appropriately compensated to account for a high wind speed SSST cool bias of - 0.14 K ±0.1 K shown in Figure 2. Global wind speed climatologies [e.g., *Woodruff et al.*, 1993] show extensive areas where $u >$ 6 m s^{-1}. These are conveniently located in regions where the collection of in situ SSST are hindered by the difficulty and cost of deployments, such as the Southern Ocean. However, there is large seasonal variability in the distribution of global wind speed and significant areas of the Oceans are characterised by $u <$ 6 m s^{-1}.

Our results provide past and future satellite SSST observations with a mechanism for widespread validation using the extensive operational BSST measurement infrastructure. This is particularly important for historical satellite archives for which no contemporaneous in situ SSST data are available. Further, this technique will facilitate the cross- and inter- calibration of satellite instruments allowing a longer multi-sensor SSST time series to be effectively screened for sensor or algorithm biases.

For low wind speed conditions, validation of satellite SSST by in situ SSST measurements is mandatory. This highlights the need for low cost autonomous in situ radiometers [e.g., *Donlon et al.*, 1998] deployed on opportunistic ship platforms. We are continuing to develop these systems aiming to generate a geographically widespread, accurate, long term, SSST validation data set.

Acknowledgments. Thanks to the Captains and ships' companies of the RRS *James Clark Ross* and the RRS *Discovery*, the Plymouth Marine Laboratory, the UK National Environmental Research Council, and the Southampton Oceanographic Centre (SOC). Craig Donlon was supported in part by NASA research grant NAGW-1110.

References

Bertie, J. E. and Z.D. Lan, Infrared intensities of liquids XX: The intensity of the OH stretching band of liquid water revisited, and the best current values of the optical constants of $H_2O(l)$ at 25°C between 15,000 and 1 cm^{-1}, *Applied Spectroscopy, 50,* 1047-1057, 1996.

Donlon, C. J. and I. S. Robinson, Observations of the oceanic thermal skin in the Atlantic Ocean, *J. Geophys. Res., 102,* 18585-18606, 1997.

Donlon, C. J., T. J. Nightingale, L. Fielder, G. Fisher, D. Baldwin and I.S.Robinson, A low cost blackbody for the calibration of sea going infrared radiometer systems, *The Journal of Atmospheric and Oceanic Technology,* In press, 1999.

Donlon, C. J., S. J. Keogh, D. J. Baldwin,I. S. Robinson, I. Ridley, T. Sheasby, I. J. Barton, E. F. Bradley, T. J. Nightingale, and W. Emery. Solid state radiometer measurements of sea surface skin temperature *J. Atmos. Oceanic. Technol., 15,* 775-787, 1998.

Grassl, H., On the dependence of the measured cool skin of the ocean on wind stress and total heat flux, *Meteorology, 10,* 465-474, 1976.

Katsaros, K. B., The surface temperature deviation at low wind speeds: Is there a limit?, *Tellus, 29,* 229-239, 1977.

Kent, E., T. Forrester, and P. K. Taylor, A comparison of the oceanic skin effect parameterizations using ship borne radiometer data, *J. Geophys. Res., 101,* 16,649-16,666, 1996.

Minnett, P. J. and J. Hanafin, At-sea measurements of the ocean thermal skin temperature and its response to surface fluxes, Proc. International geoscience and remote sensing symposium, Seattle, USA, 6-10 July, 1998.

Parkes, I. M., T. N. Sheasby, D. T. Llewellyn Jones, C. T. Mutlow, T. J. Nightingale, A. M. Zävody, R. Yokoyama, S. Tanba and C. J. Donlon, The Mutsu bay experiment,- Validation of ATSR-1 and ATSR-2 sea surface temperature (SST) in Mutsu Bay, Japan during July and August 1996, *International Journal of Remote Sensing,* in press, 1999.

Paulson, C. A., and J. J. Simpson, The temperature difference across the cool skin of the ocean, *J. Geophys. Res., 86,* 11,044-11,054, 1981.

Salisbury, J. W., D. A. D'Aria, and F. F. Sabins, Thermal infrared remote sensing of crude oil slicks, *Remote Sens. Environ., 45,* 225-231, 1993.

Saunders, P. M., The temperature at the ocean-air interface, *J. Atmos. Sci., 24,* 269-273, 1967.

Smith, S. D., Coefficients for sea surface wind stress, heat flux, and wind profiles as a function of wind speed and temperature, *J. Geophys. Res., 93,* 15,67-15,472, 1988.

Thomas J. P., R. J. Knight , H. K. Roscoe, J. Turner, and C. Symon, An evaluation of a self calibrating infrared radiometer for measuring sea surface temperature. *J. Atmos. Oceanic Technol., 12,* 301-316, 1995.

Watts, P. D., M. R. Allen, and T. J. Nightingale, Wind speed effects on sea surface emission and reflection for the along track scanning radiometer, *J. Atmos. Oceanic Technol.,13,* 126-141, 1996.

Woodruff, S.D.,S.J. Lubker, K. Wolter, S.J. Worley, and J.D. Elms, Comprehensive Ocean-Atmosphere Data Set (COADS) Release 1a, 1980-92, *Earth System Monitor, 4,* 1-8, 1993

C. J. Donlon, CEC - JRC, Space Applications Institute, Marine Environment Unit, I-21020 Ispra (VA)-ITALY, TP690, (e-mail: craig.donlon@jrc.it)

T. Nightingale, Rutherford Appleton Laboratory, Chilton, Didcot Oxon.,OX11 0QX, England. (e-mail: t.j.nightingale@rl.ac.uk)

T. Sheasby, Earth Observation Science, University of Leicester, Leicester, LE1 7RH, England. (e-mail: tns1@le.ac.uk)

J. Turner, Ice and Climate Div., British Antarctic Survey, High Cross, Cambridge, England. (e-mail: jtu@nerc-bas.ac.uk)

I. S. Robinson, School of Ocean and Earth Sciences, University of Southampton, Southampton, England, SO14 3ZH. (e-mail: isr@soc.soton.ac.uk)

W. J. Emery, Colorado Center for Astrodynamics Research, University of Colorado, Boulder, CO, 80309 USA. (e-mail: emery@colorado.edu)

(Received February 8, 1999; revised June 15, 1999; accepted June 16, 1999.)

10 References

Allen, M.R., 1993, 'The Role of Satellite Observations of Sea-Surface Temperature in the Detection of Global Change', Technical Report 93.095 (Rutherford-Appleton Laboratories).

Allen, M.R., Mutlow, C.T., Blumberg, G.M.C., Christy J.R., McNider, R.T., and Llewellyn-Jones, D.T., 1994, 'Global Change Detection', Nature, 370, 24-25.

Bailey, P., 1995, 'SADIST-2 V100 Products', ER-TN-RAL-AT-2164, Rutherford-Appleton Laboratory.

Barton, I.J., 1992, 'Satellite-derived sea surface temperature – A comparison between operational, theoretical, and experimental algorithms', Journal of Applied Meteorology, Vol. 31, 432-442.

Barton, I.J., Prata, A.J., Cechet, R.P., 1995, 'Validation of the ATSR in Australian Waters', Journal of Atmospheric and Oceanic Technology, Vol. 12, 290-300.

Brown, S.J., Harris, A.J, Mason, I.M., Závody, A.M., 1997, 'New aerosol-robust sea surface temperature algorithms for ATSR, the along track scanning radiometer', Journal of Geophysical Research, Vol. 102, 27973-27989.

Donlon, C.J., 1994, 'An Investigation of the oceanic skin temperature deviation', Ph.D. thesis, University of Southampton.

Donlon, C.J., Robinson, I.S., 1997, 'Observations of the oceanic thermal skin in the Atlantic Ocean', Journal of Geophysical Research, Vol. 102, No. C8, 18585-18606.

Donlon, C.J., Robinson, I.S., 1998, 'Radiometric Validation of ERS-1 Along-Track Scanning Radiometer Average Sea Surface Temperature in the Atlantic Ocean', Journal of Atmospheric and Oceanic Technology, Vol. 15, 647-660.

Donlon, C.J., Keogh, S.J., Baldwin, D.J., Robinson, I.S., Ridley, I., Sheasby, T., Barton, I.J., Bradley, E.F., Nightingale, T.J., Emery, W., 1998, 'Solid-State Radiometer Measurements of Sea Surface Skin Temperature', Journal of Atmospheric and Oceanic Technology, Vol. 15, 775-787.

Donlon, C.J., Nightingale, T.J., Fiedler, L., Fisher, G., Baldwin, D., Robison, I.S., 1999a, 'The Calibration and Intercalibration of Sea-Going Infrared Radiometer Systems Using a Low Cost Blackbody Cavity', Journal of Atmospheric and Oceanic Technology, Vol. 16, 1183-1197.

Donlon, C.J., Castro, S.L., Kaye, A., 1999b, 'Aircraft validation of ERS-1 ATSR and NOAA-14 AVHRR sea surface temperature measurements', International Journal of Remote Sensing, Vol. 20, No. 18, 3503-3513.

Donlon, C.J., Nightingale, T.J., Sheasby, T., Turner, J., Robinson, I.S., Emery, W.J., 1999c, 'Implications of the Oceanic Thermal Skin Temperature Deviation at High Wind Speed', Geophysical Research Letters, Vol. 26, No. 16, 2505-2508.

Downing, H.D., Williams, D, 1975, 'Optical Constants of Water in the Infrared', Journal of Geophysical Research, Vol. 80, No. 10, 1656-1661.

Emery, W.J., Schlüssel, P., 1989, 'Global Differences Between Skin and Bulk Sea Surface Temperatures', Eos, Vol. 70, No. 14, 211-212, Ed. Muench, R.D.

Ewing, G., McAlister, E.D., 1960, 'On the Thermal Boundary Layer of the Ocean', Science, 131, 1374-1376.

Harris, A.R., Saunders, M.A., Foot, J.S., Smith, K.F., Mutlow, C.T., 1995, 'Improved sea surface temperature measurements from space', Geophysical Research Letters, Vol. 22, 2159-2162.

Harris, A.R., Saunders, M.A., 1996, 'Global Validation of the along-track scanning radiometer against drifting buoys', Journal of Geophysical Research, Vol. 101, 12127-12140.

Hilton, R., 1999, 'An Investigation into the use of ATSR Sea Surface Temperature Data for Climate Detection', M.Sc. Thesis, Leicester University.

Katsaros, K. B., 1977, 'The surface temperature deviation at low wind speeds: Is there a limit?', Tellus, 29, 229-239.

Masuda, K., Takashima, T., Takayama, Y., 1988, 'Emissivity of Pure and Sea Waters for the Model Sea Surface in the Infrared Window Regions', Remote Sensing of Environment, Vol. 24, 313-329.

Merchant, C.J., 1999, web site:
http://www.met.ed.ac.uk/~chris/ATSR_coefficients/coefficients_main.shtml

Merchant, C.J., Harris, A.R., Murray, M.J., Závody, A.M., 1999, 'Toward the elimination of bias in satellite retrievals of sea surface temperature – part 1', Journal of Geophysical Research, Vol. 104, No. C10, 23565-23578.

Merchant, C.J., Harris, A.R., 1999, 'Toward the elimination of bias in satellite retrievals of sea surface temperature – part 2', Journal of Geophysical Research, Vol. 104, No. C10, 23579-23590.

Murray. J., 1995, 'Sea-surface temperatures from ATSR August 1991-July 1995', Booklet accompanying data CD-ROM.

Murray, M.J., Allen, M.R., Merchant, C.J., Harris, A.R., Donlon, C.J., 2000, 'Direct observation of skin-bulk SST variability', Geophysical Research Letters, in press.

Murray, M.J., 2000, Web site:
http://www.climate-dynamics.rl.ac.uk/~jmurray/c.html

Mutlow, C.T., Závody, A.M., Barton ,I.J., Llewellyn-Jones, D.T., 1994, 'Sea surface temperature measurements by the along-track scanning radiometer on the ERS 1 satellite: Early Results', Journal of Geophysical Research, Vol. 99, C11, 22575.

Mutlow, C.T., Murray, M.J., Bailey, P., Birks, A., Smith, D., 1999, 'ATSR-1/2 User Guide', Rutherford-Appleton Laboratories.

Mutlow, C.T., Smith, D.L., Murray, M.J., March 2000, 'The Along Track Scanning Radiometer (ATSR) Instruments on ERS-1 and –2', Earth Observation Quarterly – ATSR Special Issue, No. 65, 1-5.

Nightingale, T.J., 2000, 'SISTeR; a new high-accuracy shipborne infrared radiometer', in press.

Parkes, I.M., Sheasby, T.N., Llewellyn-Jones, D.T., Nightingale, T.J., Závody, A.M., Mutlow, C.T., Yokoyama, R., Tamba, S., Donlon, C.J., 2000, 'The Mutsu Bay Experiment: validation of ATSR-1 and ATSR-2 sea surface temperature', International Journal of Remote Sensing, In Press.

Robinson, I.S., Wells, N.C., Charnock, H., 1984, 'The sea surface thermal boundary layer and its relevance to the measurement of sea surface temperature by airborne and spaceborne radiometers', International Journal of Remote Sensing, Vol. 5, No. 1, 19-45.

Robinson, I.S., 1985, 'Satellite Oceanography: An Introduction to Oceanographers and Remote-Sensing Scientists', Ellis Horwood Ltd., Chichester.

Saunders, P. M., 1967, 'The temperature at the ocean-air interface', Journal of Atmospheric Science, 24, 269-273.

Schlüssel, P., Emery, W.J., Grassl, H., Mammen, T., 1990, 'On the Bulk-Skin Temperature Difference and its Impact on Satellite Remote Sensing of Sea Surface Temperature', Journal of Geophysical Research, Vol. 95, No. C8, 13341-13356.

Sidran, M., 1981, 'Broadband reflectance and emissivity of specular and rough water surfaces', Applied Optics, Vol. 20, No. 18, 3176- 3183.

Smith, S. D., 1988, 'Coefficients for sea surface wind stress, heat flux, and wind profiles as a function of wind speed and temperature', Journal of Geophysical Research, Vol. 93, No. C12, 15467-15472.

Smith, A.H., Saunders, R.W., Závody, A.M., 1994, 'The Validation of ATSR Using Aircraft Radiometer Data over the tropical Atlantic', Journal of Atmospheric and Oceanic Technology, Vol. 11, 789-800.

Smythe-Wright, D., 1998, 'CHAOS Cruise Outline'

Smythe-Wright, D., 1999, 'RRS Discovery Cruise 233 - A Chemical and Hydrographic Atlantic Ocean Survey: CHAOS', Southampton Oceanography Centre Cruise Report, No. 24.

Thomas, J.P., Knight, R.J., Roscoe, H.K., Turner, J., Symon, C., 1995, 'An Evaluation of a Self-Calibrating Infrared Radiometer for Measuring Sea Surface Temperature', Journal of Atmospheric and Oceanic Technology, Vol. 12, 301-316.

Thomas, J.P., Turner, J., 1995, 'Validation of Atlantic ocean sea surface temperatures measured by the ERS-1 along track scanning radiometer', Journal of Atmospheric and Oceanic Technology, Vol. 12, 1303-1312.

Watts, P.D, Myles, R.A., Nightingale, T.J., 1996, 'Wind Speed Effects on Sea Surface Emission and Reflection for the Along Track Scanning Radiometer', Journal of Atmospheric and Oceanic Technology, Vol. 13, 126-141.

Wick, G.A., 1995,'Evaluation of the variability and predictability of the bulk-skin sea surface temperature difference with application to satellite-measured seat surface temperature', Ph.D. thesis, University of Colorado.

World Climate Research Programme, 1981, 'Report of meeting on co-ordination of plans for future satellite observing systems and ocean experiment to be organised within the WCRP, Jan 1981', W.M.O. Secretariat, Geneva.

Yokoyoma, R., Tanba, S., Souma, T., 1995, 'Sea surface effects on the sea surface temperature estimation by remote sensing', International Journal of Remote Sensing, Vol. 16, No. 2, 227-238.

Yokoyoma, R., Konda, M., 1996, 'Sea surface effects on the sea surface temperature estimation by remote sensing – Part 2', International Journal of Remote Sensing, Vol. 17, No. 7, 1293-1302.

Zävody, A.M, Mutlow, C.T., Llewellyn-Jones, D.T., 1995, 'A radiative transfer model for sea surface temperature retrieval for the along-track scanning radiometer', Journal of Geophysical Research, Vol. 100, No. C1, 937-952.